Transient internal forced convection under dynamic thermal loads: in clean-tech and automotive applications

by

Mohammad Fakoor Pakdaman

M.Sc., Tehran University, 2011
B.Sc., Amirkabir University of Technology, 2008

Thesis Submitted in Partial Fulfillment of the
Requirements for the Degree of
Doctor of Philosophy

in the
School of Mechatronic Systems Engineering
Faculty of Applied Sciences

SIMON FRASER UNIVERSITY

Summer 2015

Approval

Name:	**Mohammad Fakoor Pakdaman**
Degree:	**Doctor of Philosophy**
Title:	***Transient internal forced convection under dynamic thermal loads: in clean-tech and automotive applications***
Examining Committee:	**Chair:** Behraad Bahreyni Associate Professor

Majid Bahrami
Senior Supervisor
Associate Professor

John Jones
Supervisor
Associate Professor
School of Engineering Science

Siamak Arzanpour
Supervisor
Assistant Professor

Caroline Sparrey
Internal Examiner
Assistant Professor
School of Mechatronic Systems
Engineering

Andrew Rowe
External Examiner
Professor
Department of Mechanical Engineering
University of Victoria

Date Defended/Approved: July 29, 2015

Abstract

This research aims to address the thermal behavior of emerging engineering applications with dynamic thermal characteristics. Such applications include: i) clean-tech systems, e.g., powertrain and propulsion systems of Hybrid/Electric/Fuel Cell Vehicles (HE/E/FCV); ii) sustainable/renewable power generation systems (wind, solar, tidal); and iii) information technology (IT) systems (e.g., data centers, e-houses, and telecommunication facilities).

In this research, transient internal forced-convection was used to model the thermal characteristics of the cooling systems in the above-mentioned applications. In addition, sinusoidal heat flux was considered, since arbitrary loads can be modeled by a superposition of sinusoidal waves using a Fourier transformation series. Additionally, benchmark driving cycles were used to investigate the thermal characteristics of a cooling system in the context of the real-world application of HE/E/FCV.

Firstly, the energy equation was solved analytically for a steady tube flow under an arbitrary time-dependent thermal load. Then sinusoidal heat flux was taken into account, and closed-form relationships were obtained to predict the temperature distribution inside the fluid and the Nusselt number. Finally, the presented results were validated using a commercially available software program: ANSYS Fluent.

In the next step, the energy equation was solved analytically for tube flow with an arbitrary flow rate and a given time-dependent heat flux. Sinusoidal heat flux and flow rate were then taken into account; closed-form series solutions for the temperature distribution and Nusselt number of the tube flow were presented. An independent numerical simulation was also performed to validate the models.

Additionally, new testbeds were designed and built and a comprehensive experimental study was performed to analyze the thermal behavior of a tube flow under arbitrary time-dependent heat flux. It was shown that there was an excellent agreement between the experimental data and the predictions of the developed models.

As a result of the above work, a new model was developed that predicts the minimum instantaneous flow rate to maintain the temperature at a given level under an arbitrary time-dependent heat flux. Compared to conventional steady-state designs, the developed model can result in up to a 50% energy savings while maintaining the temperature of the system below the targeted value.

Keywords: Forced convection; Transient systems; Duty cycles; Analytical solution; Experimental study; Numerical simulation

To my beloved parents, my brothers, and my lovely sister

Acknowledgements

I would like to thank my senior supervisor, Dr. Majid Bahrami, for his kind support, guidance, and insightful discussions throughout this research. It was a privilege for me to work with him and learn from his experience.

I am also indebted to Dr. John Jones and Dr. Arzanpour for the useful discussions and comments, which helped me to define the project and to pursue its goals. I would also like to thank Dr. Sparrey and Dr. Rowe for their time reading this thesis and helping to refine it.

I would like to thank my colleagues and lab mates at Laboratory for Alternative Energy Conversion at Simon Fraser University. Their helps, comments, and assistance played an important role in the development of this thesis. In particular, I want to thank Dr. Mehran Ahmadi, Mehdi Andishe-Tadbir, Dr. Wendell Huttema, Jason Wallace, and Marius Haiducu.

I have received financial support from Automotive Partnership Canada (APC), Grant No. APCPJ 401826-10, and Simon Fraser University for which I am grateful. I would also like to appreciate our industrial collaborator, Future Vehicle Technologies (FVT) for their time, help and kind cooperation.

I have to thank my family that have endlessly encouraged and supported me through all stages of my life. Without their presence and support no achievement was possible in my life. I would also like to thank my dear friends; Khorshid Fayazmanesh, Farshid Bagheri, Raana Tavasoli, Maryam Yazdanpour, Ali Gholami, Sina Salari, and Siavash Pourreza for their kind support and great memories.

Table of Contents

Approval ii
Abstract iii
Dedication iv
Acknowledgements v
Table of Contents vi
List of Tables viii
List of Figures ix
Executive Summary x
Motivation x
Objectives x
Methodology xi
Contributions xii
References xiii

Chapter 1. Introduction 1
1.1. Research Importance 1
1.2. Research Motivation 3
1.3. Research Scope 3
1.4. Organization of the dissertation 5

Chapter 2. Literature review 7
2.1. Unsteady forced convection 8
2.2. Conjugated internal heat transfer 12
2.3. Laminar pulsatile flow 14
2.4. Research Objectives 18

Chapter 3. Experimental study 19
3.1. Testbed 1 19
3.2. Test-bed 2 23
3.2.1. Time-varying load 26
3.2.2. Target temperature 26
3.2.3. Coolant flow rate 26
3.2.4. Data acquisition 27
3.3. Testbed 3 27
3.4. Uncertainty analysis 30
3.5. Experimental data 32

Chapter 4. Summary of Contributions 44
4.1. Unsteady laminar forced-convective tube flow under dynamic time-dependent heat flux 44
4.2. Unsteady internal forced-convective flow under dynamic time-dependent boundary temperature 45

4.3. Optimal unsteady convection over a cycle for arbitrary unsteady flow under dynamic thermal load....46
4.4. Temperature-aware time-varying convection over a cycle for a given system thermal-topology....47

Chapter 5. Conclusions and Future Works....48
5.1. Conclusion....48
5.2. Future Work....49

References....50
Appendix A Unsteady internal forced-convective flow under dynamic time-dependent boundary temperature....62

Appendix B Optimal unsteady convection over a duty cycle for arbitrary unsteady flow under dynamic thermal load....74

Appendix C Temperature-aware time-varying convection over a duty cycle for a given system thermal-topology....87

List of Tables

Table 2.1. Summary of literature on transient forced convection 11

Table 2.2: Summary of the literature on laminar pulsatile channel flow. 17

Table 3.1: A summary of the details of the developed testbeds. 19

Table 3.2: Technical specifications of the utilized variable-speed pump. 24

Table 3.3: Summary of calculated experimental uncertainties. 32

Table 3.4: Summary of data for outlet temperature under step heat flux $P = 100[W]$. 33

Table 3.5: Summary of data for outlet temperature under square-wave power. 34

Table 3.6: Summary of data for outlet temperature under sinusoidal power. 36

Table 3.7: Summary of data obtained for wall temperature (T_4) under step wall heat flux case. 38

Table 3.8: Summary of data obtained for wall temperature (T_4) under sinusoidal heat flux case. 39

Table 3.9: Summary of data obtained for wall temperature (T_4) under square-wave power. 41

Table 3.10: Range of dimensionless parameters in the experiments 42

Table 3.11: Range of dimensional parameters in the experiments 43

List of Figures

Figure 1.1. The roadmap and deliverables of the present research project 4

Figure 2.1. A breakdown of the literature review conducted in this study..... 7

Figure 2.2. Schematic of the two main regions adopted to find the transient thermal response of the tube flow [32]..... 9

Figure 3.1: Schematic view of the experimental setup built as testbed 1. 20

Figure 3.2: Components of the developed testbed to investigate constant flow under dynamic heat flux: (a) main reservoir (b): copper tube covered with thermal paste (c): flexible heaters wrapped around the tube (d): Insulated tube (e): flow meter (f): DAQ system and power supplies. 22

Figure 3.3: A schematic view of testbed 2. 23

Figure 3.4: (a) Single-speed and (b) variable-speed pumps used in testbed 1 and 2, respectively. 24

Figure 3.5: Pictures of testbed 3 (a) location of thermocouples on the tube (b) cold plate covered with thermal paste (c) tape heater wrapped around the cold plate (d) fiber-glass and aluminum foils around the cold plate and heater assembly (e) test section in a polystyrene box. 29

Figure 3.6: 3D schematic and exploded views of testbed 29

Executive Summary

Motivation

Efficient thermal management is a transformative technology for the development of next-generation solutions for systems that involve time-varying thermal loads. Transient thermal loads are at the core of a wide range of applications in emerging technologies including i) clean-tech systems, e.g., powertrain and propulsion systems of Hybrid/Electric/Fuel Cell Vehicles (HE/E/FCV); ii) sustainable/renewable power generation systems (wind, solar, tidal); and iii) information technology (IT) systems (e.g., data centers), e-houses, and telecommunication facilities. Substantial transitions occur in thermal loads of all of the above applications as a direct result of 1) variable load due to duty cycles; and 2) unsteady coolant flow rate. Conventionally, thermal systems are designed for nominal steady-state or worst-case scenarios, which leads to oversized heat exchangers and high parasitic power. These scenarios do not properly represent the thermal behavior of many applications or duty cycles. In this thesis, new analytical closed-form solutions are presented for internal single-phase transient heat transfer with unsteady flow under time-varying thermal loads. The results of this study provide a platform to devise efficient variable-capacity next-generation heat exchange devices for a variety of engineering applications. As such, the performance of transient heat exchangers is investigated based on the system “thermal topology”, i.e. the instantaneous thermal load within a cycle. This provides an opportunity to significantly reduce the parasitic power required for the thermal management of HE/E/FCV, telecom facilities, and sustainable power generation systems, and to improve the overall efficiency of thermal systems.

Objectives

The research objectives are summarized as follows:

- Develop a fundamental understanding of transient dynamic heat transfer for internal single-phase unsteady flows under arbitrary time-dependent thermal loads.
- Demonstrate a proof-of-concept efficient dynamic cooling system.

- Develop a complete range of analytical modelling approaches that can be applied to thermal systems with steady/unsteady flows under a given duty cycle.
- Provide a platform for designing new efficient thermal management systems that actively and/or proactively predict an optimum flow pattern over a duty cycle.

Methodology

To simulate transient thermal behaviors of the dynamic cooling systems, it is essential to evaluate the patterns and magnitudes of thermal loads over the given duty cycles. Benchmark driving cycles are an example of where dynamic thermal loads occur in automotive applications in the context of HEV/EV/FCV. These driving cycles can be used as real-time data for dynamic thermal loads. Besides in this study, sinusoidal thermal loads are studied as any arbitrary load can be modelled with oscillatory functions by using a superposition technique.

Experimental study: To obtain the experimental data required for the model development and solution validation, a new testbed is developed as a proof-of-concept demonstration in the Laboratory for Alternative Energy Conversion (LAEC) at Simon Fraser University. The main components of the testbed are i) programmable DC power supplies; ii) programmable peristaltic pump; iii) copper tube; iv) strip heaters; v) water chiller; and vi) software (LabVIEW from National Instruments) that allows for the emulation of various duty cycles, and for data acquisition.

Analytical modelling: The energy equation is solved analytically for a steady tube flow and an arbitrary time-dependent heat flux. A new all-time model is also developed to find the thermal characteristics of a steady tube flow imposed on an arbitrary time-dependent wall temperature. Then an arbitrary flow pattern for the tube flow is taken into account, and the energy equation is solved analytically for an arbitrary time-dependent heat flux. Employing the developed analytical models, the thermal characteristics of a laminar flow can be obtained for a time-dependent flow rate and heat flux.

Numerical analysis: Independent numerical simulations of the tube flow are conducted using the commercial software ANSYS Fluent. User defined codes (UDFs) are written to apply the dynamic heat flux boundary conditions on the channel wall and the transient velocity inside the tube.

As a result of the above work, a new model is developed that predicts the minimum required flow rate instantaneously to maintain the temperature at a given level under an arbitrary time-dependent heat flux. Figure 1 shows the overview and deliverables of the present research program.

Contributions

Accordingly, the list of contributions from the present study is presented below; a list of publications arising from this study is also provided at the end of the executive summary:

- Developed analytical models to predict the thermal characteristics of steady/unsteady internal flows under arbitrary time-dependent thermal loads, [1-2].
- Developed a new analytical model to predict the thermal behaviour of steady internal flow under arbitrary time-dependent surface temperature [3].
- Proposed the optimal instantaneous flow rate to maximize the Nusselt number over a given duty cycle [2].
- Designed and built a new testbed as a proof-of-concept demonstration to validate the proposed models for efficient dynamic cooling [4].
- Validated the analytical and numerical results using the obtained experimental data [4].

References

[1]M. Fakoor-Pakdaman, M. Andisheh-Tadbir, and M. Bahrami, (2014) "Unsteady laminar forced-convective tube flow under dynamic time-dependent heat flux," *ASME J. Heat Transfer*, 136 (4), 041706-1-10.

[2]M. Fakoor-Pakdaman, M. Ahmadi, M. Andisheh-Tadbir, M. Bahrami, (2014) “Optimal unsteady convection over a duty cycle for arbitrary unsteady flow under dynamic thermal load”, 78, *Int. J. Heat Mass Transfer*, pp. 1187-1198. Doi: 10.1016/j.ijheatmasstransfer.2014.07.058

[3]M. Fakoor-Pakdaman, M. Ahmadi, and Majid Bahrami, (2014) "Unsteady internal forced-convective flow under dynamic time-dependent boundary temperature", *Journal of Thermophysics and Heat Transfer*, Vol. 28, No. 3, pp. 463-473. doi: 10.2514/1.T4261

[4]M. Fakoor-Pakdaman, M. Ahmadi, M. Andisheh-Tadbir, M. Bahrami, (2015) “Temperature-aware time-varying convection over a duty cycle for a given system thermal-topology”, *International Journal of Heat and Mass Transfer,* 87, pp. 418–428.

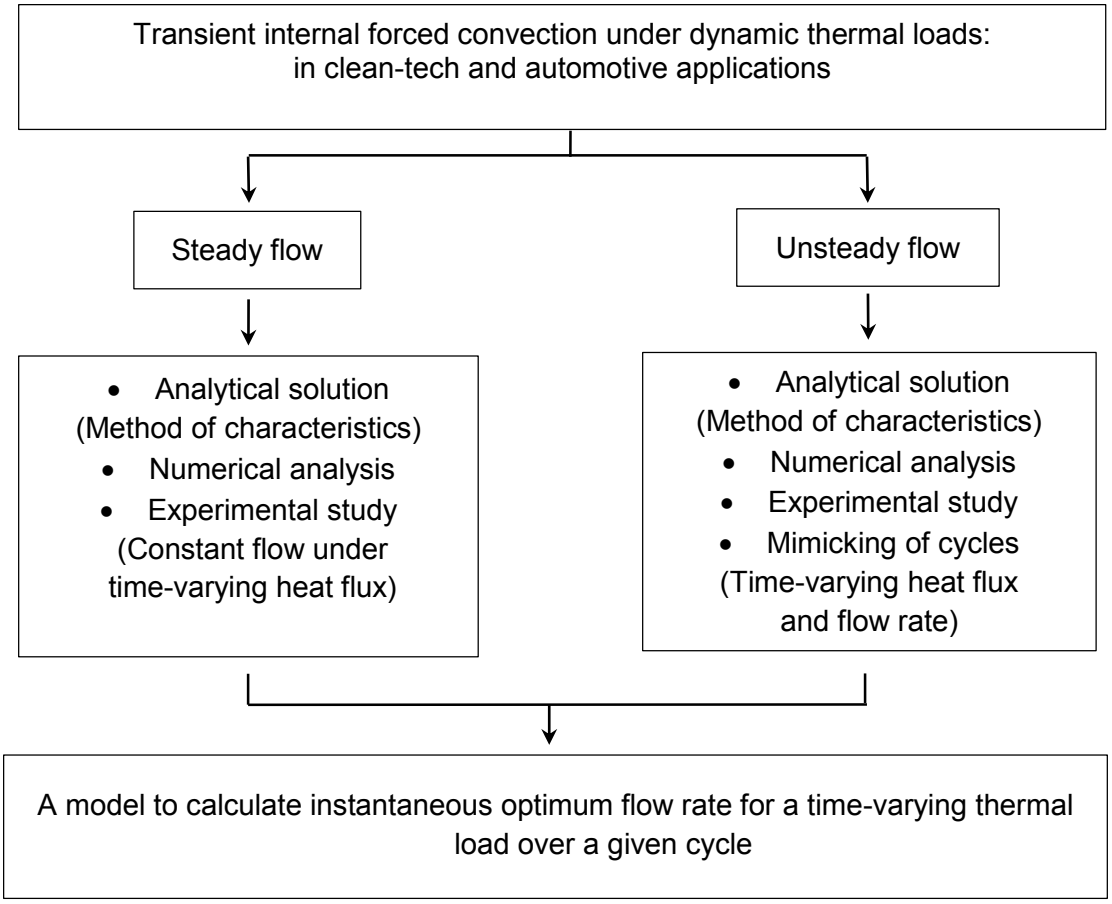

Fig.1: The present research project roadmap and deliverables

Chapter 1.

Introduction

1.1. Research Importance

Efficient thermal management is an advanced technology required for the optimal performance of a wide range of engineering applications including i) emerging clean technology systems, e.g. powertrain and propulsion systems of hybrid/electric/fuel cell vehicles (HE, E, FCV) [1–5]; ii) sustainable/renewable power generation systems (wind, solar, tidal) [6–10]; iii) information technology (IT) services (data centers) and telecommunication facilities [11–16]. In the context of electronics and power electronics, about 55% of failure mechanisms during operation have a thermal root [17]. The rate of failures due to overheating nearly doubles with every 10°C increase in the operating temperature [18]. The functionality and performance of electronic devices, and the desire for miniaturization in the industry have increased drastically over the recent years [19,20]. Thermal management has become the limiting factor in the development of new devices and reliable low-cost cooling methods are even more necessary [21–23]. The importance of the thermal management of electronic devices is also reflected in its worldwide market: the thermal management technology market was valued at $10.1 billion in 2013, reached $10.6 billion in 2014 [22] and is expected to reach $14.7 billion by 2019. Thermal management hardware, e.g. fans and heat sinks account for about 84% of the total market while other cooling product segments, e.g., software, thermal interface materials (TIM), and substrates, each account for between 4% to 6% of the market [22].

Transient thermal loads are at the core of most real applications and so should be considered when devising efficient thermal management technologies. Downing and Kojasoy [19] have predicted heat fluxes of 150-200 W/cm^2 and pulsed transient heat loads up to 400 W/cm^2 for next-generation insulated gate bipolar transistors (IGBTs).

The non-uniform and time-varying nature of the heat load is certainly a key challenge in maintaining the temperature of the heat-generating components within their safe and efficient operating limits [25]. The same challenge is observed in many other engineering applications such as sustainable/renewable power generation systems (wind, solar, tidal). About 740 MW of solar power generating capacity has been added between 2007 and the end of 2010, bringing the global total to 1095 MW [26]. Such growth is expected to continue as, in the USA, at least another 6.2 GW of capacity was expected to be in operation by the end of 2013 [26]. However, the growth of this technology is hindered by the inherent variability of solar energy, which is subject to daily and seasonal variations, as well as variability due to weather conditions [8,27,28]. To overcome the issue of intermittency, thermal energy storage (TES) systems are used to collect thermal energy to smooth out the output and shift its delivery to a later time. Single-phase sensible heating systems or latent heat storage systems utilizing phase change materials (PCM) are used in TES; transient heat exchange occurs to charge or discharge the storage material. From the technical point of view, one of the main challenges facing TES systems is designing suitable heat exchange devices to work reliably under unsteady conditions [10], a key issue that this research attempts to address.

As the systems are transient, the heat exchangers/heat sinks never attain a steady-state condition. Conventionally, cooling systems are conservatively designed for a nominal steady-state or worst-case scenario, which does not properly represent the real thermal behavior of the system [29]. The state-of-the-art approach is to utilize efficient thermal management techniques to devise a variable-capacity cooling infrastructure for next-generation dynamic heat exchange devices [30]. Thus, the performance of transient heat exchangers is optimized based on the “thermal topology” of the system, i.e. the instantaneous thermal load (heat dissipation) over a cycle. For instance, IBM utilized a variable capacity cooling strategy in a data center that led to significant energy savings, up to 20%, compared to the conventionally cooled facility [30]. In addition, in case of the HE/E/FCV, a variable capacity cooling strategy improves the overall vehicle efficiency, reliability and fuel consumption and also reduces the weight and carbon foot print of the vehicle [5].

1.2. Research Motivation

This work has been performed to assist a local start-up company, Future Vehicle Technology (FVT) located in Pitt Meadows, BC with their cooling solutions. FVT designed and developed electric drive systems with a target to meet or exceed the performance of the conventional diesel/gasoline power systems. FVT has prototyped an electric vehicle, the *eVaro.* The electric motor and inverter of the eVaro are air-cooled, and during harsh driving cycles or environmental conditions they experienced excessive heating and high temperatures. This causes reliability and performance issues, which led them to initiate this research venture, with the goal of devising effective thermal management strategies for the electric motor and inverter of the eVaro.

FVT reported a large amount of thermal load while testing the eVaro. Heat fluxes up to 50 W/cm^2 were noted in the electric motor while pulse transient heat loads up to 25 W/cm^2 were reported for the inverter. To resolve this thermal management issue, it was decided to convert the cooling systems of an FVT prototype from air-cooled to liquid cooled. The objective was to devise an efficient cooling strategy to minimize the cost, parasitic power, and size of the required heat exchangers while maintaining the temperature below the recommended value of 85°C. According to the data reported by FVT, the thermal load of the electronics was remarkably time-dependent. This translated into remarkable transient thermal behavior of the cooling systems, which in case of the eVaro led to thermal runaway during peak loads and harsh environmental conditions.

1.3. Research Scope

The goal of this project is to develop a fundamental understanding of efficient thermal management systems for engineering applications involving dynamic thermal loads. The aim is to design transient heat exchangers based on the system “thermal topology”, i.e. the instantaneous thermal load over a duty cycle. Conventionally, thermal systems are designed for nominal steady-state or worst-case scenarios, which leads to oversized heat exchangers and high parasitic power. These scenarios do not properly represent the thermal behaviour of many applications or duty cycles. The results of this study provide a platform to devise efficient variable-capacity next-generation heat

exchange devices for a variety of engineering applications. This provides an opportunity to significantly reduce the parasitic power required for the thermal management of HE/E/FCV, telecom facilities, and sustainable power generation systems, and to improve the overall efficiency of thermal systems. To achieve the above-mentioned goals, in this thesis, a model is developed as a tool for internal single-phase transient heat transfer with steady/unsteady flow under time-varying thermal loads. The roadmap of this research is presented in Figure 1.1.

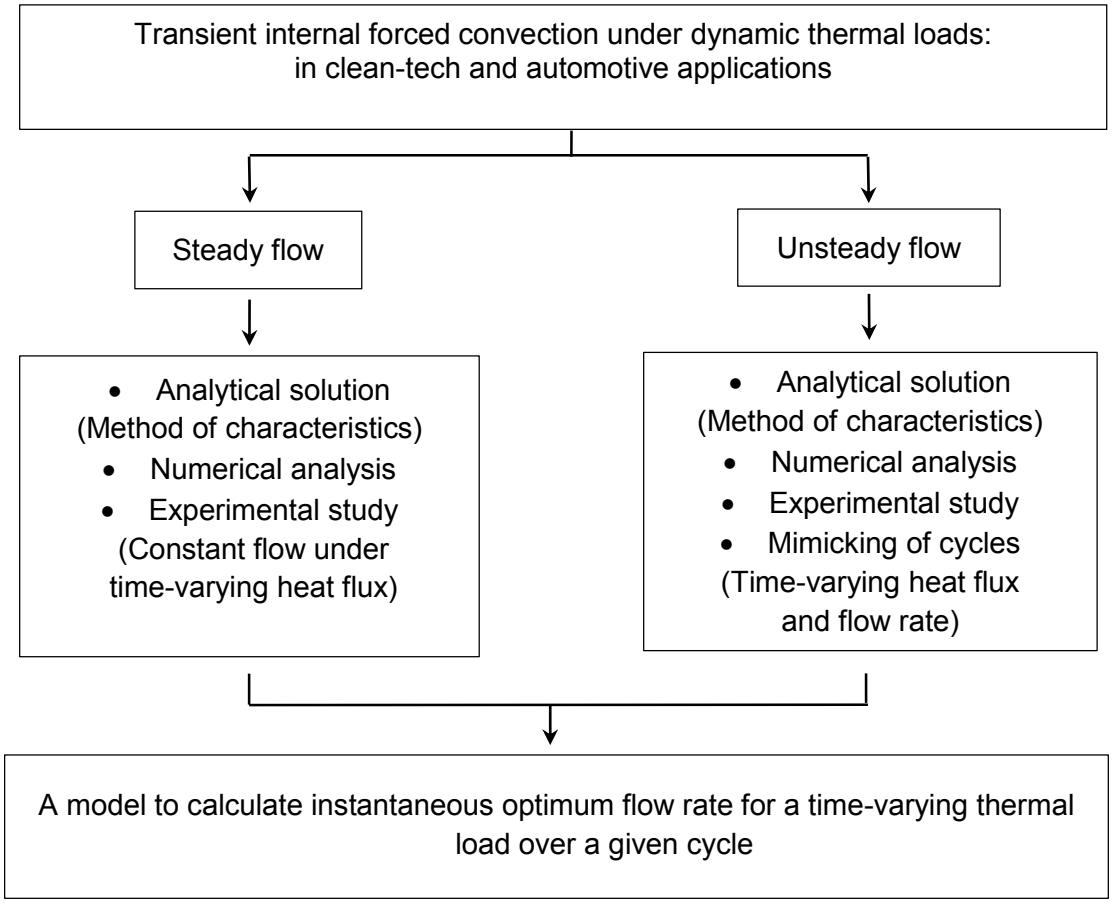

Figure 1.1. The roadmap and deliverables of the present research project

Using the developed predictive model, the temperature is maintained at a desired level for a given arbitrary thermal load. In addition, the power consumption/cooling demand will be significantly reduced by applying the minimum required flow to maintain the temperature at a given level. To obtain the experimental data required for the model

development and solution validation, a new testbed is developed as a proof-of-concept demonstration in the *Laboratory for Alternative Energy Conversion* (LAEC) at Simon Fraser University. The main components of the testbed are i) programmable DC power supplies; ii) programmable peristaltic pump; iii) copper tube; iv) strip heaters; v) water chiller; and vi) software (LabVIEW from National Instruments) that allows for the emulation of various duty cycles, and for data acquisition.

1.4. Organization of the dissertation

This dissertation is comprised of four chapters, which are organized as follows:

Chapter 1 is dedicated to the research importance and motivation of this study. In Chapter 2, a comprehensive literature review is conducted on three major aspects of this dissertation: (i) unsteady internal forced convection; (ii) unsteady conjugated forced-convection; and (iii) pulsatile flow, under dynamic thermal load. Available analytical, numerical, and experimental studies are discussed in Chapter 2, and a summary of pertinent literature is provided in a tabular form.

The details of the experimental setup are explained in Chapter 3. In addition, a description of instrumentation, data measurement and logging are presented in Chapter 3. The first testbed built to investigate constant flow under dynamic load is described in Section 3.1. The details of the second testbed which was used to study variable flow under variable load are given in Section 3.2. A cold plate was also tested for variable flow/load case, and the corresponding experimental setup is described in Section 3.3. Uncertainty analysis is then done, and the experimental data are presented in a tabular form.

Chapter 4 provides a summary of the contributions of the present research. In addition, research with the published papers attached in the appendices. In Section 4.1, an analytical model is developed to predict the thermal characteristics of a steady tube flow under a given arbitrary surface temperature. A sinusoidal surface temperature as a function of time is considered for the tube surface, and the temperature distribution inside the fluid, tube heat flux, and the Nusselt number are obtained. The analytical results are verified numerically.

An analytical model is developed in Section 4.2 that evaluates the thermal characteristics of a tube flow under dynamic thermal load and a given unsteady flow. As an example, the temperature distribution and the Nusselt number are obtained for an unsteady tube flow with sinusoidal flow rate and under a sinusoidal heat flux. The proposed models are used to show how significant enhancements or reductions in the average Nusselt number can be achieved in a tube flow by applying proper temporal flow control.

An experimental study is conducted in Section 4.3 to validate the developed analytical models in Sections 4.1-4.3. An experimental testbed is developed to apply time-dependent heat flux on a copper tube. A programmable pump is also used to apply transient flow rate inside the tube. LabVIEW software is used to simulate sinusoidal transient scenarios and benchmark driving cycles. Using the proposed models, a tool is developed to maintain the temperature of a tube flow at a given point under an arbitrary imposed heat flux. The proposed algorithm applies the minimum flow rate instantaneously to maximize the energy efficiency of the cooling system. In addition, by preventing over cooling the developed tool will minimize the cooling power of the system.

Chapter 2.

Literature review

Transient tube flow is considered as the main representative of the cooling systems in many engineering applications. Substantial transitions occur in most real applications as a direct result of 1) variable load due to duty cycles; and 2) unsteady coolant flow rate over a cycle.

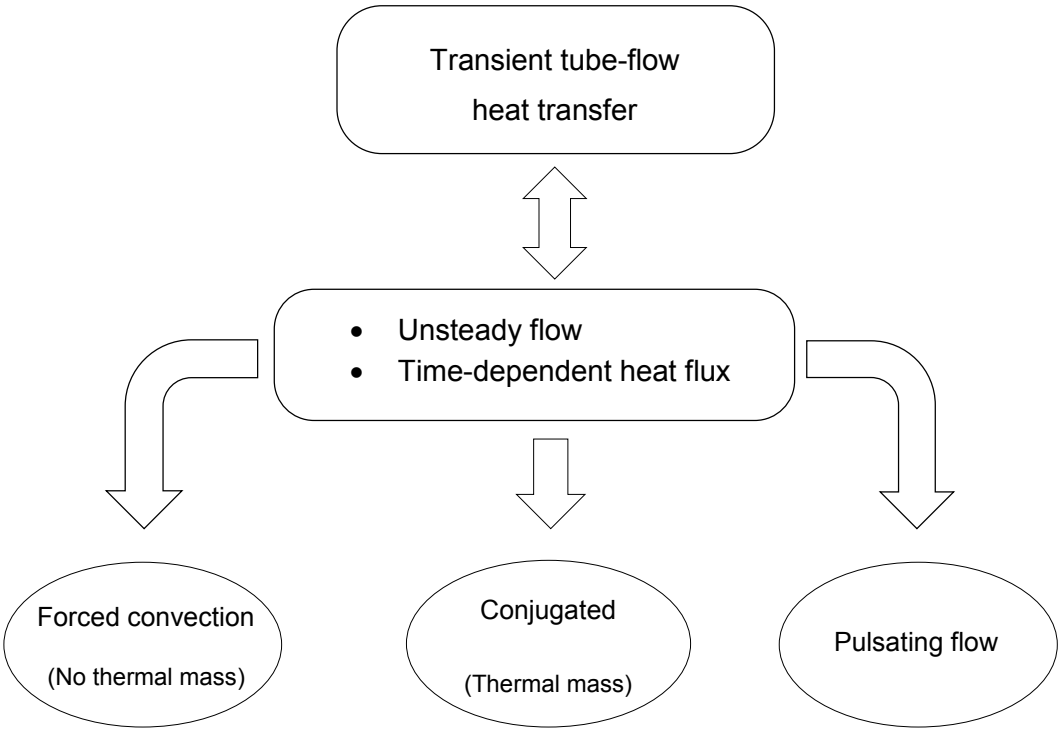

Figure 2.1. A breakdown of the literature review conducted in this study.

Depending upon the magnitude of tube thermal mass, transient conjugated heat transfer or unsteady forced convection may occur. The former happens for thermally "thick-walled" tubes (or heat exchanger) while the latter is the case when the thermal mass of the tube (or heat exchanger) is negligible. This issue will be further discussed in Sections 2.1-3. In addition, in some applications laminar pulsating flow may be subjected

to dynamic thermal loads. As such, a comprehensive literature review is conducted for i) unsteady forced-convection, ii) conjugated heat transfer, and iii) laminar pulsing flow.

2.1. Unsteady forced convection

Siegel [31-32] pioneered the study of transient laminar forced convection inside a tube. He first solved the energy equation for a tube flow with constant flow for arbitrary longitudinal variation of the wall heat flux [31]. Siegel [32] also presented a closed-form solution for transient laminar slug flow in ducts under a step heat flux. The definition of short- and long-time responses for transient forced convection were also discussed for the first time in [32]. These definitions will be used throughout this thesis. Therefore, a brief explanation is given below to define short- and long-time responses for transient forced convection [32].

As shown in Figure 2.2, in an Eulerian coordinate system, the observer is fixed at a given location x along the tube and the fluid moves by. It will take some time, $t = x/U$ for the entrance fluid to reach the axial position x. Beyond this region, i.e. at $x>U\cdot t$, where the inlet fluid will not have enough time to penetrate, convective heat transfer plays no role, thus conduction becomes the dominant mechanism for transferring heat from the wall to the fluid. The behavior in this region is similar to a tube with infinite length in both directions. This means that a pure transient “heat-conduction” process takes place. On the other hand for $x<U\cdot t$, the observer situated at axial position x feels the passing fluid that has had enough time to reach from the insulated entrance section. This region is considered as the long-time response of the fluid flow. Therefore, the solution consists of two regions that should be considered separately. The methodology considered in this study is shown schematically in Figure 2.2.

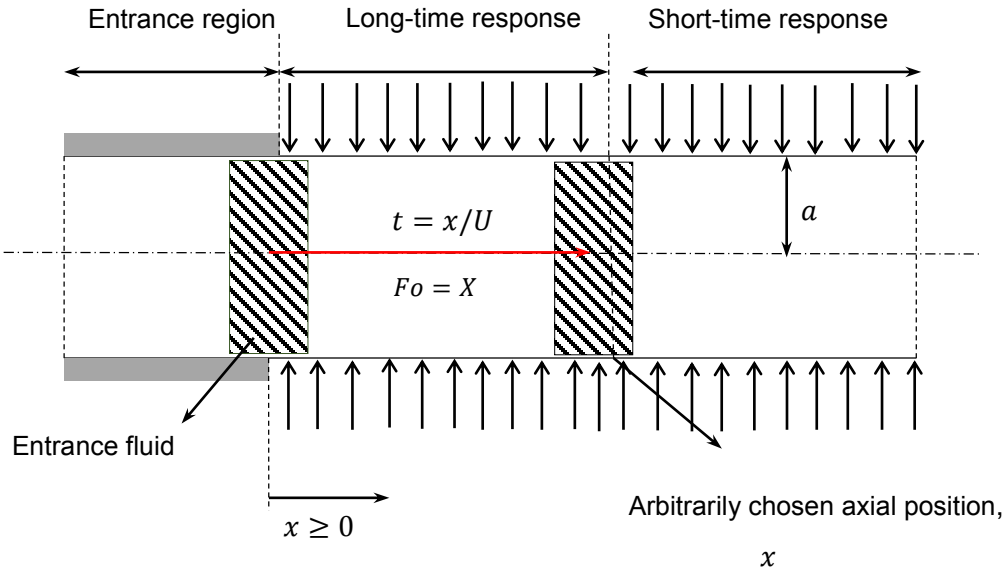

Figure 2.2. Schematic of the two main regions adopted to find the transient thermal response of the tube flow [32]**.**

Rizika [33,34] used a Laplace transform technique to find the thermal lag in a parallel flow heat exchanger with compressible/incompressible fluids. Sparrow and Siegel [35] used an integral technique to solve the integrated form of the energy equation across the boundary layer. A fully developed velocity profile was considered, and the temperature profile inside the fluid was assumed to be polynomial. The unknown coefficients were then found. They used the same technique in [36] to find the temperature distribution of laminar fully-developed flow in a parallel plate channel. Clark et al. [37,38] conducted a series of studies to evaluate the dynamic response of the bulk temperature of a coolant in a heat exchanger having time-variant heat sources. A Laplace transform technique was used, and the analytical results were validated experimentally.

Siegel [39] used eigenfunction expansion to perform analysis in the downstream region of a tube flow. It was assumed that the circular tube or a parallel-plate channel walls underwent arbitrary time-variations in temperature. Perlmutter and Siegel [40] analyzed unsteady laminar flow in a duct with unsteady heat addition. Step heat flux was considered to be imposed on the tube wall, and a few numerical examples were carried out. Bonilla et al. [41] presented solutions to the transient heat transfer in a conduit cooled on the

inside by a flowing coolant. One dimensional heat transfer was considered to evaluate the 1D temperature for a variety of cases where the internal heat generation was constant or a function of distance. Perlmutter and Siegel [42] presented analytical solutions for transient heat transfer in unsteady incompressible laminar flow between parallel plates. It was assumed that the transient was caused by simultaneously changing the driving pressure of the fluid and wall temperature with time. Siegel and Perlmutter [43] presented a methodology to analyze the laminar heat transfer in a channel with unsteady flow and wall heating varying with position and time. It was shown that quasi-steady analysis may or may not represent the thermal characteristics of a transient tube flow depending on the thermal mass of the system. Hsu [44] analyzed heat transfer in a round tube with sinusoidal wall heat flux distribution. The Nusselt number for sinusoidal wall heat flux distribution was compared with slug flow Nusselt number, and a good agreement was noted. Kays and Crawford [45] presented a methodology for solving the energy equation for tube flow under arbitrary position-dependent heat flux.

Conley et al. [46] performed a numerical study to estimate the Nusselt number at the entrance region of the Graetz problem. An explanation was then given to justify the discrepancy between the numerical and analytical results. Suces and Radley [47] analyzed unsteady forced convection in a power-law fluid, and presented an exact solution for the temperature during short-time response. Lin and Shih [48] proposed an instant-local similarity method to analyze the unsteady state Graetz problem. It was assumed that the channel wall underwent a step change in wall temperature. However, the solution was only valid for large Graetz number. Chen et al. [49] presented a numerical solution for a tube flow under a step wall temperature/heat flux. The numerical data were compared with the analytical results reported in [39]. An excellent agreement was noted especially for high Graetz numbers. Barletta and Zanchini [50] studied laminar forced convection in a circular tube under a sinusoidal axial distribution. Two cases were studied: a sinusoidal heat flux with vanishing mean value, and a sinusoidal heat flux, which did not change sign. It was shown that the Nusselt number oscillated with axial position. Some singularities were also noted in the solution when the fluid bulk and wall temperature were equal. Astaraki et al. [51] treated the same problem using a confluent hypergeometric function. The Nusselt number and temperature distribution inside the fluid were evaluated while considering the thermal mass of the tube. Transient forced convection with periodically

varying inlet temperature has been also extensively studied in the literature [52–59]; a summary of the related work is presented in Table 2.1 below.

Table 2.1. Summary of literature on transient forced convection

Author	Notes
Siegel [32]	✓ Reported temperature distribution inside a circular tube and between two parallel plates. × Limited to step wall heat flux/temperature. × Limited to slug flow condition. × Limited to an analytical-based approach without validation/verification
Siegel and Sparrow [36]	✓ Considered time-varying heat flux/temperature. ✓ Considered fully-developed velocity profile. × Limited to steady-state flow. × Limited to thermal entrance region.
Siegel [39]	✓ Reported temperature distribution inside a circular tube or between two parallel plates. ✓ Covered thermally developing and fully-developed regions. ✓ Considered fully-developed velocity profile. × Limited to step wall temperature. × Nusselt number was defined based on the tube wall and inlet fluid temperature. × Limited to an analytical-based approach without validation/verification.
Perlmutter and Siegel [40]	✓ Considered transient flow. ✓ Covered thermally developing and fully-developed regions. × Limited to step wall temperature/heat flux. × Can be used only to simulate start-up conditions.
Lin and Shih [48]	✓ Similarity solution is used to present the results. ✓ Considered non-Newtonian fluid inside the tube. × Accurate only for high Graetz numbers.
Chen et al. [49]	✓ Verified the analytical solutions presented in [32]. × Limited to a numerical (finite difference) method. × Limited to step wall tempearture/heat flux cases.

Perlmutter and Siegel [42]	✓ Considered transient flow. ✓ Considered effect of wall thermal capacity. × Limited to step wall temperature. × No experimental data are used/given even while using blending technique.
Siegel (1962) [60]	✓ Considered time-varying heat flux. ✓ Wall heat capacity is taken into account. × Limited to constant slug-flow. × Limited to a numerical method.
Suces and Radley [47]	✓ Considered wall temperature varying in a power law fashion with time. × Limited to short-time domain. × The final solutions are complex.

2.2. Conjugated internal heat transfer

Olek [61] proposed a series solution based on eigenfunction expansion to solve the steady-state two-dimensional conjugate heat transfer in rectangular or cylindrical multi-layered flow. Aleksashenko [62] performed analysis on the conjugate stationary problem of heat transfer with a moving fluid in a semi-infinite tube. The thermal mass of the tube was considered, and the viscous term in the energy equation for the fluid was also taken into account. Suces [63] presented an improved quasi-steady approach for transient conjugated forced convection. The method took into account both the effects of thermal history and thermal energy storage capacity of the fluid. The approximate analytical results were compared with finite difference solution results. In a separate study, Suces [64] reported an exact solution for transient conjugated heat transfer in the thermal entrance region of a duct, where the outside ambient fluid underwent sudden step change in temperature.

There are also a few studies on the first time domain of unsteady forced convection, i.e. before the long-time response starts. Olek [65] studied the transient conjugated heat transfer in a laminar pipe flow for early times, before the long-time response starts. A nonstandard form of separation of variables was used to present closed form solutions to evaluate the temperature distribution inside the fluid and channel wall. It was shown that the quasi-steady approach might not be a good assumption when “fast transients” were imposed on the system. Three different fields were considered: conjugate

heat transfer, forced-convection in fluids, and heat diffusion in composite media. Suces [66] analyzed transient conjugated heat transfer in a tube flow with sinusoidal heat generation and with axial position. He also performed a quasi-steady analysis, and compared the analytical and numerical results. It was stated that quasi-steady analysis was not a good assumption for a thermally “thick” wall; the tube has a high thermal mass (high specific heat and/or mass).

There are also a few numerical studies on conjugated heat transfer for a thermally thick pipe flow using finite difference method [67–70], Laplace transform technique [71–74], or perturbation method [75]. A summary of the analytical methods used to solve conjugated heat transfer problems is presented in [76]. Transient conjugated heat transfer with convective boundary condition was numerically investigated in Guedes and M. N. Özişik [79] and S. Bilir and A. Ates [80]. The effects of wall thickness ratio, wall-to-fluid conductivity ratio, wall-to-fluid thermal diffusivity ratio, and Peclet number were investigated. Peclet number is defined as the ratio between the advective transport and the diffusive transport. Several studies were also carried out to investigate the effects of wall and fluid axial conduction on the characteristics of transient conjugated heat transfer, [79–91].

Although several analytical studies were conducted on transient forced-convective tube flow and conjugated internal heat transfer, only a few experimental studies were carried out in this area. To the best knowledge of the author, the only related experimental works are in Ref. [92–94]. Koshkin et al. [92] implemented an experimental study on unsteady convective heat transfer in tubes. Stepwise heat flux and mass flow rates were implemented during the experiments, and the data were correlated to present compact easy-to-use relationships. Kawamura [93] also conducted an experimental and analytical study on the transient heat transfer for turbulent flow in a circular tube. Short-time and long-time responses were verified experimentally, and the obtained data showed good agreement with the analytical solution.

Within the context of transient forced convection, our literature review indicates:

- There is no experimental work on transient internal forced-convection under a time-varying thermal load.

- The presented models in the literature for internal flow under dynamic thermal load are limited to slug flow conditions.
- No analytical model exists to predict the thermal characteristics of fully developed flow over harmonic duty cycles.

Although encountered quite often in practice, the unsteady convection of fully-developed tube flow under time-varying thermal load has never been addressed in the open literature, either experimentally or theoretically. In other words, the answer to the following question is not clear: "*how the thermal characteristics of dynamic cooling systems vary under time-varying thermal loads (heat fluxes) of the electronics and APEEM?*"

2.3. Laminar pulsatile flow

An oscillatory flow can be classified as either a pulsatile flow (with a time-mean flow) or a reciprocating flow (with a zero time-mean flow). Oscillatory flow may be encountered in nature, circulatory and respiratory systems, and a wide range of engineering applications, e.g., reciprocating pumps, IC engines, pulse combustors, and pulsating jet cooling. Although laminar pulsatile flow was studied comprehensively in the literature for isoflux or isothermal cases, no studies were reported on pulsatile flow under dynamic load.

In earlier studies, heat and mass transfer for reciprocating flow with zero net flow received considerable attention [95–97]. In these studies, fluid reciprocates in a duct that is connected to two isothermal reservoirs. Remarkable improvement in heat and mass transfer was reported compared to the steady case. This was attributed to pure conduction occurred between the tanks. However, for pulsatile flows with non-zero mean value the results were inconsistent and sometimes contradictory. For turbulent flow, an increase in heat transfer was reported in Ref. [98], while no significant effect was observed in Ref. [99]. An increase in some cases and decrease in other cases were reported in Ref. [100] and Ref. [101] depending upon the frequency, Reynolds number, and amplitude of the pulsatile flow. For laminar flow, the pertinent literature on whether pulsatile flow increases the heat transfer can be categorized as follows:

(1) It enhances heat transfer [102], [103];

(2) It reduces the heat transfer [104–106];

(3) It does not have any effect on heat transfer [107–109]; and

(4) It either enhances or reduces heat transfer depending upon flow parameters [110–112].

In addition, Zhao and Cheng [113] performed a numerical study on laminar forced convection in a heated pipe subjected to a reciprocating flow. A correlation was presented for the Nusselt number as a function of the Reynolds number and geometrical parameters.

Siegel studied [107] pulsatile laminar flow between parallel plates under constant heat flux and constant wall temperature. The pulsations were caused by superpositioning an oscillating pressure gradient on the steady driving pressure of the flow. It was shown that the quasi-steady assumption did not give an accurate prediction of the thermal characteristics of the pulsatile flow for moderate range of pulsation frequencies [107]. Faghri et al. [103] investigated laminar pulsatile flow in a pipe. They showed that the velocity pulsation induced harmonic oscillation in temperature could be broken into a steady mean and a harmonic part. Wommersley [114] proposed a method to experimentally measure the velocity and viscous drag in arteries when the pressure gradient is known.

Guo and Sung [115] addressed the contradictory results of the Nusselt number for pulsatile flow in previous published papers. They proposed a new model for the time-averaged Nusselt number of laminar pulsatile flow under constant wall heat flux. Their definition was introduced based on the time-averaged differences between the tube-wall and fluid-bulk temperatures over a pulsation period. Kim et al. [111] showed that in the fully developed region the difference between the time-averaged heat flux and the steady heat flux was small. Moschandreou and Zamir [110] noticed positive and negative differences between the pulsating and steady Nusselt number. However, they also made a strange argument that this difference continued to grow for higher frequencies. This issue was addressed in Ref. [106]. Hemida et al. [106] argued that the small effects of

pulsation, which had been noted in previous studies, occurred as a result of the restrictive boundary conditions. Wall temperature/heat flux was assumed constant both in space and time. This may affect the heat exchange process and reduce the effects of pulsation. This showed the necessity of considering more realistic boundary conditions for the tube wall, other than constant heat flux or temperature. Less restrictive boundary conditions might manifest into greater sensitivity to pulsation [106]. This is one of the key issues addressed in this thesis.

Habib et al. [116] performed an experimental study on convective heat transfer characteristics of laminar pulsing air flow inside a duct. A significant effect was reported as a result of pulsation on the mean Nusselt number. A number of other experimental studies also studied laminar pulsating flow, [117–122]. Yu et al. [123] addressed the contradictory results for pulsating flow. They concluded that the Nusselt number fluctuated around the mean value while the time-averaged Nusselt number remains the same for all cases. Brereten and Jiang [124] introduced the idea of fluid flow modulation to increase the time-averaged Nusselt number of pulsating flow under constant heat flux. A perturbation method was used in Ref. [125] to address forced convection with laminar pulsating flow with small amplitudes. An analytical solution for laminar pulsating flow in a tube in rolling motion was presented in Ref. [126]. A number of studies were conducted on pulsating flow heat transfer inside a porous medium [127–129]. Pulsating flow for mixed convection has also been investigated in the literature, see for example [130]. There is a host of other research on laminar pulsating flow [131–143]. A summary of literature on laminar pulsating flow is presented in Table 2.2. Our literature review indicates:

- The existing models for pulsating channel flow are limited to constant wall heat flux/temperature cases.
- Effects of simultaneous oscillation of the imposed heat flux and the fluid velocity have not been investigated in the literature.
- There is no model to determine an optimal velocity frequency for a given harmonic heat flux to maximize the convective heat transfer rate.

To the best of our knowledge, the effects of non-constant boundary conditions have not been investigated in the literature either experimentally or theoretically. In other

words, the answer to the following question is not clear: "*can flow pulsation enhance the heat transfer rate in heat exchangers under arbitrary time-dependent loads*?"

Table 2.2: Summary of the literature on laminar pulsatile channel flow.

Author	Approach	Notes
Hemida et al. [106]	Analytical/numerical (Green's function solution)	✓ Reported a closed-form relationship for the temperature distribution in fully-developed region. ✓ Considered different BCs: i) isoflux; ii) wall with thermal resistance; iii) wall with thermal inertia.
Siegel and Perlmutter[107]	Analytical (Method of characteristics)	✓ Reported temperature distribution between two parallel plates. ✓ Covered thermally developing and fully-developed regions. × Limited to step wall temperature and heat flux. × Nusselt number was defined based on the tube wall and inlet fluid temperature.
Zhao and Cheng [113]	Numerical	✓ Proposed a compact relationship for the time averaged Nusselt number for reciprocating flow. ✓ Covered both thermally developing and fully-developed regions.
Ye et al. [123]	Analytical	✓ Fully-developed, time-dependent flow is taken into account. ✓ Closed-form solutions are proposed for temperature and the Nusselt number. × The short-time response is neglected.
Brereton and Jiang [124]	Analytical (Laplace transform technique)	✓ Fully-developed, time-dependent flow is taken into account. ✓ Flow unsteadiness reducing/enhancing the heat transfer are proposed and examined. × Limited to tube flow with isoflux condition. × Singularity in the solution may occur for
Nield and Kuznetsov[125]	Analytical (Perturbation method)	✓ Reported transient Nusselt number in circular tubes and parallel plates. ✓ Definition of the Nusselt number similar to [115]. × Reported singularity in the solution for $Pr = 1$. × Limited to constant wall heat flux.
Yan et al. [126]	Analytical/experimental	✓ Reported series solutions for temperature distribution and Nusselt number. × Limited to constant wall temperature.

2.4. Research Objectives

In Section 2.3 it was pointed out that most available studies on transient forced convection were focused on constant boundary conditions, e.g. isoflux or isothermal boundary conditions. In addition, most papers in this area are analytical, and there is a lack of experimental investigation. As such, the research objectives in this study are summarized as follows:

- Develop a fundamental understanding of transient dynamic heat transfer for internal single-phase unsteady flows under arbitrary time-dependent thermal loads.
- Demonstrate a proof-of-concept efficient dynamic cooling system.
- Develop a complete range of analytical modelling approaches that can be applied to thermal systems with steady/unsteady flows under a given duty cycle.
- Provide a platform for designing new efficient thermal management systems that actively and/or proactively predict optimum flow patterns.

Chapter 3.

Experimental study

New testbeds were developed to validate the proposed analytical solutions. The main differences between the testbeds were the test sections and the driving force for the fluid. The test section for testbeds 1 and 2 was a straight copper tube, while a cold plate is used in test-bed 3. Besides, a single-speed pump was utilized in test-bed 1 whereas a variable-speed pump was used in test-beds 2 and 3. The details of the test-beds are described below, and summarized in Table 1. As such, testbed 1 was developed to investigate the thermal characteristics of constant tube flow under time-dependent heat fluxes. Testbed 2 was used to study the thermal characteristics of a time-dependent flow under time-varying heat fluxes. Finally, the test section of test-bed 2 was replaced with a cold plate to simulate the thermal characteristics of heat generating components attached to a cold plate.

Table 3.1: A summary of the details of the developed testbeds.

Testbed	Test section	Fluid driving force	Heat exchanger
1	Straight tube	Single-speed pump	Tank of ice-water
2	Straight tube	Variable-speed pump	Chiller
3	Cold plate	Variable-speed pump	Chiller

The following provides a description of the above testbeds.

3.1. Testbed 1

The developed experimental setup to investigate steady flow under a time-dependent heat flux is shown schematically in Figure 3.1. Some pictures of the actual testbed are also presented in Figure 3.2. The fluid, distilled water, flowed down from a

tank installed in an elevated position to use gravity for the flow; a calming section was also included in the design to prevent any disturbances in the tube. Adjusting the installed valves, the water level inside the upper-level tank was maintained constant during each experiment to attain the desired values of the constant flow during each experiment. Following [144], the calming section was long enough so that the fluid became hydrodynamically fully-developed at the beginning of the heated section.

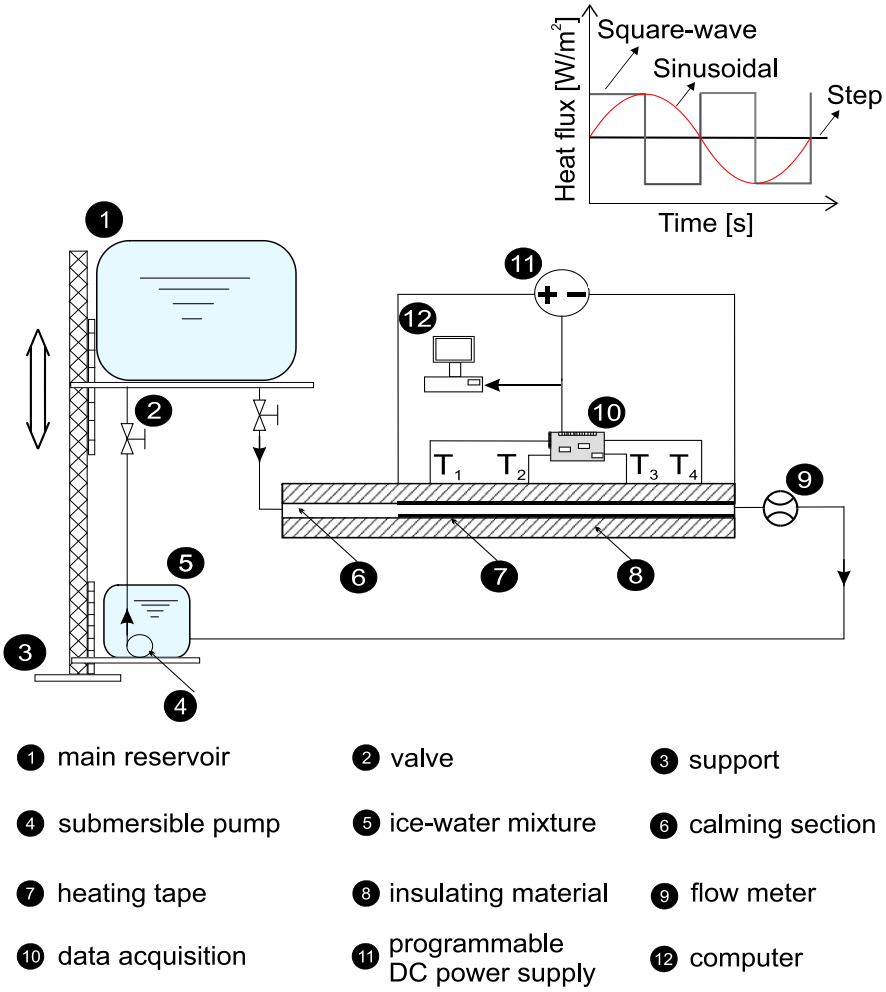

Figure 3.1: Schematic view of the experimental setup built as testbed 1.

A straight copper tube with $12.7 \pm 0.02 [mm]$ outer diameter, and $11.07 \pm 0.02 [mm]$ inner diameter was used for the calming and heated sections. The length of the former was $L_1 = 500 [mm]$, while the heated section was $L_2 = 1900 [mm]$

long. Two flexible STH062-120 heating tapes, Omega, were wrapped around the entire heated section. Four T-type thermocouples were mounted on the heated section at axial positions in [mm] of T_1(300), T_2(600), T_3(1000), and T_4(1700) from the beginning of the heated section to measure the wall temperature. In addition, two T-type thermocouples were inserted into the flow at the inlet and outlet of the test section to measure the bulk temperatures of the distilled water. The heating tapes were connected in series, while each was $240[V]$ and $940[W]$. It should be noted that a thin layer of thermal paste was used between the heaters and the tube to decrease the thermal contact resistance.

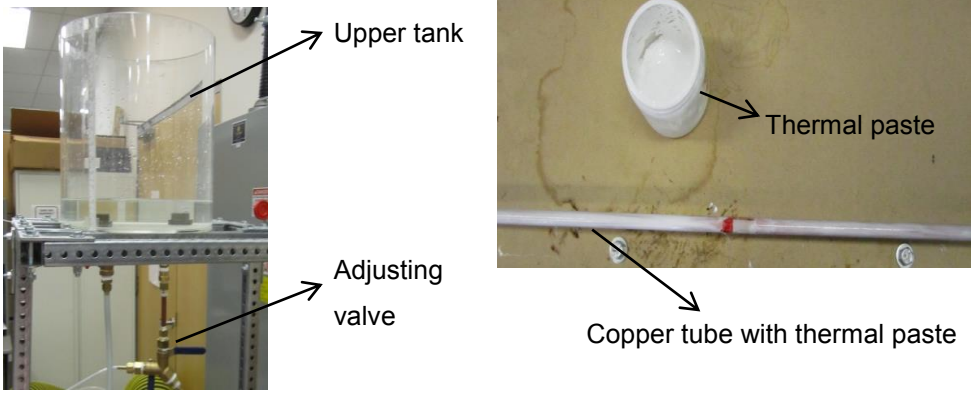

(a) (b)

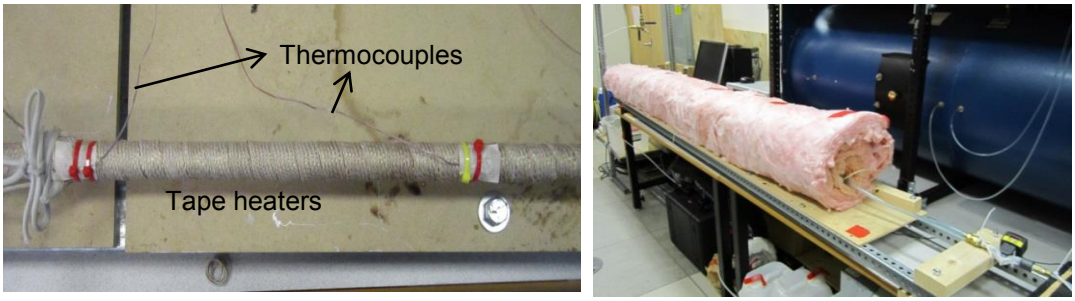

(c) (d)

(e)

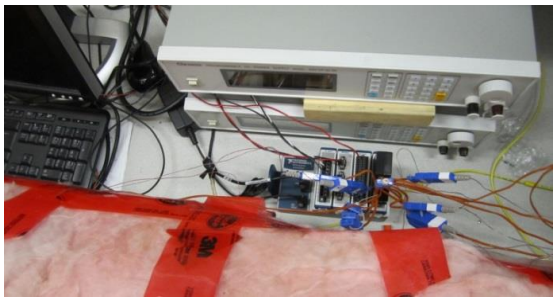

(f)

Figure 3.2: Components of the developed testbed to investigate constant flow under dynamic heat flux: (a) main reservoir (b): copper tube covered with thermal paste (c): flexible heaters wrapped around the tube (d): Insulated tube (e): flow meter (f): DAQ system and power supplies.

Data measurement implemented every 0.1 [s], and each experiment ran for 30 [min]. To apply the time-dependent power on the heated section, two programmable DC power supplies (Chroma, 62012P-100-50 and 62012P-80-60, USA) were linked in a master and slave fashion, and connected to the tape heaters. The maximum possible power was $300[\mathrm{W}]$. To reduce heat losses to the surroundings, a thick layer (5[cm]) of fiber-glass insulating blanket was wrapped around the entire test section including calming and heated sections. After the flow passed through the test section, the flow rate was measured by a precise micro paddlewheel flow meter, FTB300 series Omega. Finally, the fluid returned to the surge tank which was full of ice-water mixture. As a result, the fluid was cooled down, and then was pumped back to the main tank at the upper level. All the thermocouples were connected to a data acquisition system composed of a chassis (NI cDAQ-9174) and an NI 9213 module; all these components were supplied by National Instrument. The programmable DC power supplies were controlled via standard LabVIEW software (National Instrument), to apply the time-dependent powers. As such, different unsteady cycles were attained by applying three different scenarios for the imposed power: i) step; ii) sinusoidal; and iii) square-wave. As such, real-time data were obtained for transient thermal characteristics of the system over such cycles. The experimental results obtained by testbed 1 are presented in graphical forms in Appendix D, and tabular forms in Section 3.5.

3.2. Test-bed 2

A schematic of testbed 2 is depicted in Figure 3.3. This testbed was developed to investigate the thermal characteristics of time-dependent flow under time-varying heat fluxes. As such, a controllable variable-speed peristaltic pump (V6/YZ1515x, Baoding Shenchen Precision Pump, China) was utilized to apply different patterns of flow inside the tube. The speed range of the pump was 0.1-600 rpm, and flow rate range was 0.000067-2280ml/min. The pump had various external control modes for option, and also had programmable external control mode. It supported RS232 and RS485 communication interfaces as well as standard MODBUS communication protocol, and achieved external control under different conditions. The technical specifications of the pump are presented in Table 3.2.

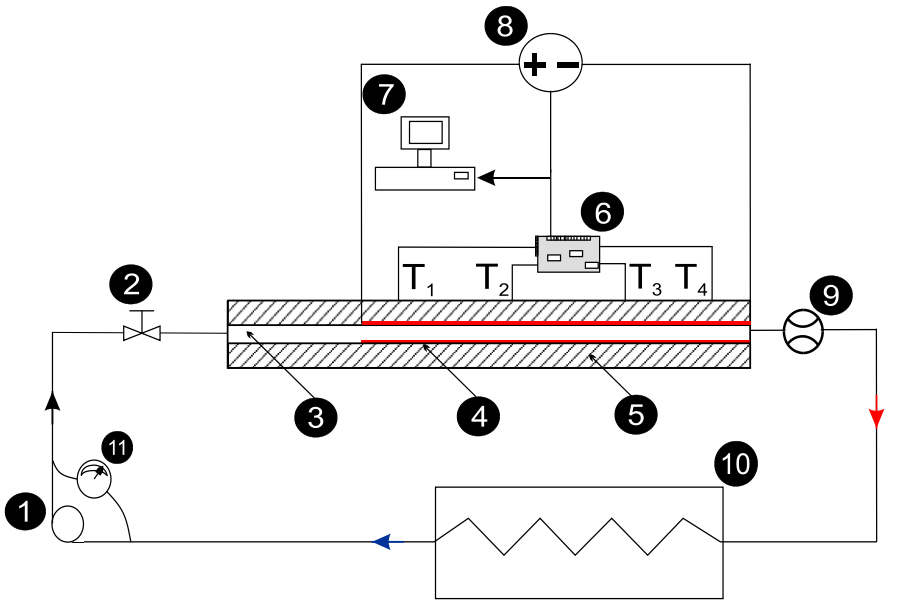

1 variable-speed pump
2 valve
3 calming section
4 heating tape
5 insulating material
6 data acquisition
7 computer
8 DC power supply
9 flow meter
10 chiller
11 clamp meter

Figure 3.3: A schematic view of testbed 2.

Besides, pictures of the single- and variable-speed pumps used in testbeds 1 and 2, respectively, are presented in Figure 3.4.

(a) (b)

Figure 3.4: (a) Single-speed and (b) variable-speed pumps used in testbed 1 and 2, respectively.

An AC clamp meter (FLUKE, I 200s) was also connected to the pump and the LabVIEW interface to monitor the pump power consumption instantaneously. The water-ice tank was also replaced by a chiller (Cole-Parmer Polystat standard 9.5L heated bath) to cool down the fluid after passing through the heated section.

Table 3.2: Technical specifications of the utilized variable-speed pump.

Technical specification:	Value/range
Flow rate	0.000067-2280ml/min
Speed range	0.1-600rpm
Speed resolution	0.01rpm
Flow rate resolution	0.001µl

Flow rate accuracy	±0.5%
Back suction angle	0-360°
Output pressure	0.1Mpa (0.86-1.0mm wall thickness tubing)
Motor type	Stepper motor
Circuit system	Shenchen-V-CIR
Operating system	Shenchen-V-EMB
Display	4.3 inch industrial grade true color LCD screen
Control method	Touch screen and membrane keypad
External cont. signal	0-5V, 0-10V, 4-20mA for option
Start/stop	Passive switch signal, such as: foot pedal
Direction signal	Active switch signal: 5V, 12V, 24V for option
Communication	RS232 and RS485, support MODBUS protocol
Output interface	Output motor working status
Drive dimension	260 × 155 × 230mm (L × W × H)
Drive weight	5.12kg
Power consumption	<50W
Environment	0-40℃
Relative humidity	<80%
IP rate	IP31

A user-friendly interface was developed in LabVIEW connecting to the DAQ system, power supplies and the pump. The developed analytical models were written as MATLAB codes and coupled with the LabVIEW interface. In this case, LabVIEW called the MATLAB functions to evaluate/apply the required flow inside the tube based on the imposed heat flux. Testbed 2 was used as a proof-of-concept demonstration as a tool to maintain the temperature of the components generating time-varying thermal loads at a desired value. Below is a brief description of how one can work with the developed setup.

3.2.1. Time-varying load

Different types of variable thermal load (heat flux) were imposed on the system: i) step, ii) sinusoidal, iii) square-wave, and iv) driving cycles. There was a module in the developed interface that enabled one to select between different scenarios to apply the heat flux. The interface then would command the power supplies to impose the heat flux on the heaters wrapped around the tube based on the specified load.

3.2.2. Target temperature

As mentioned before, the temperature of the tube was measured at 4 positions on the tube. Since the imposed heat flux was a function of time, the tube-surface temperature varied with time at any position along the tube. In addition, the temperature of the tube increased towards the downstream of the flow, as the bulk-fluid temperature raised in this direction. If one keeps the temperature at any location constant, then it will be maintained constant at any position along the tube. In this study, we tried to keep the temperature constant at T_4, as this was the hottest location between all the thermocouples along the tube.

3.2.3. Coolant flow rate

Based on the imposed heat flux and the targeted temperature, the LabVIEW interface commanded the pump to apply the required instantaneous flow rate. Two cooling-scenarios might be considered to control the pump:

Proactive cooling: the flow rate was calculated based on the developed analytical models [145–147]. The interface then commanded the pump to apply the flow inside the tube with the calculated magnitude. Note that no temperature feedback was used for this scenario, and pump modulation was only based on the applied power.

Active cooling: high and low set points around the target temperature were defined (by the user). The pump was then turned on/off by sensing the T_4 temperature, i.e. temperature feedback control. As such, when T_4 hit the maximum temperature, the user interface turned the pump on to work with the maximum capacity. Likewise, when the temperature went down below the low set point value the interface turned the pump off. Therefore, the surface temperature swung between high and low temperatures around the target temperature.

3.2.4. Data acquisition

The data acquisition system consisted of a chassis (NI cDAQ-9174) and four modules: NI 9213, NI 9205, NI 9225, and 9263. The module NI 9213 was used to record the temperature data, i.e., four surface temperatures, inlet and outlet temperatures. The module 9205 was connected to the clamp meter to measure the current of the variable-speed pump; module NI 9225 measured the voltage of the pump. In addition, NI 9263 was the voltage modulator to control the pump; this module commanded the pump by voltage output to apply the required flow rate over a cycle.

3.3. Testbed 3

The components of testbed 3 were the same as those used in testbed 2 except the test section. A cold plate was used as the test section in testbed 3, see Figure 3.5. The cold plate consisted of an aluminum heat spreader (152mm×89mm×13mm), and a U-shaped 3/8" copper tube. A tape heater, DHT 101040LD Omega, was wrapped around the cold plate to mimic the heat generating components mounted on the cold plate. The heater was 120 volt and 5.2 amps. It should be noted that a thin layer of thermal paste was used on the cold plate before wrapping the heater to decrease the thermal resistance between the heater and the cold plate. The cold plate and heater were then wrapped in a

fiber-glass blanket. The assembly was wrapped in an aluminum foil, and then insulated by 2" rigid polystyrene plates. Two T-type thermocouples were mounted on tube at axial positions in [mm] of T_1 [100], and T_2 [230] from inlet to measure the wall temperature. In addition, inlet and outlet temperatures were also measured by two T-type thermocouples. All other components including pump, chiller, and DAQ system were the same as those used in testbed 2.

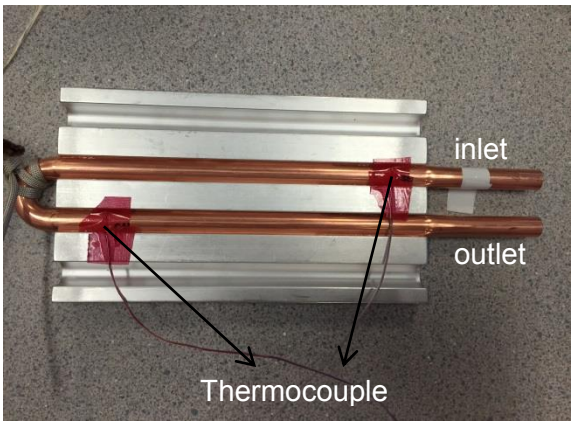

(a)

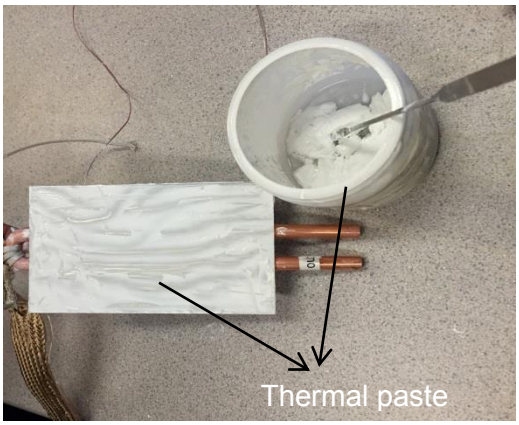

(b)

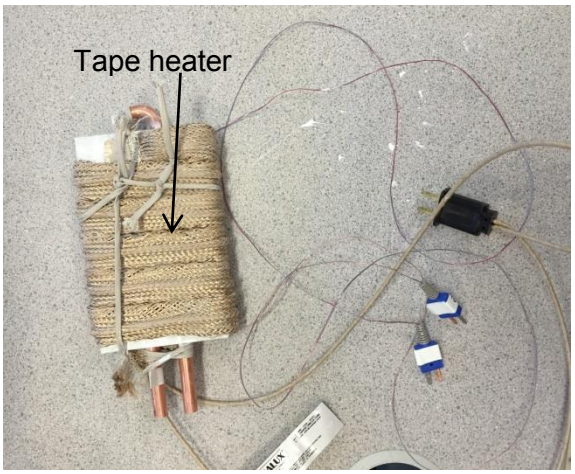

(c)

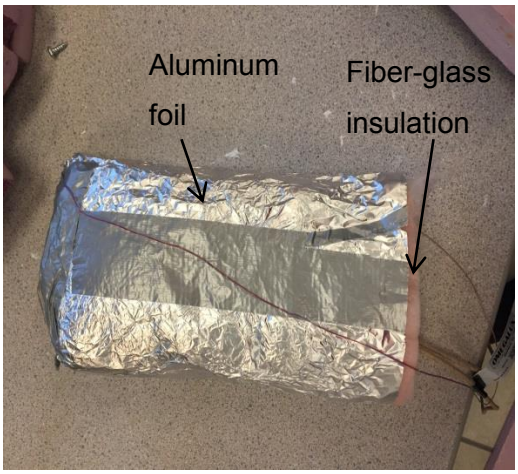

(d)

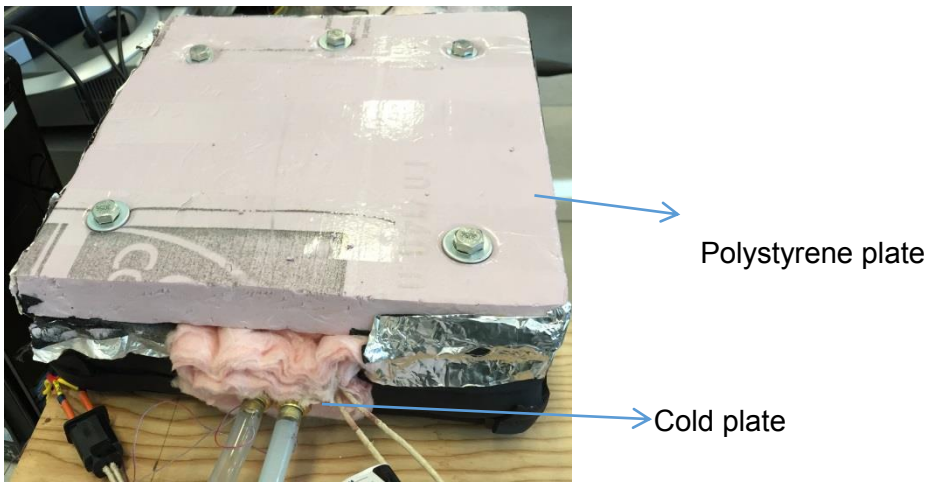

(e)

Figure 3.5: Pictures of testbed 3 (a) location of thermocouples on the tube (b) cold plate covered with thermal paste (c) tape heater wrapped around the cold plate (d) fiber-glass and aluminum foils around the cold plate and heater assembly (e) test section in a polystyrene box.

Schematic 3D view and exploded view of testbed 3 are also shown in Figure 3.6.

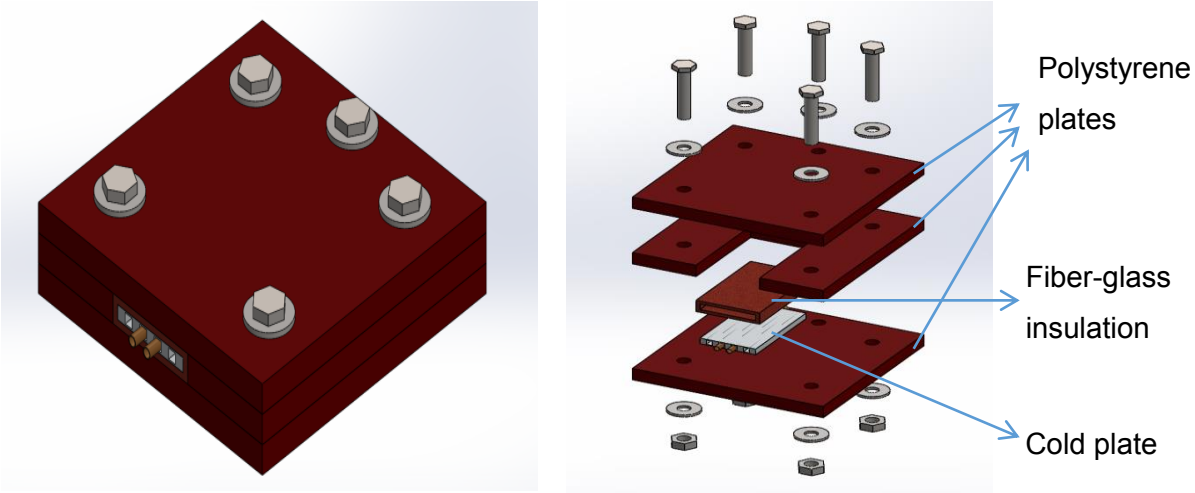

(a) (b)

Figure 3.6: 3D schematic and exploded views of testbed 3

3.4. Uncertainty analysis

The uncertainty analysis here is done based on the method presented by Moffat [149]. Suppose a set of measurements is made and the result, R, is a given function of independent variables $x_1, x_2, x_3, ..., x_n$. Thus,

$$R = R\left(x_1, x_2, x_3, ..., x_n\right) \tag{3.1}$$

To calculate the uncertainty associated with the experimental measurements, ω_R, the following relationship can be used [148]

$$\omega_R = \left[\sum\left(\frac{\partial R}{\partial x_i}\omega_i\right)^2\right]^{\frac{1}{2}} \tag{3.2}$$

where ω_i is the uncertainty of the independent variable of x_i. The heat transfer coefficient in this study is calculated by the following relationship:

$$h = \frac{P}{A\left(\bar{T}_s - T_m\right)} \tag{3.3}$$

where A is the area of the tube on which the heat flux is imposed.

$$A = \pi DL \tag{3.4}$$

It should be noted that P is the imposed power, D is the tube diameter, L is the length of the heated section, T_s denotes the average surface temperature, and T_m is the average fluid bulk temperature.

The power values $\left(P\right)$ in this study are measured directly by the power supplies and fed into LabVIEW interface. The uncertainty of the power supplies' reading is 3%. The uncertainty of the values read by thermocouples is $\pm 1°C$.

The final form of the uncertainty for the input power becomes;

$$\frac{\delta h}{h}=\left\{\left[\frac{\delta P}{P}\right]^2+\left[\frac{\delta A}{A}\right]^2+\left[\frac{\delta\left(T_s-T_m\right)}{\left(T_s-T_m\right)}\right]^2\right\}^{1/2} \quad 3.5$$

$$\frac{\delta A}{A}=\left\{\left[\frac{\delta D}{D}\right]^2+\left[\frac{\delta L}{L}\right]^2\right\}^{1/2} \quad 3.6$$

The uncertainty of the Nusselt number is calculated as follows:

$$\frac{\delta Nu}{Nu}=\left\{\left[\frac{\delta h}{h}\right]^2+\left[\frac{\delta D}{D}\right]^2\right\}^{1/2} \quad 3.7$$

In addition, the uncertainty of the applied micro flow meter was 6%, and the Reynolds number is calculated based on the flow rate as follows:

$$\mathrm{Re}=\frac{4\dot{Q}}{\pi D\nu} \quad 3.8$$

Where Re is the Reynolds number, $\dot{Q}$ is the flow rate, and ν is the fluid kinematic viscosity. Therefore, the uncertainty of Reynolds number is evaluated by the following relationship.

$$\frac{\delta \mathrm{Re}}{\mathrm{Re}}=\left\{\left[\frac{\delta \dot{Q}}{\dot{Q}}\right]^2+\left[\frac{\delta D}{D}\right]^2\right\}^{1/2} \quad 3.9$$

As such, the accuracy of the measurements and the uncertainties of the derived values are given in Table 3.3.

Table 3.3: Summary of calculated experimental uncertainties.

Primary measurements		Derived quantities	
Parameter	Uncertainties	Parameter	Uncertainties
$\dot{Q}$	6%	Re	7.6%
$P[W]$	3%	$h[W/m^2/K]$	9.1%
$T(T_s, T_m)$	$1[°C]$	Nu	9.3%

3.5. Experimental data

The experimental data logged by LabVIEW are presented in this section in tabular form. where,

$$\theta_o = \frac{T_o - T_{in}}{\pi L k} \tag{3.10}$$

$$\theta_w = \frac{T_4 - T_{in}}{\pi L k} \tag{3.11}$$

$$Fo = \frac{4\alpha t}{D^2} \tag{3.12}$$

Where θ_0 and θ_w are the dimensionless outlet and wall temperatures. T_{in}, L, k, α, D, and t are the inlet temperature, heated-section length, fluid thermal conductivity, fluid thermal diffusivity, tube diameter, and time, respectively. In addition, $\overline{T}_s$ and T_m are the average surface temperature and fluid bulk temperatures, respectively, defined as follows:

$$\overline{T}_s = \frac{T_1 + T_2 + T_3 + T_4}{4} \tag{3.13}$$

$$T_m = \frac{T_{in} + T_{out}}{2} \qquad 3.14$$

Where, T_1 to T_4 are the surface temperatures shown by the thermocouples on tube surface. T_{in} and T_{out} are the inlet and outlet fluid temperatures.

Table 3.4: Summary of data for outlet temperature under step heat flux $P = 100[W]$.

Time $[s]$	**Fourier**	**Outlet temperature** $[°C]$	**Dimensionless outlet temp.**
0	0	8.652121	0
20	0.073070866	10.10624	0.040025686
40	0.146141732	12.549207	0.132473018
60	0.219212598	15.109805	0.221365688
80	0.292283465	17.157684	0.293257951
100	0.365354331	18.658171	0.348306028
120	0.438425197	19.732985	0.387906385
200	0.730708661	21.897026	0.469270955
280	1.022992126	22.679554	0.493785602
360	1.315275591	23.075645	0.510085019
440	1.607559055	23.305574	0.518609397
520	1.89984252	23.444714	0.522274152

600	2.192125984	23.583965	0.525038826
680	2.484409449	23.687489	0.530378466
760	2.776692913	23.749674	0.533154528
840	3.068976378	23.82859	0.533630928
920	3.361259843	23.888025	0.526468097
1000	3.653543307	23.948458	0.533630928
1080	3.945826772	24.001013	0.530049513
1160	4.238110236	24.052935	0.530049513
1240	4.530393701	24.108883	0.530049513
1320	4.822677165	24.158482	0.526468097
1400	5.11496063	24.231794	0.530049513
1480	5.407244094	24.302246	0.533630928
1560	5.699527559	24.374794	0.537212344
1640	5.991811024	24.438641	0.530049513
1720	6.284094488	24.504465	0.530049513
1800	6.576377953	24.563236	0.526468097

Table 3.5: Summary of data for outlet temperature under square-wave power.

Time $[s]$	**Fourier**	**Outlet temperature** $[°C]$	**Dimensionless outlet**
0	0	6.114547	0

20	0.073070866	6.126176	0.000238761
40	0.146141732	6.805634	0.014335523
60	0.219212598	9.214728	0.070194361
80	0.292283465	11.522184	0.124762171
100	0.365354331	13.323492	0.167624099
120	0.438425197	15.138761	0.21165505
200	0.730708661	16.401608	0.24313352
280	1.022992126	16.901848	0.257298616
360	1.315275591	16.079029	0.236044347
440	1.607559055	14.32583	0.193032094
520	1.89984252	12.952079	0.163718136
600	2.192125984	13.973857	0.185800237
680	2.484409449	17.077087	0.259586305
760	2.776692913	17.960108	0.281197498
840	3.068976378	15.784777	0.223415798
920	3.361259843	13.815901	0.1775302
1000	3.653543307	13.262111	0.165287823
1080	3.945826772	15.008973	0.201269279
1160	4.238110236	17.755644	0.268896863
1240	4.530393701	17.782726	0.267653539
1320	4.822677165	15.10263	0.203215611
1400	5.11496063	13.863958	0.1729659

1480	5.407244094	14.362059	0.180778472
1560	5.699527559	17.18248	0.247021672
1640	5.991811024	18.575022	0.282830504
1720	6.284094488	17.135864	0.245519794
1800	6.576377953	14.601091	0.184463128

Table 3.6: Summary of data for outlet temperature under sinusoidal power.

Time $[s]$	**Fourier**	**Outlet temperature** $[°C]$	**Dimensionless outlet temp.**
0	0	5.953964	0
10	0.073070866	5.962303	0
20	0.146141732	6.050928	0.017907078
30	0.219212598	6.365502	0.046558403
40	0.292283465	6.988284	0.08
60	0.365354331	8.570149	0.12
80	0.438425197	9.889353	0.161163703
100	0.730708661	10.835764	0.179070781
190	1.022992126	11.394756	0.195249934
270	1.315275591	9.77809	0.127531274
350	1.607559055	9.366815	0.114473432

430	1.89984252	11.099916	0.177148564
500	2.192125984	12.621054	0.234825758
580	2.484409449	12.255813	0.217096104
660	2.776692913	10.356788	0.149979658
740	3.068976378	9.57959	0.123023525
820	3.361259843	11.073767	0.17908679
900	3.653543307	12.843814	0.23272293
980	3.945826772	12.436004	0.223319207
1060	4.238110236	10.52688	0.153819796
1140	4.530393701	9.737215	0.121445661
1220	4.822677165	11.222397	0.174943128
1300	5.11496063	12.977089	0.238186666
1700	5.407244094	13.130026	0.242722816
1740	5.699527559	13.231096	0.223818385
1760	5.991811024	13.042304	0.210056321
1780	6.284094488	12.701344	0.208587482
1800	6.576377953	12.280485	0.187907078

Table 3.7: Summary of data obtained for wall temperature (T_4) under step wall heat flux case.

Time $[s]$	Fourier	Surface temperature $[°C]$	Dimensionless surface temp.
0	0	10.68254	0.047731124
10	0.073070866	14.96912	0.164758205
20	0.146141732	18.72503	0.272042099
30	0.219212598	21.89111	0.357101822
40	0.292283465	24.37288	0.424357089
60	0.365354331	26.20711	0.475896056
80	0.438425197	27.38911	0.509310774
100	0.730708661	29.80251	0.578768473
190	1.022992126	30.73983	0.601890396
270	1.315275591	31.23809	0.617243015
350	1.607559055	31.51533	0.625103644
430	1.89984252	31.71952	0.629714799
500	2.192125984	31.8814	0.632464941
580	2.484409449	32.02506	0.637677967
660	2.776692913	32.11748	0.64064652
740	3.068976378	32.21215	0.64052241
820	3.361259843	32.30006	0.64052241

900	3.653543307	32.37025	0.641624384
980	3.945826772	32.4381	0.64052241
1060	4.238110236	32.50194	0.64052241
1140	4.530393701	32.57132	0.64052241
1220	4.822677165	32.62973	0.64052241
1300	5.11496063	32.69118	0.64052241
1700	5.407244094	32.77278	0.64052241
1740	5.699527559	32.84833	0.64052241
1760	5.991811024	32.91961	0.64052241
1780	6.284094488	32.97911	0.647409748
1800	6.576377953	33.0427	0.64052241

Table 3.8: Summary of data obtained for wall temperature (T_4) under sinusoidal heat flux case.

Time $[s]$	**Fourier**	**Surface temperature** $[°C]$	**Dimensionless surface temp.**
0	0	5.594989	0
10	0.073070866	6.427629	0.052436
20	0.146141732	7.966392	0.123565
30	0.219212598	9.409614	0.172585

40	0.292283465	10.74359	0.221282
60	0.365354331	13.00501	0.251245
80	0.438425197	14.69914	0.291258
100	0.730708661	15.84321	0.348339
190	1.022992126	15.63427	0.347084
270	1.315275591	12.82175	0.236538
350	1.607559055	12.89849	0.240957
430	1.89984252	16.28808	0.362958
500	2.192125984	18.39426	0.441588
580	2.484409449	17.04655	0.388672
660	2.776692913	13.74689	0.271393
740	3.068976378	13.14058	0.250557
820	3.361259843	16.20562	0.36288
900	3.653543307	18.73777	0.44381
980	3.945826772	17.33389	0.398733
1060	4.238110236	14.01521	0.278752
1140	4.530393701	13.37528	0.25174
1220	4.822677165	16.40709	0.360628
1300	5.11496063	18.91915	0.450997
1700	5.407244094	19.08217	0.450885
1740	5.699527559	18.86472	0.431254
1760	5.991811024	18.36598	0.422145

1780	6.284094488	17.66911	0.401735
1800	6.576377953	16.82465	0.38

Table 3.9: Summary of data obtained for wall temperature (T_4) under square-wave power.

Time $[s]$	**Fourier**	**Surface temperature** $[°C]$	**Dimensionless surface temp.**
0	0	5.953983	0
10	0.073070866	7.60235	0.033357998
20	0.146141732	9.814568	0.083446674
30	0.219212598	13.443272	0.169482209
40	0.292283465	14.889111	0.205151271
60	0.365354331	17.475941	0.266768404
80	0.438425197	18.631804	0.317461146
100	0.730708661	19.570225	0.42647354
190	1.022992126	20.450476	0.31363956
270	1.315275591	21.75922	0.268109215
350	1.607559055	23.368286	0.402929338
430	1.89984252	25.126925	0.452313167
500	2.192125984	25.36282	0.38258162
580	2.484409449	25.552137	0.307786525

660	2.776692913	23.910202	0.276681882
740	3.068976378	22.447247	0.399664376
820	3.361259843	21.218746	0.453461465
900	3.653543307	20.253191	0.408928591
980	3.945826772	19.710888	0.283007641
1060	4.238110236	19.277061	0.401003539
1140	4.530393701	18.847506	0.459296426
1220	4.822677165	18.546677	0.411503008
1300	5.11496063	18.338228	0.317037823
1700	5.407244094	18.185852	0.290964782
1740	5.699527559	18.839071	0.411458192
1760	5.991811024	20.624666	0.464826681
1780	6.284094488	22.015427	0.412749603
1800	6.576377953	23.192247	0.317488078

Table 3.10: Range of dimensionless parameters in the experiments

Parameter	Reynolds number	Prandtl number	Fourier number	Nusselt number
Range	100-1500	1.8-6.5	0-10	0-8

Table 3.11: Range of dimensional parameters in the experiments

Parameter	Surface temperature $[^{\circ}C]$	Outlet temperature $[^{\circ}C]$	Inlet temperature $[^{\circ}C]$	Time $[s]$	Power $[W]$	Flow rate $[ml/\min]$
Range	10-100	20-90	0-10	0-1800	0-800	0-800

Chapter 4.

Summary of Contributions

The results of this study are published in four journal papers. A summary of the presented results is reported below.

4.1. Unsteady laminar forced-convective tube flow under dynamic time-dependent heat flux

A new analytical model was developed for steady tube flow under dynamic time-dependent heat flux. The solution to the time dependent energy equation for a step heat flux boundary condition was generalized for arbitrary time variations in surface heat flux using a Duhamel's integral technique. A sinusoidal heat flux was considered as an example, and closed-form relationships were proposed for (i) temperature distribution inside the fluid, (ii) fluid bulk temperature, and (iii) Nusselt number. For the first time, a new definition was introduced for the Nusselt number, i.e. cyclic fully developed Nusselt number. Such Nusselt number is associated with the thermally developed region where the Nusselt number does not vary with axial location but is arbitrary in time. It was shown that the temperature inside the fluid varies with the angular frequency of the imposed heat flux. Fluctuations happen around the response for the step heat flux boundary condition. It was shown that the amplitude of temperature fluctuations decreases towards the centerline of the tube, which is attributed to the increase in thermal inertia towards the center of the tube. At any given axial position there is an initial transient period, which can be considered as pure conduction, i.e. the short time response. However, each axial position shows steady oscillatory behavior at the long-time response when convection begins. The analytical results show that at two limiting cases the temperature response approaches that of step heat flux: (i) heat flux with zero angular frequency and (ii) heat flux with very high angular frequency. The latter is called "fast transient"; for such rapid transient the fluid does not follow the details of the heat flux, and yields the response of step heat flux. This is attributed to the thermal inertia of the fluid. Time- and space-averages of the Nusselt number were obtained, along with the optimum angular frequency

to maximize the Nusselt number. It was also seen that conventional models deviate considerably from the newly developed transient results. The proposed analytical models were verified numerically, and the maximum difference was found to be around 5%.

4.2. Unsteady internal forced-convective flow under dynamic time-dependent boundary temperature

The results of this study are presented in Appendix B. A new full-time model was developed for steady tube flow under dynamic surface temperature. Using Duhamel's theorem, closed-form solutions were developed to predict (i) temperature distribution inside the fluid, (ii) wall heat flux, and (iii) Nusselt number. Both circular tube and parallel plate geometries were considered, and the proposed relationships can be used for both configurations. It was shown that for an imposed cyclic wall temperature, the fluid temperature oscillates around the associated response for the step surface temperature. Fluctuations occur with the angular frequency that the system is excited with. The shift between the peaks of the temperature profiles at different radial positions shows a "thermal lag" (phase shift) for the fluid flow, which increases towards the centerline of the tube. This thermal lag is attributed to the thermal inertia of the fluid. The phase lag between the imposed temperature and the heat flux was obtained, and presented as an easy-to-use relationship. It was noted that the Nusselt number experiences discontinuities, soaring to plus infinity and then returning from minus infinity. These excursions occur when the wall and fluid bulk temperature are equal but the heat flux is not zero. In fact, the Nusselt number loses its significance at these points. In addition, it was observed that when the angular frequency of the imposed surface temperature is very high, the fluid does not follow the imposed transient, and yields the response for step wall temperature. The amplitude of temperature fluctuations inside the tube is a function of the imposed frequency. At very high and small values of angular frequency, the amplitude approaches zero, i.e. step wall temperature response. Finally, an arbitrary time-dependent temperature was imposed on the tube wall, and the fluid response was obtained using a superposition technique. The analytical results were verified numerically using ANSYS Fluent.

4.3. Optimal unsteady convection over a cycle for arbitrary unsteady flow under dynamic thermal load

The results of this study are presented in Appendix C. A new analytical model was presented to predict the thermal characteristics of a tube flow with arbitrary unsteadiness in flow under arbitrary time-dependent heat flux. Exact relationships were obtained to find (i) the temperature distribution for the fluid; (ii) the fluid bulk temperature, and (iii) the local and time averaged Nusselt number. New compact relationships were proposed for the thermal entrance length and the cyclic fully-developed Nusselt number. It was shown that the period of the Nusselt number oscillations is the least common multiple of the periods of the imposed harmonic heat flux and the pulsating flow. For the first time, a new definition, cut-off angular frequency, was proposed to set a criterion for “fast” transients. As such, when the angular frequency of the imposed heat flux is beyond the cut-off angular frequency, the fluid feels the heat flux as constant at the average value. A relationship was obtained for the dimensionless cut-off angular frequency of pulsating flow, beyond which the heat transfer does not feel the pulsation. The dimensionless cut-off frequency is a function of pulsation angular frequency, channel geometry, and fluid thermal diffusivity. It was shown that the Nusselt number is a function of the imposed heat flux, and the fluid pulsation frequency. As a result, the Nusselt number can be altered by changing the frequency of the imposed heat flux or fluid pulsation. Optimum flow patterns that can increase the Nusselt number over a duty cycle were obtained, i.e. an optimal pulsating flow velocity with optimum frequency that enhances the time averaged Nusselt number by up to 27%. The model was presented for a general time-dependent heat flux and fluid flow, however, sinusoidal heat flux and fluid flow were considered as examples for presenting the closed-form relationships. Thermal lag inside the system was found to be a function of the angular frequency of the imposed heat flux and pulsating flow. The developed models show that downstream of the channel, the pulsation effects decrease, as a result, the heat transfer enhancement drops. The optimum frequency depends on the angular frequency of the imposed heat flux. In other words, for an imposed harmonic wall heat flux, there is an optimum value for the pulsation frequency which maximizes the heat transfer enhancement. Finally, it is indicated that the time averaged Nusselt number of pulsating flow is equal to that of steady flow over a period of fluctuation.

4.4. Temperature-aware time-varying convection over a cycle for a given system thermal-topology

An experimental study was implemented to investigate the thermal behavior of a steady fully-developed tube flow under time-dependent heat fluxes. To simulate duty cycles three different transient scenarios were implemented: (i) step; (ii) sinusoidal; and (iii) square-wave time-varying thermal loads. An experimental testbed was developed as a proof-of-concept demonstration for efficient dynamic cooling. The setup consists of (i) programmable power supplies, (ii) programmable pump, (iii) copper tube, and (iv) a data acquisition system. LabVIEW was used to control the power supplies, and apply the time-varying heat fluxes. Based on the proposed methodology in Appendix A, analytical expressions were proposed as closed-form solutions to predict temperature distribution and Nusselt number under step, sinusoidal, and square wave heat fluxes. The obtained experimental data were compared with the developed analytical models, with maximum relative difference of less than 15%. The new definition that was proposed analytically in Appendix C as cut-off angular frequency was tested/validated experimentally. In addition, a blending technique was used to propose an all-time model for the Nusselt number under step wall heat flux. This study was conducted to validate the analytical results obtained by the author, and it was used, for the first time, as a proof-of-concept demonstration of efficient variable-capacity liquid cooled systems. In fact, these analyses led to devising ‘‘temperature-aware’’ cooling solutions based on the system thermal topology (power management) over a given duty cycle. The results of this work provide a platform for the design, validation and building of new smart thermal management systems that can actively and proactively control the cooling systems of APEEMs and similar applications. The results of this study are presented in Appendix D.

Chapter 5.

Conclusions and Future Works

5.1. Conclusion

In this thesis, new analytical models are presented to predict the thermal characteristics of a cooling system with unsteady flow under time-dependent heat flux. It is shown that when a system is excited by a harmonic heat flux, the temperature inside the system is fluctuating with the same angular frequency. In addition, a thermal lag is observed between the applied heat flux, and the temperature response. A fully-developed cyclic Nusselt number is defined which does not vary with axial distance, but arbitrary with time. It is noted that the fluctuations occur around the response for the time-averaged heat flux.

Finally, an experimental study is performed to analyze the thermal behavior of a tube flow under an arbitrary time-dependent heat flux. Several forms of heat flux are taken into consideration including step, sinusoidal, and square wave. It is shown that there is an excellent agreement between the obtained experimental data and those predicted by the developed models.

The question "*whether the flow pulsation increases or reduces the heat transfer rate of convective cooling systems under time dependent thermal load?"* is answered here as follows: "the time averaged Nu number of pulsating flow is equal to that of steady flow over a period of fluctuation.

Several case studies are also considered to address the following question "*how the thermal characteristics of the dynamic cooling systems vary over a duty cycle?"*. The imposed heat flux (thermal load) is the dominant parameter that characterizes the thermal behavior of a cooling system. In other words, all the thermal characteristics of a transient system are a function of the imposed heat flux. For a sinusoidal heat flux, the temperature varies sinusoidally while for a square-wave load the temperature follows the same pattern.

As a result of this work, a new model is developed that predicts the minimum required flow rate instantaneously to maintain the temperature at a given level under an arbitrary time-dependent heat flux. As such, thermal stresses within the heat generating components will be reduced and their durability will increase remarkably. The developed model also predicts the minimum cooling demand of a system under a given heat flux based on the set point for the temperature. The results of this study provide a platform to devise efficient variable-capacity next-generation heat exchange devices for a variety of engineering applications. Compared to conventional steady-state designs, the developed model can lead to up to 50% energy saving while maintaining the temperature at the desired value.

5.2. Future Work

The following research directions can be considered as the continuation of this dissertation:

- Extend the analysis to hydrodynamically developing region. The results of this study are presented for slug flow and fully-developed flow cases. However, consideration of hydrodynamicaaly developing region can be a good addition to this work.
- Investigate the effect of interrupted wall heating. In fact, interrupted wall heating leads to resetting the thermal boundary layer and increases the heat transfer rate. As such, the heat flux pattern on the wall can be modeled by the models presented in this dissertation, and best dimensions of interruptions can be obtained.
- Extend the analysis to cases with high thermal inertial. There is no analytical relationship in the literature to predict transient conjugated forced convection.
- Investigate the effects of dynamic thermal load on mixed convection. There is no study in literature on effects of time-varying thermal load on mixed convection and natural convection.
- Investigate the effect of tube surface features, e.g. roughness, grooves, or fins on transient forced convection under a dynamic thermal load.

References

[1] Bennion, K., and Thornton, M., 2010, “Integrated vehicle thermal management for advanced vehicle propulsion technologies,” SAE Tec. Pap. 2010-01-0836, pp. 1–15.

[2] Boglietti, A., Member, S., Cavagnino, A., Staton, D., Shanel, M., Mueller, M., and Mejuto, C., 2009, “Evolution and modern approaches for thermal analysis of electrical machines,” IEEE Trans. Ind. Electron., **56**(3), pp. 871–882.

[3] Canders, W.-R., Tareilus, G., Koch, I., and May, H., 2010, “New design and control aspects for electric vehicle drives,” 14th International Power Electronics and Motion Control Conference (EPE-PEMC), Ohrid, Macedonia, pp. 1–8.

[4] Johnson, R. W., Evans, J. L., Jacobsen, P., Thompson, J. R. R., and Christopher, M., 2004, “The changing automotive environment: high-temperature electronics,” IEEE Trans. Electron. Packag. Manuf., **27**(3), pp. 164–176.

[5] Mi, C., Peng, F. Z. ., Kelly, K. J. ., Keefe, M. O. ’, and Hassani, V., 2008, “Topology, design, analysis and thermal management of power electronics for hybrid electric vehicle applications,” Int. J. Electr. Hybrid Veh., **1**(3), pp. 276–294.

[6] Garrison, J., and Webber, M., 2012, “Optimization of an integrated energy storage scheme for a dispatchable wind powered energy system,” ASME 2012 6th International Conference on Energy Sustainability, Parts A and B San Diego, California, USA, pp. 1009–1019.

[7] Garrison, J., and Webber, M., 2011, “An integrated energy storage scheme for a dispatchable solar and wind powered energy system and analysis of dynamic parameters,” J. Renew. Sustain. Energy, **3**(4), pp. 1–11.

[8] Agyenim, F., Hewitt, N., Eames, P., and Smyth, M., 2010, “A review of materials, heat transfer and phase change problem formulation for latent heat thermal energy storage systems (LHTESS),” J. Renew. Sustain. Energy Rev., **14**(2), pp. 615–628.

[9] Kurklo, A., 1998, “Energy storage applications in greenhouses by means of phase change materials (PCMs): a review,” J. Renew. Energy, **13**(1), pp. 89–103.

[10] Sharma, A., Tyagi, V. V., Chen, C. R., and Buddhi, D., 2009, “Review on thermal energy storage with phase change materials and applications,” J. Renew. Sustain. Energy Rev., **13**(2), pp. 318–345.

[11] Tang, Q., Gupta, S. K. S., and Varsamopoulos, G., 2008, “Energy-efficient thermal-aware task scheduling for homogeneous high-performance computing data centers: a cyber-physical approach,” IEEE Trans. Parallel Distrib. Syst., **19**(11), pp. 1458–1472.

[12] Bash, C., Patel, C., and Sharma, R., 2003, “Efficeint thermal management of data centers-immediate and long-term research needs,” J. HVAC&R Res., **9**(2), pp. 137–152.

[13] Beloglazov, A., Abawajy, J., and Buyya, R., 2012, “Energy-aware resource allocation heuristics for efficient management of data centers for Cloud computing,” J. Futur. Gener. Comput. Syst., **28**(5), pp. 755–768.

[14] Beloglazov, A., and Buyya, R., 2010, “Energy efficient resource management in virtualized Cloud data centers,” 2010 10th IEEE/ACM Int. Conf. Clust. Cloud Grid Comput., pp. 826–831.

[15] Chen, Y., Gmach, D., Hyser, C., Wang, Z., Bash, C., Hoover, C., and Singhal, S., 2010, “Integrated management of application performance, power and cooling in data centers,” IEEE Netw. Oper. Manag. Symp. (NOMS 2010), pp. 615–622.

[16] Crawford, C., 2005, “Balance of power: dynamic thermal mangement for Internet data centers,” IEEE Internet Comput., **9**(1), pp. 42–49.

[17] Anandan, S., and Ramalingam, V., 2008, “Thermal management of electronics: A review of literature,” Int. J. Therm. Sci., **12**(2), pp. 5–26.

[18] Gurrum, S. P. S. P., Suman, S. K., Shivesh, K., Joshi, Y. K., and Fedorov, A. G., 2004, “Thermal Issues in Next-Generation Integrated Circuits,” IEEE Trans. Device Mater. Reliab., **4**(4), pp. 709–714.

[19] Scott Downing, R., and Kojasoy, G., 2002, “Single and two-phase pressure drop characteristics in miniature helical channels,” J. Exp. Therm. Fluid Sci., **26**(5), pp. 535–546.

[20] Joshi, Y., and Wei, X., 2005, “Micro and meso scale compact heat exchangers in electronics thermal management-a review,” Enhanced, Compact and Ultra-Compact Heat Exchangers: Science, Engineering and Technology (CHE-2005), pp. 162–179.

[21] Wankhede, M., Khaire, V., and Goswami, A., 2007, “Evaluation of cooling solutions for outdoor electronics,” 13th International Conference on Thermal Investigation of ICs and Systems, ©EDA Publishing, Budapest, Hungary, pp. 1–6.

[22] Jahkonen, J., Puolakka, M., and Halonen, L., 2013, “Thermal management of outdoor LED lighting systems and streetlights variation of ambient cooling conditions,” J. Illum. Eng. Soc. North Am., **9**(3), pp. 155–176.

[23] Christensen, A., Ha, M., and Graham, S., 2007, “Thermal management methods for compact high power LED arrays,” 7th International Conference on Solid State Lighting, SPIE UK, San Diego, California, USA, pp. 1–19.

[24] BCCResearch, 2014, The Market for Thermal Management Technologies, Wellesley, MA, USA.

[25] Garimella, S. V, Yeh, L., and Persoons, T., 2012, “Thermal management challenges in telecommunication systems and data centers,” CTRC Res. Publ., pp. 1–26.

[26] Sawin, J. L., and E. Martinot, 2011, Renewables Bounced Back in 2010, Finds REN21 Global Report.

[27] Ulf Herrmann, and Kearney, D. W., 2002, “Survey of thermal energy storage for parabolic trough power plants,” ASME J. Sol. Energy Eng., **124**(2), pp. 145–152.

[28] Garrison, J. B., and E. Webber, M., 2012, “Optimization of an integrated energy storage for a dispatchable wind powered energy system,” ASME 2012 6th International Conference on Energy Sustainability, pp. 1–11.

[29] O’Keefe, M., and Bennion, K., 2007, “A comparison of hybrid electric vehicle power electronics cooling options,” Vehicle Power and Propulsion Conference, pp. 116–123.

[30] Joshi, Y., Kumar, P., Sammakia, B., and Patterson, M., 2012, Energy efficient thermal management of data centers, Springer US, Boston, MA.

[31] Siegel, R., Sparrow, E. M., and Hallman, T. M., 1958, “Steady laminar heat transfer in a circular tube with prescribed wall heat flux,” Appl. Sci. Res. Sect. A, **7**(5), pp. 386–392.

[32] Siegel, R., 1959, “Transient heat transfer for laminar slug flow in ducts,” Trans. ASME, **81**, pp. 140–142.

[33] Rizika, J. W., 1954, “Thermal lags in flowing systems containing heat capacitors,” Trans. ASME, **76**, pp. 411–420.

[34] Rizika, J. W., 1956, “Thermal lags in flowing incompressible fluid systems containing heat capacitors,” Trans. ASME, **78**, pp. 1407–1412.

[35] Sparrow, E. M., and Siegel, R., 1958, “Thermal entrance region of a circular tube under transient heating conditions,” Third U. S. National Congress for Applied Mechanics, pp. 817–826.

[36] Siegel, R., and Sparrow, E. M., 1959, “Transient heat transfer for laminar forced convection in the thermal entrance region of flat ducts,” Trans. ASME, **81**(C), pp. 29–36.

[37] Clarck, J. A., Arpaci, V. S., and Treadwell, K. M., 1958, “Dynamic response of heat exchangers having internal heat sources-Part I,” Trans. ASME, **80**, pp. 612–624.

[38] Clark, J. A., and Arpaci, V. S., 1958, “Dynamic response of heat exchangers having internal heat sources- Part II,” Trans. ASME, **80**, pp. 625–634.

[39] Siegel, R., 1960, “Heat transfer for laminar flow in ducts with arbitrary time variations in wall tempearture,” Trans. ASME, **82**(E), pp. 241–249.

[40] Perlmutter, M., and Siegel, R., 1961, “Unsteady laminar flow in a duct with unsteady heat addition,” Trans. ASME, **83**(C), pp. 432–440.

[41] Bonilla, C. F., Busch, J. S., Landau, H. G., and Lynn, L. L., 1961, “Formal heat transfer solutions,” Nucl. Sci. Eng., **9**, pp. 323–331.

[42] Perlmutter, M., and R. Siegel, 1961, “Two-dimensional unsteady incompressible laminar duct flow with a step change in wall tempearture,” Int. J. Heat Mass Transf., **3**, pp. 94–107.

[43] Siegel, R., and Perlmutter, M., 1963, “Laminar heat transfer in a channel with unsteady flow and wall heating varying with position and time,” Trans. ASME, **85**, pp. 358–365.

[44] HSU, C.-J., 1965, “Heat transfer in a round tube with sinusoidal wall heat flux distribution,” J. Am. Inst. Chem. Eng., **11**(4), pp. 690–695.

[45] Kays, W. M., and Crawford, M. E., 1993, Convective heat and mass transfer, McGraw-Hill, New York.

[46] Conley, N., Lawal, A., and Mujumdar, A. S., 1985, “An assessment of the accuracy of numerical solutions to the Graetz problem,” J. Int. Commun. Heat Mass Transf., **12**, pp. 209–218.

[47] Sucec, J., and Radley, D., 1990, “Unsteady forced convection heat transfer in a channel,” Int. J. Heat Mass Transf., **33**(4), pp. 683–690.

[48] Lin, H. T., and Shih, Y. P., 1981, “Unsteady thermal entrance heat transfer of power-law fluids in pipes and plate slits,” Int. J. Heat Mass Transf., **24**(9), pp. 1531–1539.

[49] Chen, S. C., Anand, N. K., and Tree, D. R., 1983, “Analysis of transient laminar convective heat transfer inside a circular duct,” ASME J. Heat Transf., **105**, pp. 922–924.

[50] Barletta, a., and Zanchini, E., 1995, “Laminar forced convection with sinusoidal wall heat flux distribution: axially periodic regime,” J. Heat Mass Transf., **31**(1), pp. 41–48.

[51] Astaraki, M. R., Tabari, N. G., and Rudhelepur, a., 2013, “Analytical Solution of Periodic Laminar Forced Convection via Confluent Hypergeometric Function,” J. Thermophys. Heat Transf., pp. 1–5.

[52] Kakac, S., and Yener, Y., 1973, “Exact solution of the transient forced convection energy equation for timewise variation of inlet temperature,” Int. J. Heat Mass Transf., **16**, pp. 2205–2214.

[53] Cotta, R. M., Mikhailov, M. D., and Ozisik, M. N., 1987, “Transient conjugated forced convection in ducts with peridically varying inlet temperature,” Int. J. Heat Mass Transf., **30**(10), pp. 2073–2082.

[54] Cotta, R. M., and Ozisik, M. N., 1986, “Laminar forced convection inside ducts with periodic variation of inlet temperature,” Int. J. Heat Mass Transf., **29**(10), pp. 1495–1501.

[55] Hadiouche, a., and Mansouri, K., 2010, “Analysis of the effects of inlet temperature frequency in fully developed laminar duct flows,” J. Eng. Phys. Thermophys., **83**(2), pp. 380–392.

[56] Kakac, S., Ding, Y., and Li, W., 1988, “Experimental study on unsteady laminar forced convection in ducts for timewise varying inlet tempearture,” Proceedings of the First World Conference on Experimental Heat Transfer, Fluid mechanics, and Thermodynamics, pp. 1177–1184.

[57] Kakac, S., Li, W., and Cotta, R. M., 1990, “Unsteady laminar forced convection in ducts with periodic variation of inlet temperature,” J. Mech. Des., **112**, pp. 913–920.

[58] Sparrow, E. M., and Farias, F. N. De, 1968, “Unsteady heat transfer in ducts with time-varying inlet tempearture and participating walls,” Int. J. Heat Mass Transf., **11**, pp. 837–853.

[59] Weigong, L., and Kakac, S., 1991, “Unsteady thermal entrance heat transfer in laminar flow with a periodic variation of inlet temperature,” Int. J. Heat Mass Transf., **34**(10), pp. 2581–2592.

[60] Siegel, R., 1963, “Forced convection in a channel with wall heat capacity and with wall heating variable with axial position and time,” Int. J. Heat Mass Transf., **6**, pp. 607–620.

[61] Olek, S., 1999, “Multiregion Conjugate Heat Transfer,” J. Hybrid Methods Eng., **1**, pp. 119–137.

[62] Aleksashenko, V. A., 1968, “Conjugate stationary problem of heat transfer with a moving fluid in a semi-infinite tube allowing for viscous dissipation,” J. Eng. Phys., **14**(1), pp. 100–107.

[63] Sucec, J., 1981, “An improved quasi-steady approach for transient conjugated forced convection problems,” Int. J. Heat Mass Transf., **24**(10), pp. 1711–1722.

[64] Sucec, J., 1987, “Exact solution for unsteady conjugated heat transfer in the thermal entrance region of a duct,” ASME J. Heat Transf., **109**(2), pp. 295–299.

[65] Olek, S., Elias, E., Wacholder, E., and Kaizerman, S., 1991, “Unsteady conjugated heat transfer in laminar pipe flow,” Int. J. Heat Mass Transf., **34**(6), pp. 1443–1450.

[66] Sucec, J., 2002, “Unsteady forced convection with sinusoidal duct wall generation: the conjugate heat transfer problem,” Int. J. Heat Mass Transf., **45**(8), pp. 1631–1642.

[67] Lin, T. F., and Kuo, J. C., 1988, “Transient conjugated heat transfer in fully developed laminar pipe flows,” Int. J. Heat Mass Transf., **31**(5), pp. 1093–1102.

[68] Schutte, D. J., Rahman, M. M., and Faghri, A., 1992, “Transient conjugate heat transfer in a thick-walled pipe with developing laminar flow,” J. Numer. Heat Transf. Part A, **21**, pp. 163–186.

[69] Yan, W. M., Tsay, Y. L., and Lin, T. F., 1989, “Transient conjugated heat transfer in laminar pipe flows,” Int. J. Heat Mass Transf., **32**(4), pp. 775–777.

[70] Luna, N., Méndez, F., and Mar, E., 2003, “Transient analysis of the conjugated heat transfer in circular ducts with a power-law fluid,” J. Nonnewton. Fluid Mech., **111**(2-3), pp. 69–85.

[71] Travelho, J. S., and Santos, W. F. N., 1998, “Unsteady conjugate heat transfer in a circular duct with convection from the ambient and periodically varying inlet temperature,” ASME J. Heat Transf., **120**(2), pp. 506–510.

[72] Hadiouche, A., and Mansouri, K., 2010, “Application of integral transform technique to the transient laminar flow heat transfer in the ducts,” Int. J. Therm. Sci., **49**(1), pp. 10–22.

[73] Kiwan, S. M., and Al-Nimr, M. a., 2002, “Analytical solution for conjugated heat transfer in pipes and ducts,” J. Heat Mass Transf., **38**(6), pp. 513–516.

[74] Al-Nimr, M. A., and Ei-Shaarawi, M. A. I., 1992, “Analytical solutions for transient conjugated heat transfer in a parallel plate and circular ducts,” J. Int. Commun. Heat Mass Transf., **19**, pp. 869–878.

[75] Khadrawi, A. F., and Al-nimr, M. A., 2003, “A perturbation technique to solve conjugated heat transfer problems in circular ducts,” J. Heat Mass Transf., **39**, pp. 125–130.

[76] Luikov, A. V., Aleksashenko, V. A., and Aleksashenko, A. A., 1971, “Analytical methods of solution of conjugated problems in convective heat transfer,” Int. J. Heat Mass Transf., **14**, pp. 1047–1056.

[77] Guedes, R. O. C., and Özişik, M. N., 1992, “Conjugated turbulent heat transfer with axial conduction in wall and convection boundary conditions in a parallel-plate channel,” Int. J. Heat Fluid Flow, **13**(4), pp. 322–328.

[78] Bilir, S., and Ates, A., 2003, “Transient conjugated heat transfer in thick walled pipes with convective boundary condition,” Int. J. Heat Mass Transf., **46**(2), pp. 2701–2709.

[79] Bilir, S., 1995, “Laminar flow heat transfer in pipes including two-dimensional wall and fluid axial conduction,” Int. J. Heat Mass Transf., **38**, pp. 1619–1625.

[80] Bilir, S., 2002, “Transient conjugated heat transfer in pipes involving two-dimensional wall and axial fluid conduction,” Int. J. Heat Mass Transf., **45**, pp. 1781–1788.

[81] Cotta, R. M., Mikhailov, M. D., and Özişik, M. N., 1987, “Transient conjugated forced convection in ducts with periodically varying inlet temperature,” Int. J. Heat Mass Transf., **30**, pp. 2073–2082.

[82] Sucec, J., and Weng, H. Z., 2002, “Unsteady conjugated duct heat transfer solution with wall heating,” J. Thermophys. Heat Transf., **16**, pp. 128–134.

[83] Wijeysundera, N. E., 1986, “Laminar forced convection in circular and flat ducts with wall axial conduction and external convection,” Int. J. Heat Mass Transf., **29**, pp. 797–807.

[84] Guedes, R. O. C., and Cotta, R. M., 1991, “Periodic laminar forced convection within ducts including wall heat conduction effects,” Int. J. Eng. Sci., **29**(5), pp. 535–547.

[85] Karvinen, R., 1988, “Transient conjugated heat transfer to laminar flow in a tube or channel,” Int. J. Heat Mass Transf., **31**(6), pp. 1326–1328.

[86] Soliman, H. M., and Rahman, M. M., 2005, “Analytical solution of conjugate heat transfer and optimum configurations of flat-plate heat exchangers with circular flow channels,” J. Heat Mass Transf., **42**(7), pp. 596–607.

[87] Soliman, H. M., 1984, “Analysis of low-Peclet heat transfer during slug flow in tubes with axial wall conduction,” ASME J. Heat Transf., **106**, pp. 782–788.

[88] Barozzi, G. S., and Pagliarini, G., 1985, “A method to solve conjugate heat transfer problems: the case of fully developed laminar flow in a pipe,” ASME J. Heat Transf., **107**, pp. 77–83.

[89] Faghri, M., and Sparrow, E. M., 1980, “Simultaneous wall and fluid axial conduction in laminar pipe-flow heat transfer,” ASME J. Heat Transf., **102**(58), pp. 58–63.

[90] Papoutsakis, E., and Ramkrishna, D., 1981, “Conjugated Graetz problem-I. General formalism and a class of solid-fluid problems,” J. Chem. Eng. Sci., **36**, pp. 1381–1391.

[91] Papoutsakis, E., and Ramkrishna, D., 1981, “Conjugated Graetz problem-II. General formalism and a class of fluid-fluid problems,” J. Chem. Eng. Sci., **36**, pp. 1393–1399.

[92] Koshkin, V. K., Kalinin, E. K., Dreitser, G. A., Galitseisky, B. M., and Izosimov, V. G., 1970, “Experimental study of unsteady convective heat transfer in tubes,” Int. J. Heat Mass Transf., **13**, pp. 1271–1281.

[93] Kawamura, H., 1977, “Experimental and analytical study of transient heat transfer for turbulent flow in a circular tube,” Int. J. Heat Mass Transf., **20**, pp. 443–450.

[94] Barozzi, G. S., and Pagliarini, G., 1984, “Experimental investigation of coupled conduction and laminar convection in a circular tube,” Int. J. Heat Mass Transf., **27**(12), pp. 2321–2329.

[95] Watson, E. J., 1983, “Diffusion in oscillatory pipe flow,” J. Fluid Mech., **133**, pp. 233–244.

[96] Joshi, C. H., Kamm, R. D., Drazen, J. M., and Slutsky, A. S., 1983, “An experimental study of gas exchange in laminar oscilltory flow,” J. Fluid Mech., **133**, pp. 245–254.

[97] Kurzweg, U. H., 1985, “Enhanced heat conduction in oscillating viscous flows within parallel-plate channels,” J. Fluid Mech., **156**, pp. 291–300.

[98] West, F. B., and Taylor, A. T., 1952, “The effect of pulsations on heat transfer; turbulet flow of water inside tubes,” J. Chem. Eng. Prog., **48**(1), pp. 39–43.

[99] Martinelli, R. C., Boelter, L. M. K., Weinberg, E. B., and Yakahi, S., 1943, “Heat transfer to a fluid flowing periodically at low frequencies in a vertical tube,” Trans. ASME, **65**, pp. 789–798.

[100] Havemann, H., and Rao, N., 1954, “Heat transfer in pulsating flow,” J. Nat., **174**, p. 41.

[101] Darling, G. B., 1959, “Heat transfer to liquids in intermittent flow,” J. Pet., **22**, pp. 177–178.

[102] Hwang, M. F., and Dybbs, A., 1983, “Heat transfer in a tube with oscillatory flow,” ASME paper 83-WA/Ht-90, pp. 1–12.

[103] Faghri, M., Javdani, K., and Faghri, A., 1979, “Heat transfer with laminar pulsating flow in a pipe,” J. Lett. Heat Mass Transf., **6**(4), pp. 259–270.

[104] R. Siegel, 1987, “Influence of oscillaation diffusion on heat transfer in a uniformly heated channel,” Trans. ASME, **109**, pp. 244–249.

[105] Mamayev, V., Nosov, V., and Syromyatnikov, N., 1976, “Investigation of heat transfer in pulsed flow of air in pipes,” J. Heat Transf. Res., **8**(3), pp. 111–116.

[106] Hemida, H. N., Sabry, M. N., Abdel-Rahim, A., and Mansour, H., 2002, “Theoretical analysis of heat transfer in laminar pulsating flow,” Int. J. Heat Mass Transf., **45**(8), pp. 1767–1780.

[107] Siegel, R., and Perlmutter, M., 1962, “Heat transfer for pulsating laminar duct flow,” ASME J. Heat Transf., **84**(2), pp. 111–122.

[108] Mackley, M. R., Tweddle, G. M., and Wyatt, I. D., 1990, “Experimental heat transfer measurement for pulsatile flow in baffled tubes,” J. Chem. Sci. Eng., **45**(5), pp. 1237–1242.

[109] Mackley, M. R., and Stonestreet, P., 1995, “Heat transfer and associated energy dissipation for oscialltory flow in baffled tubes,” J. Chem. Sci. Eng., **50**(14), p. 1995.

[110] Moschandreou, T., and Zamir, M., 1997, “Heat transfer in a tube with pulsating flow and constant heat flux,” Int. J. Heat Mass Transf., **40**(10), pp. 2461–2466.

[111] Kim, S. Y., Kang, B. H., and Hyun, J. M., 1993, “Heat transfer in the thermally developing region of a pulsating channel flow,” Int. J. Heat Mass Transf., **36**(17), pp. 4257–4266.

[112] Cho, H. W., and Hyun, J. M., 1990, “Numerical solution of pulsating flow and heat transfer characteristics in a pipe,” Int. J. Heat Fluid Flow, **11**(4), pp. 321–330.

[113] Zhao, T., and Cheng, P., 1995, “A numerical solution of laminar forced convection in a heated pipe subjected to a reciprocating flow,” Int. J. Heat Mass Transf., **38**(16), pp. 3011–3022.

[114] Wommersley, J. R., 1955, “Method for the calculation of velocity, rate of the flow and viscous drag in arteries when the pressure gradient is known,” J. Physiol., **127**, pp. 553–563.

[115] Guo, Z., and Sung, H., 1997, “Analysis of the Nusselt number in pulsating pipe flow,” Int. J. Heat Mass Transf., **40**(10), pp. 2486–2489.

[116] Habib, M. a., Attya, a. M., Eid, a. I., and Aly, a. Z., 2002, “Convective heat transfer characteristics of laminar pulsating pipe air flow,” J. Heat Mass Transf., **38**(3), pp. 221–232.

[117] Gupta, S. K., Patel, R. D., and Ackerberg, R. C., 1982, “Wall heat/mass transfer in pulsatile flow,” J. Chem. Eng. Sci., **37**(12), pp. 1727–1739.

[118] Krishnan, K. N., and Sastri, V. M. K., 1989, “Heat transfer in laminar pulsating flows of fluids with tempearture dependent viscosities,” J. Warme Stoffubertragung, **24**, pp. 37–42.

[119] Lemlich, R., 1961, “Vibration and pulsation boost heat transfer,” J. Chem. Eng., **68**, pp. 171–176.

[120] Lemlich, R., and Hwu, C., 1961, “The effect of acoustic vibration on forced convective heat transfer,” Am. Inst. Chem. Eng., **21**, pp. 197–199.

[121] Niida, T., Yoshida, T., Yamashita, R., and Nakayama, S., 1974, “The influence of pulsation on laminar heat transfer in pipes,” J. Heat Transf. Res., **3**(3), pp. 19–28.

[122] Shuai, X., Cheng, S., and Antonni, G., 1994, “Pulsation effects on convective heat transfer in the laminar flow of a viscous fluid,” Can. J. Chem. Eng., **72**, pp. 468–475.

[123] Yu, J.-C., Li, Z.-X., and Zhao, T. S., 2004, “An analytical study of pulsating laminar heat convection in a circular tube with constant heat flux,” Int. J. Heat Mass Transf., **47**(24), pp. 5297–5301.

[124] Brereton, G. J., and Jiang, Y., 2006, “Convective heat transfer in unsteady laminar parallel flows,” J. Phys. Fluids, **18**(10), pp. 1–15.

[125] Nield, D. a., and Kuznetsov, a. V., 2007, “Forced convection with laminar pulsating flow in a channel or tube,” Int. J. Therm. Sci., **46**(6), pp. 551–560.

[126] Yan, B. H., Yu, L., and Yang, Y. H., 2010, “Forced convection with laminar pulsating flow in a tube,” J. Heat Mass Transf., **47**(2), pp. 197–202.

[127] Paek, J. W., Kang, B. H., and Hynn, J. M., 1999, “Transient cool-down of a porous medium in pulsating flow,” Int. J. Heat Mass Transf., **42**, pp. 3523–3527.

[128] Fu, H. L., Leong, K. C., Huang, X. Y., and Liu, C. Y., 2001, “An experimental study of heat transfer of a porous channel subjected to oscillating flow,” ASME J. Heat Transf., **123**, pp. 162–170.

[129] Leong, K. C., and Jin, L. W., 2005, “Heat transfer of oscillating flow and steady flows in a channel filled with an aluminum foam,” Int. J. Heat Mass Transf., **48**, pp. 243–253.

[130] Myrum, T. A., Acharya, S., and Inamdar, S., 1997, “Laminar pulsed forced and mixed convection in a vertical isothermal tube,” J. Thermophys. Heat Transf., **11**, pp. 423–428.

[131] Bandyopadhyay, S., and Mazumder, B. S., 1999, “Unsteady convective diffusion in a pulsatile flow through a channel,” J. Acta Mech., **134**(1), pp. 1–16.

[132] Lee, D., Park, S., and Rot, S. T., 1995, “Heat transfer by oscillating flow in a circular pipe with a sinusoidal wall temperature distribution,” Int. J. Heat Mass Transf., **38**(14), pp. 2529–2537.

[133] Lin, T. F., Hawks, K. H., Leidenfrost, W., and Ausgleichsvorg, Z., 1983, “Transient thermal entrance heat transfer in laminar pipe flows with step change in pumping pressure,” J. Wärme - und Stoffübertragung, **17**, pp. 201–209.

[134] Lin, T. F., Hawks, K. H., and Leidenfrost, W., 1983, “Unsteady thermal entrance heat transfer in laminar pipe flows with step change in ambient temperature,” J. Wärme - und Stoffübertragung, **17**(3), pp. 125–132.

[135] Loudon, C., and Tordesillas, A., 1998, “The use of the dimensionless Womersley number to characterize the unsteady nature of internal flow,” J. Theor. Biol., **191**(1), pp. 63–78.

[136] Uchida, S., 1956, “The pulsating viscous flow superposed on the steady laminar motion of incompressible fluid in a circular pipe,” J. Zeitschrift für Angew. Math. und Phys., **7**(5), pp. 403–422.

[137] Zhao, T. S., and Cheng, P., 1996, “Oscillatory heat transfer in a pipe subjected a periodically reversing flow,” ASME J. Heat Transf., **118**, pp. 592–598.

[138] Zhao, T. S., and Cheng, P., 1996, “Experimental investigations of the onset of turbulence and frictional losses in an oscillatory pipe flow,” Int. J. Heat Fluid Flow, **17**, pp. 356–362.

[139] Zhao, T. S., and Cheng, P., 1996, “Oscillatory pressure drops through a woven-screen packed column subjected to a cyclic flow,” J. Cryog., **36**, pp. 333–341.

[140] Gibson, M. M., and Diakoumakos, E., 1993, “Oscillating turbulent boundary layer on a heated wall,” Ninth Symposium on Turbulent Shear Flows, pp. 16–18.

[141] Ramaprian, B. R., and Tu, S. W., 1981, “Periodic turbulent pipe flow at high frequencies of oscillation,” IUTAM Symposium, pp. 47–58.

[142] Ohmi, M., Usui, T., Tanaka, O., and Toyama, M., 1976, “Pressure and velocity distributions in pulsating turbulent pipe flow,” Bull. JSME, **19**(134), pp. 951–957.

[143] Parikh, P. G., Reynolds, W. C., Jaydraman, R., and Carr, L. W., 1981, “Dynamic behavior of an unsteady turbulent boundary layer,” IUTAM Symposium, pp. 35–47.

[144] Incropera, F. P., Dewitt, D. P., Bergman, T. L., and Lavine, A. S., 2007, Introduction to heat transfer, John Wiley & Sons, USA.

[145] Fakoor-Pakdaman, M., Andisheh-Tadbir, M., and Bahrami, M., 2013, “Unsteady laminar forced-convective tube flow under dynamic time-dependent heat flux,” J. Heat Transfer, **136**(4), pp. 041706–1–10.

[146] Fakoor-Pakdaman, M., Ahmadi, M., and Bahrami, M., 2014, “Unsteady internal forced-convective flow under dynamic time-dependent boundary temperature,” J. Thermophys. Heat Transf., **28**(3), pp. 463–473.

[147] Fakoor-Pakdaman, M., Ahmadi, M., Andisheh-Tadbir, M., and Bahrami, M., 2014, “Optimal unsteady convection over a duty cycle for arbitrary unsteady flow under dynamic thermal load,” Int. J. Heat Mass Transf., **78**, pp. 1187–1198.

[148] Fakoor-Pakdaman, M., Ahmadi, M., Andisheh-Tadbir, M., Bahrami, M., (2015) “Temperature-aware time-varying convection over a duty cycle for a given system thermal-topology”, Int. J. Heat Mass Transf., **87**, pp. 418–428.

[149] Moffat, R. J., 1988, “Describing the uncertainties in experimental results,” Exp. Therm. Fluid Sci., **1**(1), pp. 3–17.

Appendix A

Unsteady internal forced-convective flow under dynamic time-dependent boundary temperature

JOURNAL OF THERMOPHYSICS AND HEAT TRANSFER
Vol. 28, No. 3, July–September 2014

Unsteady Internal Forced-Convective Flow Under Dynamic Time-Dependent Boundary Temperature

M. Fakoor-Pakdaman,* Mehran Ahmadi,† and Majid Bahrami‡
Simon Fraser University Surrey, British Columbia V3T 0A3, Canada

DOI: 10.2514/1.T4261

A new all-time analytical model is developed to predict transient internal forced-convection heat transfer under arbitrary time-dependent wall temperature. Slug flow condition is assumed for the velocity profile inside the tube. The solution to the time-dependent energy equation for a step wall temperature is generalized for arbitrary time variations in surface temperature using Duhamel's theorem. A harmonic boundary temperature is considered, and new compact closed-form relationships are proposed to predic: 1) fluid temperature distribution; 2) fluid bulk temperature; 3) wall heat flux; and 4) the Nusselt number. An optimum value is found for the dimensionless angular frequency of the wall temperature to maximize the heat transfer rate of the studied unsteady forced-convective process. Such dimensionless parameter depends upon the imposed-temperature angular frequency, fluid thermophysical properties, and tube geometrical parameters. A general surface temperature is considered, and the temperature field inside the medium is obtained using a superposition technique. An independent numerical simulation is performed using ANSYS® Fluent. The comparison between the obtained numerical data and the present analytical model shows good agreement: a maximum relative difference less than 4.9%.

Nomenclature

A	=	cross-sectional area, Eq. (13), m^2
a	=	half-width of spacing between parallel plates, or circular tube radius, m
c_p	=	heat capacity, $J/kg \cdot K$
Fo	=	Fourier number; $\alpha t/a^2$
J	=	Bessel function, Eq. (6a)
k	=	thermal conductivity, $W/m \cdot K$
Nu	=	Nusselt number, ha/K
n	=	positive integer, Eq. (6b)
p	=	0 for parallel plate and 1 for circular tube, Eqs. (3) and (14)
Pr	=	Prandtl number (ν/α)
q_w^*	=	dimensionless wall heat flux
Re	=	Reynolds number, $2Ua/\nu$
r	=	radial coordinate measured from circular tube centerline, m
T	=	temperature, K
U	=	velocity magnitude, m/s
$\boldsymbol{u}$	=	velocity vector, Eq. (2)
x	=	axial distance from the entrance of the heated section, m
y	=	normal coordinate measured from centerline of parallel plate channel, m
α	=	thermal diffusivity, m^2/s
γ	=	function for circular tube [Eq. (6a)] or for parallel plate [Eq. (6b)]
$\Delta\varphi$	=	thermal lag (phase shift)
ζ	=	dummy X variable
η	=	dimensionless radial/normal coordinate for circular tube equal to r/a or for parallel plate equal to y/a
θ	=	dimensionless temperature; $(T - T_0)/\Delta T_R$
λ_n	=	eigenvalues, Eq. (6)
ν	=	kinematic viscosity, m^2/s
ξ	=	dummy Fo variable
ρ	=	fluid density, kg/m^3
ψ	=	arbitrary function of Fo
Ω	=	imposed-temperature angular frequency, rad/s
ω	=	dimensionless temperature angular frequency,

Subscripts

m	=	mean or bulk value
R	=	reference value
s	=	step wall (surface) temperature
w	=	wall
0	=	inlet

Received 23 August 2013; revision received 23 November 2013; accepted for publication 9 January 2014; published online 21 April 2014.

*Laboratory for Alternative Energy Convection, School of Mechatronic Systems Engineering, No. 4300, 250-13450 102nd Avenue; mfakoorp@sfu.ca.

†Laboratory for Alternative Energy Convection.

‡Laboratory for Alternative Energy Convection; mbahrami@sfu.ca.

I. Introduction

DEVELOPING an in-depth understanding of unsteady forced-convection heat transfer is crucial for optimal design and accurate control of heat transfer in emerging sustainable energy applications and next-generation heat exchangers. The origin of thermal transients in sustainable energy applications include the variable thermal load on 1) thermal solar panels in thermal energy storage (TES) systems [1–3]; 2) power electronics of solar/wind/tidal energy conversion systems [4,5]; and 3) power electronics and electric motor (PEEM) of hybrid electric vehicles (HEVs), electric vehicles (EVs), and fuel cell vehicles (FCVs) [6–9].

Solar thermal systems are widely used in solar powerplants and are being widely commercialized. Solar powerplants have seen about 740 MW of generating capacity added between 2007 and the end of 2010, bringing the global total to 1095 MW [5]. Such growth is expected to continue, as in the United States at least another 6.2 GW capacity is expected to be in operation by the end of 2013 [5]. However, the growth of such technology is hindered by the inherent variability of solar energy subjected to daily variation, seasonal variation, and weather conditions [1,4,10]. To overcome the issue of the intermittency, TES systems are used to collect thermal energy to smooth out the output and shift its delivery to a later time. Single-phase sensible heating systems or latent heat storage systems using phase change materials are used in TES; transient heat exchange occurs to charge or discharge the storage material [11]. From the technical point of view, one of the main challenges facing TES systems is designing suitable heat exchangers to work reliably under unsteady conditions [11]: a key issue that this research attempts to address.

To assure reliable performance of electronic components, the temperature of different components should be maintained below

recommended values. The temperature of power electronics can vary significantly with the fluid flow and the applied heat flux over time [12]. Thus, it is important to investigate the transient thermal behavior of these systems, especially during peak conditions [13]. Furthermore, new application of transient forced convection has emerged by the advent of HEVs, EVs, and FCVs. Since introduced, the sales of such vehicles have grown at an average rate of more than 80% per year. As of October 2012, more than 5.8 million HEVs have been sold worldwide since their inception in 1997 [14]. Their hybrid powertrain and power electronics electric motors undergo a dynamic thermal load as a direct result of driving/duty cycle and environmental conditions. Conventional cooling systems are designed based on a nominal steady state, typically a worst-case scenario [15], which may not properly represent the thermal behavior of various applications or duty cycles. This clearly indicates the enormity of the pending need for in-depth understanding of the instantaneous thermal characteristics of the aforementioned thermal systems [16]. Successful and intelligent thermal design of such dynamic systems leads to the design of new efficient heat exchangers to enhance the overall efficiency and reliability of TES and PEEM cooling solutions, which in the cases of the HEVs/EVs/FCVs means significant improvement in vehicle efficiency/reliability and fuel consumption [15–18].

In all the aforementioned applications, transient heat transfer occurs in heat exchangers subjected to arbitrary time-dependent duct wall temperature. This phenomenon can be represented by an unsteady forced-convective tube flow, which is the ultimate goal of this study.

Siegel pioneered the study of transient internal forced convection by investigating a duct flow following a step change in wall heat flux or temperature [19,20]. Later, Sparrow and Siegel [21,22] used an integral technique to analyze transient heat transfer in the thermal entrance region of a Poiseuille flow under step wall temperature/heat flux. Moreover, the tube wall temperature of channel flows for particular types of position/time-dependent heat fluxes was studied in the literature [23–27]. A number of studies were conducted on effects of periodic inlet temperature on the heat transfer characteristics of a convective tube flow under step wall temperature [28–33]. Most studies on unsteady internal forced convection are limited to homogeneous/constant boundary conditions at the tube wall, i.e., isothermal or isoflux; a summary of the available studies is presented in Table 1.

Our literature review indicates the following:

1) The effects of periodic/arbitrary time-dependent surface temperatures on thermal performance of an internal forced-convective flow have not been investigated.

2) There is no model to predict the fluid temperature distribution, wall heat flux, and the Nusselt number of a tube flow under arbitrary time-dependent surface temperatures.

3) No study has been conducted to determine the optimum conditions that maximize the convective heat transfer rate in tube flows under harmonic boundary conditions.

4) The parameters, including temperature amplitude, angular frequency, and fluid thermal lag (phase shift), affecting the unsteady internal forced convection have not been presented in the literature.

In previous work [34,35], a comprehensive study was carried out on the thermal characteristics of a convective tube flow under dynamically varying heat flux. In the present study, a new analytical all-time model is developed in Cartesian and cylindrical coordinates to accurately predict 1) fluid temperature distribution; 2) fluid bulk temperature; 3) wall heat flux; and 4) the Nusselt number, for a tube flow under arbitrary time-dependent temperature. New dimensionless variables are introduced that characterize transient forced convection inside a conduit under a time-dependent boundary temperature. An optimum condition is presented that maximizes the heat transfer rate of internal forced convection under a harmonic boundary temperature. The present paper provides new insight on unsteady heat transfer, and it serves as a platform and an engineering tool to investigate and develop intelligent transient thermal systems for a wide variety of engineering applications.

To develop the present analytical model, the fluid flow response for a step surface temperature is taken into account. Using Duhamel's theorem [36], the thermal characteristics of the fluid flow are determined analytically under a periodic time-dependent surface temperature. New dimensionless variables are introduced, and the system is optimized to maximize the heat transfer rate under harmonic boundary temperature. Any type of time-dependent surface temperature can be decomposed into sinusoidal functions using a sine Fourier series transformation [36]. Thus, the present model for the harmonic excitation is applied to find the temperature distribution of a tube flow under a general time-dependent boundary condition.

II. Governing Equations

Figure 1 shows a laminar forced-convective internal flow inside a parallel plate or a circular tube. The tube is thermally insulated in the first subregion, $x \leq 0$, and at $t = 0$; the second subregion of tube wall at $x \geq 0$ is instantaneously subjected to an arbitrary time-dependent temperature, $T_w = \varphi(t)$. The tube and fluid are assumed to be initially isothermal at initial temperature T_0. The entering fluid temperature is also maintained at T_0 throughout the heating period. The tube is assumed long enough so that it covers both thermally developing and fully developed regions; see Fig. 1. It is intended to determine the evolution of the fluid temperature, wall heat flux, and the Nusselt number as a function of time and space for the entire range of the Fourier number under arbitrary time-dependent wall temperature.

The assumptions made in deriving the mathematical model of the proposed unsteady heat convection process are 1) laminar incompressible flow; 2) negligible tube wall thermal inertia; 3) constant thermophysical properties; negligible viscous dissipation; negligible axial heat conduction, i.e., $Pe = Re \times Pr > 10$ [37]; 4) no thermal energy sources within the fluid; and 5) uniform velocity profile along the tube, i.e., slug flow.

Slug flow assumption can predict the thermal behavior of any type of fluid flow close to the tube entrance where the velocity profile is developing and has not reached the fully developed condition [24].

As such, the energy equation for a fluid flowing inside a duct in vectorial notation in this at any instance is shown by Eq. (1):

$$\frac{\partial T}{\partial t} + \boldsymbol{u} \cdot \nabla T = \alpha \cdot \nabla^2 T \tag{1}$$

where $\boldsymbol{u}$ and α are the velocity and the thermal diffusivity of the fluid, respectively. For the case of slug flow, the flow is considered one-dimensional and fluid velocity inside the duct is considered constant, as indicated by Eq. (2):

$$\boldsymbol{u} = U\hat{\boldsymbol{i}}, \qquad U = \text{const} \tag{2}$$

Accordingly, the dimensionless energy equation in Cartesian and cylindrical coordinates can be written in a unified form as follows:

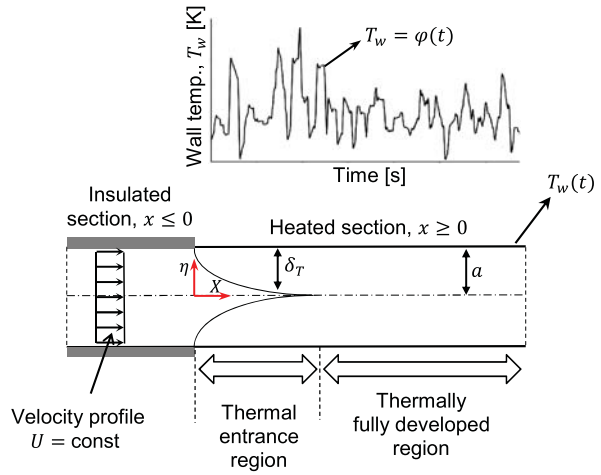

Fig. 1 Schematic of laminar forced-convective tube flow under arbitrary time-dependent wall temperature inside a parallel plate or a circular tube.

$$\frac{\partial\theta}{\partial Fo}+\frac{\partial\theta}{\partial X}=\frac{1}{\eta^p}\frac{\partial}{\partial\eta}\left(\eta^p\frac{\partial\theta}{\partial\eta}\right) \tag{3}$$

It should be noted that superscript p takes the values of 0 and 1, respectively, for Cartesian and cylindrical coordinates. In fact, the former is attributed to the fluid flow between parallel plates, and the latter indicates the fluid flow inside a circular tube. The dimensionless variables are

$$\theta=\frac{T-T_0}{\Delta T_R},\qquad Fo=\frac{\alpha t}{a^2},\qquad X=\frac{2\frac{x}{a}}{Re\cdot Pr},$$
$$Re_a=\frac{2Ua}{\upsilon},\qquad Pr=\frac{\upsilon}{\alpha},\qquad Nu_a=\frac{ha}{k}$$

where ΔT_R is the amplitude of the imposed temperature, Fo is the Fourier number, and X is the dimensionless axial position. In addition, for parallel plate and circular tube, $\eta=\frac{y}{a}$ and $\eta=\frac{r}{a}$, respectively.

Equation (4) is subjected to the following boundary and initial conditions:

$$\theta(0,\eta,Fo)=0\quad\text{at } X=0,\qquad Fo>0,\qquad 0\le\eta\le 1 \tag{4a}$$

$$\frac{\partial\theta(X,0,Fo)}{\partial\eta}=0\quad\text{at }\eta=0,\qquad X>0,\qquad Fo>0 \tag{4b}$$

$$\theta(X,1,Fo)=\psi(Fo)\quad\text{at }\eta=1,\qquad X>0,\qquad Fo>0 \tag{4c}$$

$$\theta(X,\eta,0)=0\quad\text{at } Fo=0,\qquad X>0,\qquad 0\le\eta\le 1 \tag{4d}$$

where $\psi(Fo)$ is an arbitrary time-dependent temperature imposed on the tube wall.

III. Model Development

In this section, a new all-time model is developed in Cartesian and cylindrical coordinates, considering 1) short-time response; and 2) long-time response. As such, the presented model predicts the temperature distribution inside a convective tube flow under an arbitrary time-dependent temperature imposed on the tube wall.

For a duct flow at uniform temperature T_0, instantaneously subjected to a step surface temperature, the temperature response is given in [19]:

$$\theta_s=\frac{T_w-T_0}{\Delta T_R}\left[1-2\sum_{n=1}^{\infty}\gamma_n(\eta)\exp(-\lambda_n^2 Fo)\right] \tag{5}$$

1) In cylindrical coordinate, i.e., flow inside a circular tube,

$$\gamma_n(\eta)=\frac{J_0(\lambda_n\eta)}{\lambda_n J_1(\lambda_n)},\quad\text{and}\quad J_0(\lambda_n)=0,\qquad \lambda_n>0 \tag{6a}$$

2) In Cartesian coordinate, i.e., flow between parallel plates,

$$\gamma_n(\eta)=\frac{(-1)^{n-1}}{\lambda_n}\cos(\lambda_n\eta),\ \text{and}\ \lambda_n=\frac{2n-1}{2}\pi,\quad n=1,2,3,\ldots \tag{6b}$$

where θ_s is the dimensionless temperature of the fluid under step wall temperature. J_0 and J_1 are the zero- and first-order Bessel functions of the first kind, and λ_n are the eigenvalues in cylindrical or Cartesian coordinates: Eqs. (6a) and (6b), respectively. The energy equation for a tube flow is linear; Eq. (4). This shows the applicability of a superposition technique to extend the response of the fluid flow for a step surface temperature to the other general cases, as discussed in [25]. As such, byusing Duhamel's theorem [36], the thermal response for a step surface temperature [Eq. (6)] can be generalized for an arbitrary time variation in surface temperature [Eq. (4c)]:

$$\theta=\frac{T-T_0}{\Delta T_R}=2\sum_{n=1}^{\infty}\lambda_n^2\gamma(\eta)\exp(-\lambda_n^2 Fo)\times\int_0^{Fo}\psi(\xi)\exp(\lambda_n^2\xi)\,\mathrm{d}\xi \tag{7}$$

This expression is valid only if the element is initially isothermal, so the solution here is limited to the cases where the channel is initially isothermal. However, the extension to the other cases, e.g., when the fluid initially has a steady state temperature distribution, can be obtained by superposition techniques, as discussed in [25].

As shown in Fig. 2, in an Eulerian coordinate system, the observer is fixed at a given location x along the tube and the fluid moves by. It will take some time, $t=x/U$, $Fo=X$, for the entrance fluid to reach the axial position X. Beyond this region, i.e., $X\ge Fo$, where the inlet fluid will not have enough time to penetrate, convection heat transfer plays no role; hence, the conduction becomes the dominant mechanism for transferring heat from the wall to the fluid. The behavior in this region is similar to a tube with infinite length in both directions. This means that the convective term in the energy equation [Eq. (1)] drops and a pure transient "heat-conduction" process takes place. On the other hand, for $X<Fo$, the observer situated at axial position X feels the passing fluid that has had enough time to reach from the insulated entrance section. This region is considered as the long-time response of the fluid flow [25]. Therefore, the solution consists of two regions that should be considered separately. The methodology considered in this study is shown schematically in Fig. 2.

A. Short-Time Response, $X\ge Fo$

For the sake of generality, we consider a case in which the surface temperature varies with both time and space, $\psi(X,Fo)$. We first consider the region where $X\ge Fo$. A fluid element that reaches X at time Fo was already in the heated section at the location $X-Fo$ at the beginning of the transient. As this element moves along, it is subjected to the surface temperature variations in both time and space. At a time ξ between 0 and Fo, the element is arrived to the location $X-Fo+\xi$. Thus, the tube wall temperature that the element is subjected to at that time is $\psi(X-Fo+\xi,\xi)$. This is substituted into Eq. (7) to find the short-time response for the fluid temperature distribution inside a circular tube and parallel plate, respectively [24]:

$$\theta(X,\eta,Fo)=\frac{T-T_0}{\Delta T_R}=2\sum_{n=1}^{\infty}\lambda_n^2\gamma_n(\eta)\exp(-\lambda_n^2 Fo)$$
$$\times\int_0^{Fo}\psi(X-Fo+\xi,\xi)\exp(\lambda_n^2\xi)\,\mathrm{d}\xi \tag{8}$$

It should be noted that, according to Eq. (8), when the imposed tube wall temperature is only a function of time $\psi=\psi(Fo)$, the short-time thermal response of the fluid flow is not dependent upon the

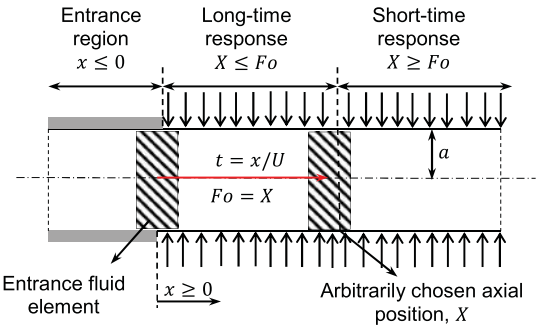

Fig. 2 Schematic of the two main regions adopted to find the transient thermal response of the tube flow.

axial position. However, it is a function of time and the characteristics of the imposed surface temperature.

B. Transition Time, $X = Fo$

For each axial position, the short-time and long-time responses are equal at $X = Fo$. This is the dimensionless transition time for a given axial position. Therefore, the time $Fo = X$ can be considered a demarcation between the short-time and long-time responses for each axial position. For instance, for an arbitrarily-chosen axial position $X = 1.2$, the dimensionless transition time is $Fo = 1.2$.

C. Long-Time Response, $X < Fo$

Now, we consider the region where $X < Fo$. The element that reaches X at time Fo has entered the channel at the time $Fo - X$ and begun to be heated. As time elapses from when the transition begins, this element will reach the location ζ at the time $Fo - X + \zeta$. Thus, the surface temperature that the element is subjected to at that location is $\psi(\zeta, Fo - X + \zeta)$. Substituting this into Eq. (7) results in Eq. (9), which represents the long-time response of the flow inside a circular tube or a parallel plate [24]:

$$\theta(X,\eta,Fo) = \frac{T - T_0}{\Delta T_R} = 2\sum_{n=1}^{\infty} \lambda_n^2 \gamma_n(\eta) \exp(-\lambda_n^2 Fo) \times \int_0^{Fo} \psi(\zeta, Fo - X + \zeta) \exp(\lambda_n^2 \xi)\, \mathrm{d}\xi \tag{9}$$

According to Eq. (9), the long-time thermal response of the fluid flow is a function of time, axial position, and characteristics of the imposed tube wall temperature.

IV. Harmonic Thermal Transients

In this section, thermal response of a tube flow is obtained under a harmonic wall temperature, prescribed as follows:

$$T_w = T_0 + \Delta T_R[1 + \sin(\Omega t)] \tag{10}$$

where ΔT_R K and Ω rad/s are the amplitude and the angular frequency of the imposed wall temperature. The analytical model is presented in form of 1) closed-form series solutions; and 2) approximate compact easy-to-use relationships.

Any type of prescribed time-dependent wall temperature can be decomposed into simple oscillatory functions using a Fourier series transformation [36]. Using a superposition technique, the results can be extended to the cases with an arbitrary time-dependent wall temperature as a general boundary condition; see Sec. IV.H.

A. Exact Series Solutions

The dimensionless form of Eq. (10) is as follows:

$$\theta_w(\omega, Fo) = \frac{T_w - T_0}{\Delta T_R} = 1 + \sin(\omega Fo) \tag{11}$$

where $\omega = \Omega a^2/\alpha$ is the dimensionless angular frequency. Substituting Eq. (11) into Eqs. (8) and (9), after some algebraic manipulations, the short-time and long-time temperature distributions inside the fluid are obtained. In this study, we considered the first 60 terms of the series solutions; using more terms does not affect the results up to four decimal digits.

1) Short-time fluid temperature distribution, $X \geq Fo$,

$$\theta(\omega,\eta,Fo) = 1 + \sin(\omega Fo) + 2\sum_{n=1}^{\infty} \gamma_n(\eta) \times \left\{ \frac{[\omega\lambda_n^2 - (\omega^2 + \lambda_n^4)]\exp(-\lambda_n^2 Fo) - \omega^2 \sin(\omega Fo) - \omega\lambda_n^2 \cos(\omega Fo)}{\omega^2 + \lambda_n^4} \right\} \tag{12a}$$

2) Long-time fluid temperature distribution, $X \leq Fo$,

$$\theta(\omega, X, \eta, Fo) = 1 + \sin(\omega Fo) + 2\sum_{n=1}^{\infty} \gamma_n(\eta) \times \left\{ \frac{\dfrac{-\lambda_n^2\omega\cos(\omega Fo) - \omega^2 \sin(\omega Fo)}{\omega^2 + \lambda_n^4} - \dfrac{\left\{\lambda_n^4 \sin[\omega(Fo - X)] - \lambda_n^2\omega \cos[\omega(Fo - X)] - (\omega^2 + \lambda_n^4)\right\} \times \exp(-\lambda_n^2 X)}{\omega^2 + \lambda_n^4}}{} \right\} \tag{12b}$$

It should be noted that the definition of $\gamma_n(\eta)$ and the eigenvalues λ_n have been previously given by Eqs. (6a) and (6b) for a circular tube and a parallel plate, respectively. In addition, the fluid bulk temperature can be obtained by Eq. (13) [38]:

$$\theta_m(\omega, X, Fo) = \frac{1}{A} \iint_A \theta \, \mathrm{d}A \tag{13}$$

where A is the cross-sectional area of the tube at any arbitrary axial position. After performing the integration in Eq. (13), the following relationships are obtained to evaluate the fluid bulk temperature.

Short-time dimensionless fluid bulk temperature, $X \geq Fo$,

$$\theta_m(\omega, Fo) = 1 + \sin(\omega Fo) + 2^p \sum_{n=1}^{\infty} \times \frac{[\omega\lambda_n^2 - (\omega^2 + \lambda_n^4)]\exp(-\lambda_n^2 Fo) - \omega^2 \sin(\omega Fo)\omega\lambda_n^2 \cos(\omega Fo)}{\lambda_n^2(\omega^2 + \lambda_n^4)} \tag{14a}$$

Long-time dimensionless fluid bulk temperature, $X \leq Fo$,

$$\theta_m(\omega, X, Fo) = 1 + \sin(\omega Fo) + 2^p \sum_{n=1}^{\infty} \left\{ \frac{\dfrac{-\lambda_n^2\omega \cos(\omega Fo) - \omega^2 \sin(\omega Fo)}{\lambda_n^2(\omega^2 + \lambda_n^4)} - \dfrac{\{\lambda_n^4 \sin[\omega(Fo - X)] + \lambda_n^2\omega \cos[\omega(Fo - X)] - (\omega^2 + \lambda_n^4)\} \times \exp(-\lambda_n^2 X)}{\lambda_n^2(\omega^2 + \lambda_n^4)}}{} \right\} \tag{14b}$$

The eigenvalues λ_n for the fluid flow inside a circular tube and a parallel plate can be obtained by Eqs. (6a) and (6b), respectively.

The dimensionless heat flux at the tube wall can be evaluated by

$$q_w^* = \left.\frac{\partial\theta}{\partial\eta}\right|_{\eta=1} \tag{15}$$

Differentiating the fluid temperature [Eqs. (12a) and (12b)] at the tube wall, we obtain the following:

Short-time dimensionless wall heat flux, $X \geq Fo$,

$$q_w^*(\omega, Fo) = -2\sum_{n=1}^{\infty} \times \frac{[\omega\lambda_n^2 - (\omega^2 + \lambda_n^4)]\exp(-\lambda_n^2 Fo) - \omega^2 \sin(\omega Fo) - \omega\lambda_n^2 \cos(\omega Fo)}{\omega^2 + \lambda_n^4} \tag{16a}$$

Long-time dimensionless wall heat flux, $X \leq Fo$,

$$q_w^*(\omega, X, Fo) = -2\sum_{n=1}^{\infty} \times \frac{\omega\lambda_n^2 \sin(\omega Fo) - \omega^2 \cos(\omega Fo) - \{\lambda_n^4 \cos[\omega(Fo - X)] + \lambda_n^2\omega \sin[\omega(Fo - X)]\} \times \exp(-\lambda_n^2 X)}{\omega^2 + \lambda_n^4} \tag{16b}$$

In this study, the local Nusselt number is defined based on the difference between the tube wall and fluid bulk temperatures; see Bejan [39]:

$$Nu_a(\omega, X, Fo) = \frac{ha}{k} = \frac{q_w^*}{\theta_w - \theta_m} = \frac{q_w^*}{[1 + \sin(\omega Fo)] - \theta_m} \tag{17}$$

It should be noted that the characteristics length α for the Nusselt number is the half-width of a parallel plate in the Cartesian coordinate and the tube radius in the cylindrical coordinate. Therefore, the short-time Nusselt number can be obtained by substituting Eqs. (14a) and (14b) into Eq. (17); similarly, substituting Eqs. (16a) and (16b) into Eq. (17) indicates the long-time Nusselt number.

To optimize the transient internal forced convection, we define a new parameter, the average dimensionless wall heat flux, as follows:

$$\bar{q}_w^*(\omega) = \frac{1}{Fo \times X} \int_{\xi=0}^{Fo} \int_{\zeta=0}^{X} q_w^* \, \mathrm{d}\zeta \, \mathrm{d}\xi \tag{18}$$

where Fo is the Fourier number (dimensionless time), and X is an arbitrarily chosen axial position. Equation (18) shows the average heat transfer rate over an arbitrary period of time Fo and length of the tube X. This will be discussed in more detail in Sec. VI.

B. Approximate Compact Relationships

Since using the series solutions presented in Section IV.E is tedious, the following new compact easy-to-use relationships are proposed to predict 1) dimensionless fluid bulk temperature; 2) dimensionless wall heat flux; and 3) Nusselt number, for fluid flow inside a parallel plate. As such, the MATLAB curve fitting tool was used to find the proposed compact relationships. Therefore, analytical results for different dimensionless numbers were curve fitted to find the most appropriate form of the compact relationships with minimum relative difference compared to the obtained series solutions. The proposed compact relationships are compared with the exact series solutions in graphical form in Sec. VI.

1. *Dimensionless Fluid Bulk Temperature*

For $\omega \geq \pi$, the following compact relationships predict the exact series solutions for the fluid bulk temperature [Eqs. (14a) and (14b)] by the maximum relative difference less than 9.1%.

1) Compact short-time fluid bulk temperature, $X \geq Fo$,

$$\theta_m(\omega, Fo) = \frac{1.078 \times Fo}{Fo + 0.1951} + \left(\frac{1.616}{\omega + 1.023}\right) \times \exp\left(-\frac{0.3748 \times \omega + 28.78}{\omega + 9.796} \times Fo\right) + \frac{0.0934 \times \omega + 2.86}{\omega + 1.802} \times \sin\left(\omega Fo + \frac{-0.78\omega^2 + 17.8 \times \omega - 160.9}{\omega^2 - 22.3 \times \omega + 200.7}\right) \tag{19a}$$

2) Compact long-time fluid bulk temperature, $X \leq Fo$,

$$\theta_m(\omega, X, Fo) = \frac{1.078 \times X}{X + 0.1951} + \frac{0.1167 \times \omega + 3.575}{\omega + 1.802} \times \sin\left(\omega Fo + \frac{-0.78\omega^2 + 17.8 \times \omega - 160.9}{\omega^2 - 22.3 \times \omega + 200.7}\right) \tag{19b}$$

2. *Dimensionless Wall Heat Flux*

For $Fo \geq 0.05$ and $\omega \geq \pi$, the dimensionless wall heat flux can be obtained by the following compact relationships. The maximum relative difference between the developed compact relationships [Eqs. (20a) and (20b)] and the exact series solutions [Eqs. (16a), (16b)] is less than 5.1%.

1) Compact short-time wall heat flux, $X \geq Fo$,

$$q_w^*(\omega, Fo) = \frac{-0.206 \times Fo + 0.449}{Fo + 0.132} + \frac{14.73 \times \omega + 103.2}{\omega + 70.74} \times \sin\left(\omega Fo + \frac{-0.77\omega^2 - 23.45 \times \omega + 215.3}{\omega^2 - 30.51 \times \omega + 280.5}\right) \tag{20a}$$

2) Compact long-time wall heat flux, $X \leq Fo$,

$$q_w^*(\omega, X, Fo) = 3.037 \times \exp(-4.626X) + \frac{-0.206 \times X + 0.449}{X + 0.132} + \frac{14.73 \times \omega + 103.2}{\omega + 70.74} \times \sin\left(\omega Fo + \frac{-0.77\omega^2 - 23.45 \times \omega + 215.3}{\omega^2 - 30.51 \times \omega + 280.5}\right) \tag{20b}$$

3. *Nusselt Number*

Using the definition of the Nusselt number [Eq. (17)], a compact closed-form relationship can also be obtained for Nusselt number. The short-time Nusselt number can be developed by substituting

Eqs. (17a) and (20a) into Eq. (17). Similarly, the long-time Nusselt number can be obtained by substituting Eqs. (19b) and (20b) into Eq. (17).

We believe that the form of the compact relationships presented in this section reveals the nature of the transient problem herein under consideration. This will be discussed in detail in Sec. VI.

V. Numerical Study

To verify the presented analytical solution, an independent numerical simulation of the planar flow inside a parallel plate is performed using the commercial software ANSYS® Fluent. User-defined codes are written to apply the harmonic and arbitrary time-dependent temperatures on the tube wall: Eqs. (10) and (22), respectively. Model geometry and boundary conditions are similar to what is shown in Fig. 1. Furthermore, the assumptions stated in Sec. II are used in the numerical analysis; however, the fluid axial conduction is not neglected in the numerical analysis. Grid independency of the results is tested for three different grid sizes: 20×100 and 40×200, as well as 80×400. Finally, 40×200 is selected as the final grid size, since the maximum difference in the predicted values for the fluid temperature by the two latter grid sizes is less than 1%. The geometrical and thermal properties used in the baseline case for the numerical simulation are listed in Table 2. The maximum relative difference between the analytical results and the numerical data is less than 4.9%, which is discussed in detail in Sec. VI.

VI. Results and Discussion

A. Harmonic Prescribed Temperature

Although the methodology developed in Sec. III is presented for Cartesian and cylindrical coordinates, only the results for the former are discussed in this section in a graphical form. The trends for the cylindrical coordinate are similar.

Variations of the dimensionless centerline temperature against the Fo number [Eqs. (12a) and (12b)] for a few axial positions along the tube are shown in Fig. 3 and compared with the numerical data obtained in Sec. V. Periodic temperature is imposed on the tube wall; Eq. (11). The solid lines in Fig. 3 represent our analytical results, and the markers show the obtained numerical data. There is an excellent agreement between the analytical results [Eqs. (12a) and (12b)] and the obtained numerical data, with a maximum relative difference less than 4.9%.

The following is shown in Fig. 3:

1) The present model predicts an abrupt transition between the short-time and long-time responses. The numerical results, however, indicate a smooth transition. This causes the numerical data to deviate slightly from the analytical results as the long-time response begins. Such transitions are demarcated by dashed lines on the figure.

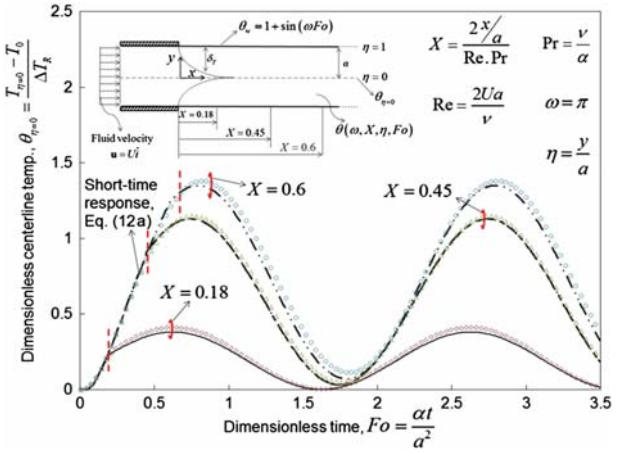

Fig. 3 Variations of centerline temperature versus the dimensionless time (Fourier number) for different axial positions [Eqs. (12a) and (12b)] and comparison with the obtained numerical data (markers).

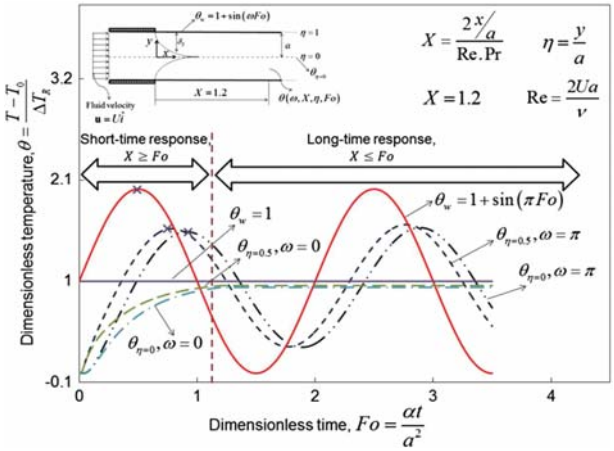

Fig. 4 Dimensionless fluid temperature against Fo number for cyclic and step heat fluxes.

2) The abrupt transition from short-time to long-time responses is attributed to the analytical method that Siegel [19] used to solve the transient energy equation for a step wall temperature. This is discussed in detail in [19].

3) There is an initial transient period of "pure conduction" during which all the curves follow along the same line, $X \geq Fo$; Eq. (12a).

4) When $Fo = X$, each curve moves away from the common line, i.e., pure conduction response, and adjusts toward a steady oscillatory behavior at a long-time response; Eq. (12b). The wall temperatures increase for larger X values, as expected; this is due to the increase of the fluid energy (bulk temperature) along the axial direction.

5) Increasing length-to-diameter ratio increases the axial position number, which in turn increases the temperature inside the fluid.

6) The higher the velocity inside the tube, the higher the Re number, which in turn decreases the axial position number, $X = (2x/a)/(Re_a \cdot Pr)$ and leads to lower temperature inside the fluid.

Figure 4 shows the variations of the dimensionless fluid temperature at different radial positions across the tube versus the Fo number; Eqs. (12a) and (12b). Harmonic and step temperatures are imposed at the tube wall, i.e., $\theta_w = 1 + \sin(\pi Fo)$ and $\theta_w = 1$, respectively. As such, the short-time and long-time fluid temperatures at different radial positions at an arbitrarily chosen axial position, $X = 1.2$, are obtained using Eqs. (12a) and (12b).

From Fig. 4, the following conclusions can be drawn:

1) As expected at any given axial position, the fluid temperature oscillates with time in the case of a prescribed harmonic wall temperature. For a step surface temperature, $\omega = 0$, the solution does not fluctuate over time.

2) At any given axial position, there is an initial transient period, which can be considered as pure conduction, i.e., the short-time response for $X \geq Fo$. However, as pointed out earlier, each axial position shows steady oscillatory behavior for $X \leq Fo$ at the long-time response. Therefore, for the arbitrarily chosen axial position of $X = 1.2$, the long-time response begins at $Fo = 1.2$ and shows the same behavior all-time thereafter.

3) For an imposed cyclic wall temperature, the fluid temperature oscillates around the associated response for the step surface temperature with the same angular frequency at which the system is excited.

4) The shift between the peaks of the temperature profile is marked at different radial positions. This shows a "thermal lag" (phase shift) of the fluid flow, which increases toward the centerline of the tube. This thermal lag is attributed to the fluid thermal inertia.

Figure 5 shows the variations of the dimensionless centerline temperature at a given axial position of $X = 1.2$ versus the Fourier number and the angular frequency; Eqs. (12a) and (12b).

The following can be concluded from Fig. 5:

1) At the two limiting cases where 1) $\omega \to 0$ and 2) $\omega \to \infty$, the fluid flow response yields that of a step surface temperature (isothermal boundary condition).

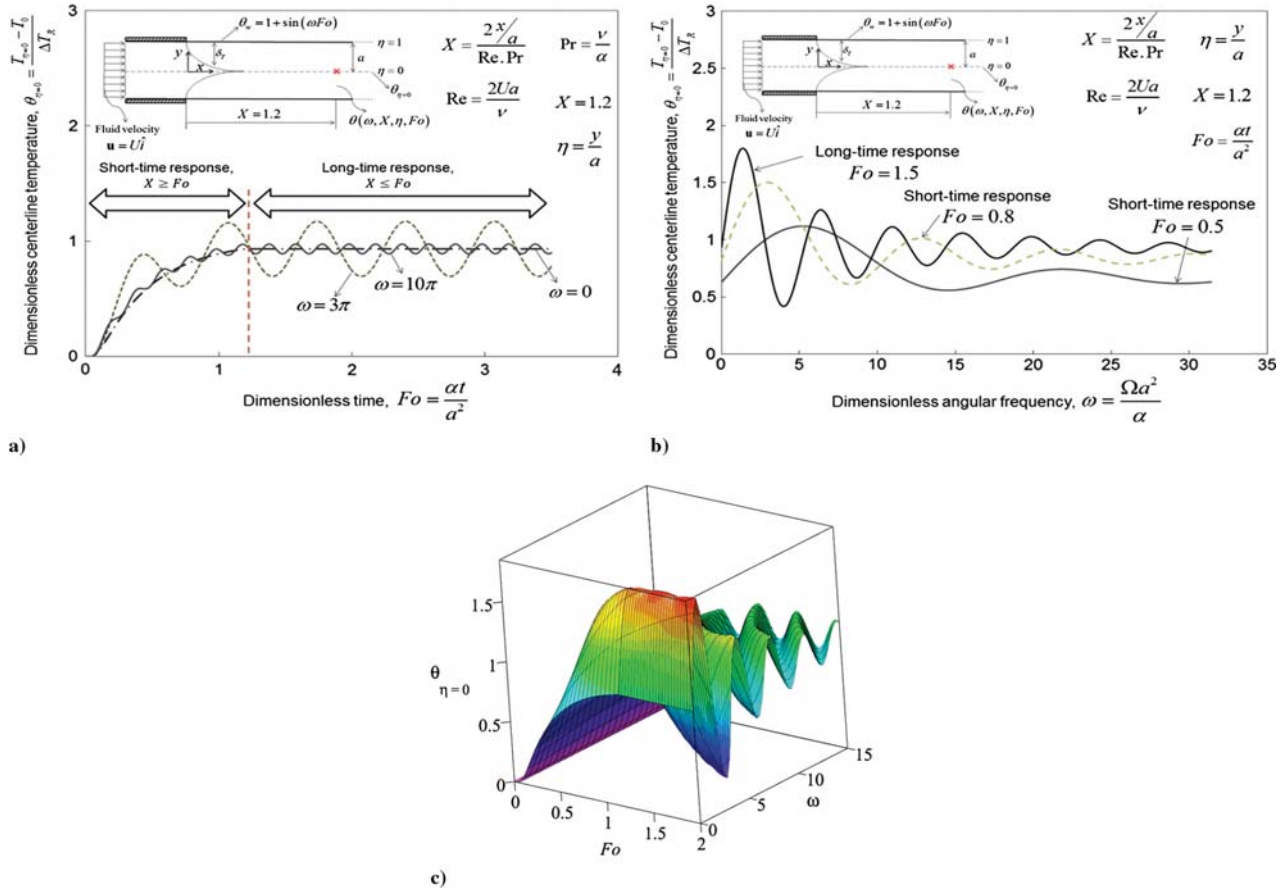

Fig. 5 Centerline temperature against: a) *Fo* number, b) angular frequency, and c) *Fo* and angular frequency.

2) When a sinusoidal cyclic wall temperature with high angular frequency is imposed on the flow, the fluid does not follow the details of the imposed temperature behavior. Therefore, for high angular frequencies, the flow acts as if the imposed temperature is constant at "the average value" associated with zero frequency [Eq. (11)] for the sinusoidal heat flux in this case, in mathematical terms $\theta_{\omega\to\infty} \approx \theta_{\omega\to 0}$.

3) A conventional way to decrease the temperature of the working fluid inside the heat exchangers is to cool down the surface temperature. However, it is shown that changing the surface temperature frequency can also dramatically alter the fluid temperature.

4) The highest temperature for the centerline temperature occurs for small values of angular frequency. Considering Eq. (12b), the highest long-time centerline temperature occurs at

$$\frac{\mathrm{d}\theta_{\eta=0}}{\mathrm{d}\omega} = 0 \Rightarrow \omega \approx \pi \text{ (rad)} \tag{21}$$

At a given axial position, the maximum long-time centerline temperature is remarkably higher than that of the short-time response.

Figure 6 shows the variations of the dimensionless wall heat flux at a given arbitrary axial position of $X = 1.2$ versus the Fourier number and the dimensionless angular frequency; Eqs. (16a) and (16b). In addition, a comparison is made between the exact series solutions [Eqs. (16a) and (16b)] and the developed compact relationships [Eqs. (20a) and (20b)]. As seen from Fig. 6, there is an excellent agreement between the exact solution and the compact relationships; the maximum relative difference less than 4.6%.

From Fig. 6, one can conclude the following:

1) The dimensionless wall heat flux oscillates with the angular frequency of the imposed wall temperature. This is indicated by the developed compact relationships; Eqs. (20a) and (20b).

2) The dimensionless wall heat flux oscillates around the step wall heat flux response. In other words, as $\omega \to 0$, the dimensionless wall heat flux yields the response of the step wall temperature condition.

3) Regardless of the angular frequency, at a very initial transient period, the dimensionless wall heat flux is much higher than that of the long-time response.

4) The amplitude of the dimensionless wall heat flux increases with the angular frequency of the imposed wall temperature. It should be noted that increasing the angular frequency does not affect the amplitude of the imposed wall temperature; see Eq. (9). However, as mentioned before, it decreases the amplitude of the fluid temperature toward the centerline. Therefore, as the angular frequency of the

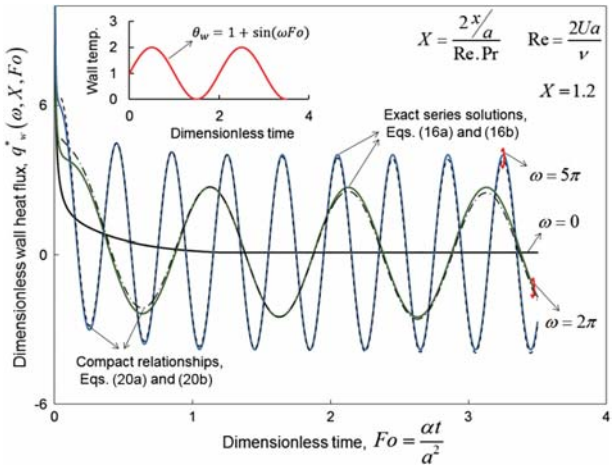

Fig. 6 Exact and approximate wall heat fluxes versus *Fo* number for different angular frequencies.

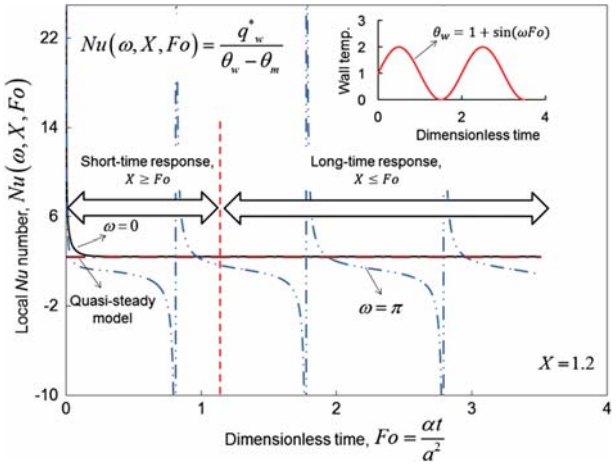

Fig. 7 Local Nu number against Fo number for different angular frequencies.

imposed temperature rises, the amplitude of the temperature gradient and heat flux in consequent increases.

5) The phase lag of the dimensionless wall heat flux is only a function of dimensionless angular frequency of the imposed wall temperature, as indicated by Eqs. (20a) and (20b), i.e.,

$$\Delta\varphi = \frac{-0.77\omega^2 - 23.45 \times \omega + 215.3}{\omega^2 - 30.51 \times \omega + 280.5}$$

As mentioned before, the dimensionless angular frequency is a function of temperature frequency, fluid thermophysical properties, and tube geometrical parameters.

Figure 7 shows the variations of the Nusselt number at a given arbitrary axial position of $X = 1.2$ versus the Fourier number for different angular frequencies; Eq. (17). In addition, the transient Nusselt number developed in this study [Eq. (17)] is compared with the conventional "quasi-steady" model, which is a simplified model assuming that the convective heat transfer coefficient is constant, equal to the fully developed condition in the channel [25].

The following can be concluded from Fig. 7:

1) The values of the transient Nusselt number deviate considerably from the ones predicted by the conventional quasi-steady model. Therefore, the conventional models fail to predict the transient Nusselt number accurately.

2) When $Fo \geq 0.2$, as the fluid flow becomes thermally fully developed, the presented model approaches the quasi-steady model for $\omega \to 0$, i.e., the step wall temperature condition.

3) The Nusselt number is positive when the heat flow is from the wall to the fluid, i.e., $\theta_w > \theta_m$. However, when the fluid bulk temperature is higher than the wall temperature, $\theta_m > \theta_w$, the Nusselt number is negative.

4) At some particular Fo numbers, the Nusselt number experiences discontinuities, soaring to plus infinity and then returning from minus infinity. These excursions occur when the wall and fluid bulk temperature are equal, $\theta_w = \theta_m$, but the heat flux is not zero; see Eq. (17). In fact, the Nusselt number loses its significance at such particular points. The same behavior for the Nusselt number was reported for the periodic inlet fluid temperature [40] and variable x-dependent wall temperature [41].

5) Comparing the results of this study with [40,41], when there is a periodic boundary condition for a convective duct flow, the temperature field inside the fluid fluctuates with the agitation angular frequency of the boundary.

6) Accordingly, we believe that the Nusselt number is not a proper candidate to represent the thermal characteristics of transient systems under harmonic prescribed temperature. Therefore, dimensionless wall heat flux can be considered as the best representative of the thermal behavior of a convective tube flow.

Figure 8 depicts the variations of the average dimensionless wall heat flux [Eq. (18)] against the dimensionless angular frequency and compared with the quasi-steady model. It should be noted that arbitrary intervals of axial positions are considered to calculate the integral in Eq. (18), i.e., $0 \leq X \leq 0.2$ and $0 \leq X \leq 1$. In addition, an arbitrary time interval of 0.8 is considered for the Fo number, $0 \leq Fo \leq 0.8$, over which the double integral in Eq. (18) is performed. Since the parameters are dimensionless, the same trend is observed for other arbitrarily chosen intervals of axial position X and Fo number.

One can conclude the following from Fig. 8:

1) The maximum average heat flux occurs at the dimensionless angular frequency of

$$\omega_{\text{opt.}} = \left(\frac{\Omega \times a^2}{\alpha}\right)_{\text{opt.}} = 2.4 \text{ rad}$$

2) Therefore, the optimum excitation angular frequency, Ω rad/s, is a function of the fluid properties and the geometrical parameters of the tube, $\Omega_{\text{opt.}} = 2.4 \times (\alpha/a^2)$ rad/s.

3) The values of the averaged wall heat flux vary significantly with the angular frequency of the imposed wall temperature, whereas the conventional models, e.g., quasi-steady model, fail to predict such variations of the dimensionless heat flux with time.

4) As an example for the optimum angular frequency, when $0 \leq X \leq 1$ and $0 \leq Fo \leq 0.8$, the value of the averaged dimensionless wall heat flux is almost 52% higher than the corresponding value for isothermal boundary condition (step wall temperature).

5) Regardless of the chosen intervals of Fo and X, the value of the optimum dimensionless angular frequency remains the same, $\omega_{\text{opt.}} = 2.4$ rad.

B. Arbitrary Time-Dependent Prescribed Temperature

In this section, a superposition technique is applied to the results for harmonic boundary condition, see Sec. VI.A. It is intended to obtain the temperature distribution inside a tube for an arbitrary time-dependent wall temperature and compare it with the numerical simulation data. The results presented here are dimensional; we believe this will provide one with a sense for the actual values of the discussed dimensionless variables of transient internal forced convection.

Consider a parallel plate with half-width $\alpha = 0.31$ cm, in which water is flowing at uniform velocity, $U = 2.4$ cm/s. The thermophysical properties of the working fluid and the geometrical parameters are previously presented in Table 2. The prescribed temperature is considered arbitrarily in the following general form:

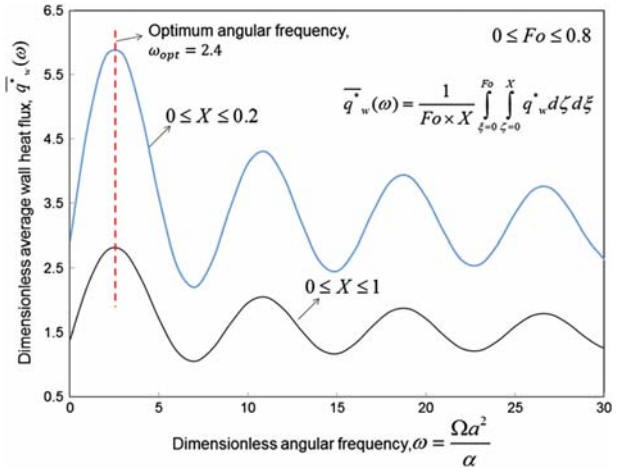

Fig. 8 Variations of the average dimensionless wall heat flux [Eq. (18)] with the angular frequency over arbitrarily chosen intervals of axial positions and Fo number.

Table 1 Summary of the literature regarding unsteady internal forced convection

Author	Velocity profile	Notes
Siegel [19]	Slug flow	Reported temperature distribution inside the fluid in Cartesian and cylindrical coordinates. Limited to step wall temperature/heat flux.
Siegel [20]	Poiseuille flow	Reported temperature distribution inside the fluid in cylindrical coordinate. Limited to step wall temperature condition.
Sparrow and Siegel [21,22]	Poiseuille flow	Reported tube wall temperature/heat flux. Limited to homogenous boundary conditions, i.e., step wall temperature/heat flux. Limited to thermal entrance region.
Perlmutter and Siegel [26]	Poiseuille flow	Evaluated tube wall temperature considering the wall thermal inertia. Limited to step wall temperature condition.
Sucec [27]	Slug flow	Evaluated fluid temperature under sinusoidal wall heat flux. Limited to quasi-steady assumption.

Table 2 Fluid properties and dimensions of the tube for the baseline case in numerical simulation[a]

Parameter	Value
Thermal conductivity k, W/m/k	0.64
Thermal diffusivity α, m^2/s	1.6E-7
Kinematic viscosity ν, m^2/s	5.66E-7
Tube half-width a, m	0.003
Tube length L, cm	250

[a]$Re_a = 100$.

Table 3 Parameters in Eq. (22)

Parameter	Value
T_0, K	300
Ω_1, rad/s	0.06
Ω_2, rad/s	0.12
Ω_3, rad/s	0.24
Ω_4, rad/s	0.1
$\Delta T_{R,1}$, K	1
$\Delta T_{R,2}$, K	4
$\Delta T_{R,3}$, K	10
$\Delta T_{R,4}$, K	8
T_1, K	5
T_2, K	10
T_3, K	15
T_4, K	20

$$T_w = T_0 + \sum_{i=1}^{4}[T_i + \Delta T_{R,i}\sin(\Omega_i t)] \tag{22}$$

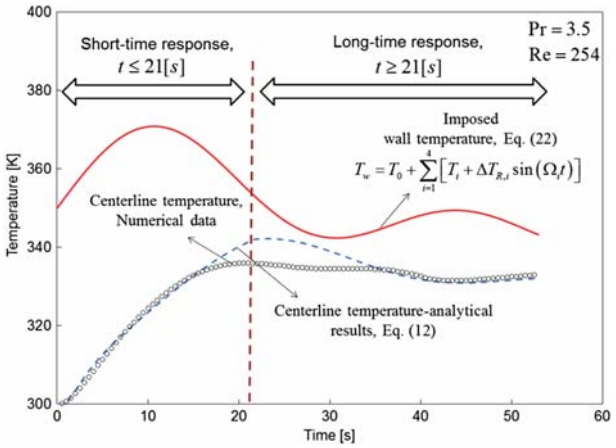

Fig. 9 Centerline temperature [Eq. (11)] versus time, and comparison with the obtained numerical data for a general boundary condition [Eq. (20)].

The parameters in Eq. (22) are introduced in Table 3. It should be noted that T_0 is the initial temperature of the fluid, and T_i and $\Delta T_{R,i}$ are the constant values and the amplitudes of the imposed wall temperature, respectively. The values for the parameters in Eq. (22) are arbitrarily chosen, and a similar approach can be taken for other forms of time-dependent boundary conditions.

Figure 9 displays the transient centerline temperature, at an arbitrarily chosen axial position, $x = 50$ cm, under a time-dependent wall temperature [Eq. (22)] in comparison with the obtained numerical data. The imposed wall temperature is also depicted in Fig. 9 by a solid line. The markers in Fig. 9 are the numerical data, and the solid lines are the analytical results. There is a good agreement between the analytical results and the numerical simulation data; the maximum relative difference is less than 5%.

The following can be concluded from Fig. 9:

1) The short-time response, $t \le 21$ s, at which pure conduction heat transfer occurs is much lower than the long time response, $t \ge 21$ s.

2) The presented model can be applied to find the fluid temperature inside a tube under any type of arbitrary time-dependent wall temperature.

3) The maximum discrepancy between the analytical results and the obtained numerical data occurs around the transition time, as stated for the trends in Fig. 3. This occurs since the analytical model predicts an abrupt arrival from short-time to long-time response, whereas the numerical simulation predicts a smooth transition; see [19] for more detail.

VII. Conclusions

A new full-time-range analytical model is developed to predict the transient thermal performance of forced-convective tube flow under an arbitrary time-dependent wall temperature. The methodology is presented in Cartesian and cylindrical coordinates. The slug flow condition is considered for the velocity distribution inside a circular tube. As such, new all-time models are developed to evaluate 1) temperature distribution inside the fluid; 2) fluid bulk temperature; 3) dimensionless wall heat flux; and 4) Nusselt number. Furthermore, compact closed-form relationships are proposed to predict such thermal characteristics of the tube flow with the maximum relative difference of less than 10%. A new heat transfer enhancement technique is presented for convective tube flow under harmonic boundary temperature. Optimizing the angular frequency of the imposed wall temperature can remarkably increase the overall heat transfer rate of a convective tube flow. The analytical results are verified successfully with the obtained numerical data. The maximum relative difference between the analytical results and the numerical data is less than 4.9%. The highlights of the present study can be listed as follows:

1) There is a thermal lag in the thermal response of the fluid temperature that increases toward the centerline of the tube due to the thermal inertia of the fluid.

2) The fluid temperature, dimensionless wall heat flux, and Nusselt number oscillate with the angular frequency of the imposed wall temperature.

3) At the two limiting cases, the thermal response of the fluid yields that of the step wall temperature: 1) $\omega \to 0$ and 2) $\omega \to \infty$.

4) There is an optimum value for the dimensionless angular frequency of the imposed harmonic wall temperature that maximizes the average dimensionless wall heat flux:

$$\omega_{\text{opt.}} = \left(\frac{\Omega \times a^2}{\alpha}\right)_{\text{opt.}} = 2.43 \text{ rad}$$

Acknowledgments

This work was supported by Automotive Partnership Canada, grant no. APCPJ 401826-10. The authors would like to thank the support of the industry partner Future Vehicle Technologies, Inc. (British Columbia, Canada).

References

[1] Agyenim, F., Hewitt, N., Eames, P., and Smyth, M., "A Review of Materials, Heat Transfer and Phase Change Problem Formulation for Latent Heat Thermal Energy Storage Systems (Lhtess)," *Renewable and Sustainable Energy Reviews*, Vol. 14, No. 2, Feb. 2010, pp. 615–628. doi:10.1016/j.rser.2009.10.015

[2] Cabeza, L. F., Mehling, H., Hiebler, S., and Ziegler, F., "Heat Transfer Enhancement in Water when Used as PCM in Thermal Energy Storage," *Applied Thermal Engineering*, Vol. 22, No. 10, July 2002, pp. 1141–1151. doi:10.1016/S1359-4311(02)00035-2

[3] Kurklo, A., "Energy Storage Applications in Greenhouses by Means of Phase Change Materials (PCMs): A Review," *Renewable Energy*, Vol. 13, No. 1, 1998, pp. 89–103. doi:10.1016/S0960-1481(97)83337-X

[4] Garrison, J. B., and Webber, E. M., "Optimization of an Integrated Energy Storage for a Dispatchable Wind Powered Energy System," *ASME 2012 6th International Conference on Energy Sustainability*, American Soc. of Mechanical Engineers, Fairfield, NJ, 2012, pp. 1–11.

[5] Sawin, J. L., and Martinot, E., "Renewables Bounced Back in 2010, Finds REN21 Global Report," *Renewable Energy World*, 2011, Data available online at http://www.renewableenergyworld.com/rea/news/article/2011/09/renewables-bounced-back-in-2010-finds-ren21-global-report [retrieved 2014].

[6] Bennion, K., and Thornton, M., "Integrated Vehicle Thermal Management for Advanced Vehicle Propulsion Technologies," National Renewable Energy Lab. NREL/CP-540-47416, Golden, CO, 2010.

[7] Boglietti, A., Member, S., Cavagnino, A., Staton, D., Shanel, M., Mueller, M., and Mejuto, C., "Evolution and Modern Approaches for Thermal Analysis of Electrical Machines," *IEEE Transactions on Industrial Electronics*, Vol. 56, No. 3, 2009, pp. 871–882. doi:10.1109/TIE.2008.2011622

[8] Canders, W.-R., Tareilus, G., Koch, I., and May, H., "New Design and Control Aspects for Electric Vehicle Drives," *2010 14th International Power Electronics and Motion Control Conference (EPE/PEMC)*, IEEE Xplore, Sept. 2010, pp. S11-1, S11-8. doi:10.1109/EPEPEMC.2010.5606528

[9] Hamada, K., "Present Status and Future Prospects for Electronics in Electric Vehicles/Hybrid Electric Vehicles and Expectations for Wide Bandgap Semiconductor Devices," *Physica Status Solidi (B)*, Vol. 245, No. 7, July 2008, pp. 1223–1231. doi:10.1002/pssb.v245:7

[10] Hale, M., "Survey of Thermal Storage for Parabolic Trough Power Plants," National Renewable Energy Lab. NREL/SR-550-27925, Golden, CO, 2000, pp. 1–28.

[11] Sharma, A., Tyagi, V. V., Chen, C. R., and Buddhi, D., "Review on Thermal Energy Storage with Phase Change Materials and Applications," *Renewable and Sustainable Energy Reviews*, Vol. 13, No. 2, Feb. 2009, pp. 318–345. doi:10.1016/j.rser.2007.10.005

[12] März, M., Schletz, A., Eckardt, B., Egelkraut, S., and Rauh, H., "Power Electronics System Integration for Electric and Hybrid Vehicles," *Integrated Power Electronics Systems (CIPS)*, IEEE Xplore, March 2010, pp. 1–10, 16–18, Data available online at http://ieeexplore.ieee.org/stamp/stamp.jsp?tp=&=5730643&=5730626.

[13] Nerg, J., Rilla, M., and Pyrhönen, J., "Thermal Analysis of Radial-Flux Electrical Machines with a High Power Density," *IEEE Transactions on Industrial Electronics*, Vol. 55, No. 10, 2008, pp. 3543–3554. doi:10.1109/TIE.2008.927403

[14] "Cumulative Sales of TMC Hybrids Top 2 Million Units in Japan," Toyota Motor Corporation, Japan, 2012, Data available online at http://www.toyotabharat.com/inen/news/2013/april_17.aspx [retrieved 2014].

[15] O'Keefe, M., and Bennion, K., "A Comparison of Hybrid Electric Vehicle Power Electronics Cooling Options," *IEEE Vehicle Power and Propulsion Conference (VPPC)*, IEEE Xplore, 2007, pp. 116–123, 9–12. doi:10.1109/VPPC.2007.4544110

[16] Bennion, K., and Thornton, M., "Integrated Vehicle Thermal Management for Advanced Vehicle Propulsion Technologies," National Renewable Energy Lab. NREL/CP-540-47416, Golden, CO, 2010.

[17] Johnson, R. W., Evans, J. L., Jacobsen, P., Thompson, J. R. R., and Christopher, M., "The Changing Automotive Environment: High-Temperature Electronics," *IEEE Transactions on Electronics Packaging Manufacturing*, Vol. 27, No. 3, July 2004, pp. 164–176. doi:10.1109/TEPM.2004.843109

[18] Kelly, K., Abraham, T., and Bennion, K., "Assessment of Thermal Control Technologies for Cooling Electric Vehicle Power Electronics," National Renewable Energy Lab. NREL/CP-540-42267, Golden, CO, 2008.

[19] Siegel, R., "Transient Heat Transfer for Laminar Slug Flow in Ducts," *Applied Mechanics*, Vol. 81, No. 1, 1959, pp. 140–144.

[20] Siegel, R., "Heat Transfer for Laminar Flow in Ducts with Arbitrary Time Variations in Wall Temperature," *Journal of Applied Mechanics*, Vol. 27, No. 2, 1960, pp. 241–249. doi:10.1115/1.3643945

[21] Sparrow, E. M., and Siegel, R., "Thermal Entrance Region of a Circular Tube Under Transient Heating Conditions," *Third U.S. National Congress of Applied Mechanics*, ASME Trans., 1958, pp. 817–826.

[22] Siegel, R., and Sparrow, E. M., "Transient Heat Transfer for Laminar Forced Convection in the Thermal Entrance Region of Flat Ducts," *ASME Heat Transfer*, Vol. 81, No. 1, 1959, pp. 29–36.

[23] Perlmutter, M., and Siegel, R., "Unsteady Laminar Flow in a Duct with Unsteady Heat Addition," *Heat Transfer*, Vol. 83, No. 4, 1961, pp. 432–439. doi:10.1115/1.3683662

[24] Siegel, R., "Forced Convection in a Channel with Wall Heat Capacity and with Wall Heating Variable with Axial Position and Time," *International Journal of Heat Mass Transfer*, Vol. 6, No. 7, 1963, pp. 607–620. doi:10.1016/0017-9310(63)90016-4

[25] Siegel, R., and Perlmutter, M., "Laminar Heat Transfer in a Channel with Unsteady Flow and Wall Heating Varying with Position and Time," *Journal of Heat Transfer*, Vol. 85, No. 4, 1963, pp. 358–365. doi:10.1115/1.3686125

[26] Perlmutter, M., and Siegel, R., "Two-Dimensional Unsteady Incompressible Laminar Duct Flow with a Step Change in Wall Temperature," *Journal of Heat Transfer*, Vol. 83, No. 4, 1961, pp. 432–440. doi:10.1115/1.3683662

[27] Sucec, J., "Unsteady Forced Convection with Sinusoidal Duct Wall Generation: The Conjugate Heat Transfer Problem," *International Journal of Heat and Mass Transfer*, Vol. 45, No. 8, April 2002, pp. 1631–1642. doi:10.1016/S0017-9310(01)00275-7

[28] Kakac, S., Li, W., and Cotta, R. M., "Unsteady Laminar Forced Convection in Ducts with Periodic Variation of Inlet Temperature," *Heat Transfer*, Vol. 112, No. 4, 1990, pp. 913–920. doi:10.1115/1.2910499

[29] Weigong, L., and Kakac, S., "Unsteady Thermal Entrance Heat Transfer in Laminar Flow with a Periodic Variation of Inlet Temperature," *International Journal of Heat and Mass Transfer*, Vol. 34, No. 10, Oct. 1991, pp. 2581–2592. doi:10.1016/0017-9310(91)90098-Y

[30] Kakac, S., and Yener, Y., "Exact Solution of the Transient Forced Convection Energy Equation for Timewise Variation of Inlet Temperature," *International Journal of Heat Mass Transfer*, Vol. 16, No. 12, 1973, pp. 2205–2214. doi:10.1016/0017-9310(73)90007-0

[31] Cotta, R. M., and Özişik, M. N., "Laminar Forced Convection Inside Ducts with Periodic Variation of Inlet Temperature," *International Journal of Heat and Mass Transfer*, Vol. 29, Oct. 1986, pp. 1495–1501. doi:10.1016/0017-9310(86)90064-5

[32] Kakac, S., "A General Analytical Solution to the Equation of Transient Forced Convection with Fully Developed Flow," *International Journal of Heat Mass Transfer*, Vol. 18, No. 12, 1975, pp. 1449–1454. doi:10.1016/0017-9310(75)90259-8

[33] Hadiouche, A., and Mansouri, K., "Application of Integral Transform Technique to the Transient Laminar Flow Heat Transfer in the Ducts," *International Journal of Thermal Sciences*, Vol. 49, No. 1, Jan. 2010, pp. 10–22. doi:10.1016/j.ijthermalsci.2009.05.012

[34] Fakoor-Pakdaman, M., Andisheh-Tadbir, M., and Bahrami, M., "Transient Internal Forced Convection Under Arbitrary Time-Dependent Heat Flux," *Proceedings of the ASME 2013 Summer Heat Transfer Conference HT2013*, ASME-17148, Minneapolis, MN, 2013.
[35] Fakoor-Pakdaman, M., Andisheh-Tadbir, M., and Bahrami, M., "Unsteady Laminar Forced-Convective Tube Flow Under Dynamic Time-Dependent Heat Flux," *Journal of Heat Transfer*, Vol. 136, No. 4, Nov. 2013, Paper 041706. doi:10.1115/1.4026119
[36] Kreyszig, E., Kreyzig, H., and Norminton, E. J., *Advanced Engineering Methematics*, Wiley, New York, 2010, pp. 473–490.
[37] Campo, A., Morrone, B., and Manca, O., "Approximate Analytic Estimate of Axial Fluid Conduction in Laminar Forced Convection Tube Flows with Zero-to-Uniform Step Wall Heat Fluxes," *Heat Transfer Engineering*, Vol. 24, No. 4, July 2003, pp. 49–58. doi:10.1080/01457630304027
[38] Incropera, F. P., Dewitt, D. P., Bergman, T. L., and Lavine, A. S., *Introduction to Heat Transfer*, Wiley, New York, 2007, p. 458.
[39] Bejan, A., *Convection Heat Transfer*, Wiley, New York, 2004, p. 119.
[40] Sparrow, E. M., and Farias, F. N. De., "Unsteady Heat Transfer in Ducts With Time-Varying Inlet Tempearture and Participating Walls," *International Journal of Heat Mass Transfer*, Vol. 11, No. 5, 1968, pp. 837–853. doi:10.1016/0017-9310(68)90128-2
[41] Kays, W. M., and Crawford, M. E., *Convective Heat and Mass Transfer*, McGraw–Hill, New York, 1993, pp. 140–146.

Appendix B

Optimal unsteady convection over a duty cycle for arbitrary unsteady flow under dynamic thermal load

International Journal of Heat and Mass Transfer 78 (2014) 1187–1198

Contents lists available at ScienceDirect

International Journal of Heat and Mass Transfer

journal homepage: www.elsevier.com/locate/ijhmt

Optimal unsteady convection over a duty cycle for arbitrary unsteady flow under dynamic thermal load

M. Fakoor-Pakdaman *, Mehran Ahmadi, Mehdi Andisheh-Tadbir, Majid Bahrami

Laboratory for Alternative Energy Conversion (LAEC), School of Mechatronic Systems Engineering, Simon Fraser University, Surrey, BC, Canada

ARTICLE INFO

Article history:
Received 30 April 2014
Received in revised form 18 July 2014
Accepted 20 July 2014
Available online 15 August 2014

Keywords:
Convection
Dynamic systems
Pulsating flow
Transient
Optimal frequency
APEEM

ABSTRACT

Developing next generation transient heat exchangers is a transformative technology for efficient thermal management of advanced power electronics and electric machines (APEEM) inside hybrid electric, electric, and fuel cell vehicles as well as renewable energies (wind, solar, tidal). Optimal design criteria for such dynamic heat exchangers should be achieved through addressing internal forced convection with arbitrary flow unsteadiness under dynamic time dependent thermal loads. Exact analytical solutions were obtained for laminar forced-convective heat transfer under arbitrary time-dependent heat flux for steady flow inside a tube (Fakoor-Pakdaman *et al.*, 2014). In this study, the energy equation is solved analytically for arbitrary unsteady flow between parallel plates under dynamic time and position dependent heat flux. As such, laminar pulsating flow between two parallel plates is considered under a harmonic wall heat flux. Exact relationships are obtained to find; (i) temperature distribution for the fluid; (ii) fluid bulk temperature; and (iii) the local and time averaged Nusselt number. New compact relationships are proposed to find the thermal entrance length and the cyclic fully-developed Nusselt number. It is shown that the period of the Nusselt number oscillations is the least common multiple of the periods of the imposed harmonic heat flux and the pulsating flow. We obtained a relationship for the 'cut-off' angular frequency of pulsating flow beyond which the heat transfer does not feel the pulsation. This study also shows that for a given harmonic wall heat flux, there is an optimal pulsating flow velocity, with optimum frequency, which enhances the time averaged Nusselt number by up to 27%.

1. Introduction

Optimal design of transient single-phase heat exchangers is a key to developing innovative technology for the next generation advanced power electronics and electric machines (APEEM). APEEM has applications in emerging cleantech systems such as powertrain and propulsion systems of hybrid electric, electric vehicles (EV), and emerging fuel cell vehicles (FCV) [1,2] and green power systems (wind, solar, tidal) [3,4]. Heat generation in APEEM undergo substantial transitions as a direct result of; (i) variable load due to duty cycle, [5–8] and (ii) unsteady coolant flow rate over a duty cycle [9,10]. As such, the heat exchangers/heat sinks associated with APEEM operate periodically over time and never attain a steady-state condition. Conventionally, cooling systems are designed based on a nominal steady-state or a "worst" case scenario, which may not properly represent the thermal behavior of various applications or duty cycles [7]. Downing and Kojasoy [11] predicted heat fluxes of $150-200\,[W/cm^2]$ and pulsed transient heat loads up to $400\,[W/cm^2]$, for the next-generation insulated gate bipolar transistors (IGBTs) which are used in the design of inverter units of HEVs.

Processes such as start-up, shut down, and pump/fan failure are other typical examples of arbitrary flow unsteadiness for dynamic/transient heat exchangers [12–15]. Besides, depending on the functionality of APEEM over a duty cycle, the coolant flow rate inside the heat exchangers/heat sinks of HE/E/FCV is varying arbitrarily over time [16]. Conventionally mechanical water pumps, directly coupled to the engine, are used in gasoline/diesel vehicles. However, electric vehicles can use variable-speed electric water pump using a separate electric motor and a controller, therefore maintaining an 'optimal' and variable flow rate of the coolant is possible over a driving cycle [9,10]. This provides an opportunity to significantly reduce the parasitic power required for the cooling of HE/E/FCV APEEM and improve the overall efficiency of the vehicle. There are only a few studies in the open literature on this topic. Therefore, there is a pending need for an in-depth understanding of instantaneous thermal characteristics of transient cooling systems

* Corresponding author. Tel.: +1 (778) 782 8538; fax: +1 (778) 782 7514.
E-mail addresses: mfakoorp@sfu.ca (M. Fakoor-Pakdaman), mahmadi@sfu.ca (M. Ahmadi), mandishe@sfu.ca (M. Andisheh-Tadbir), mbahrami@sfu.ca (M. Bahrami).

http://dx.doi.org/10.1016/j.ijheatmasstransfer.2014.07.058
0017-9310/

Nomenclature

a	Half width of the parallel plates, [m]
c_p	heat capacity, [J/kg K]
f	Arbitrary function of time, Eq. (2), $=\frac{u(t)}{u_r}$
F_n	Eigen values, Eq. (7)
Fo	Fourier number, $=\alpha t/R^2$
h	Local heat transfer coefficient, Eq. (23), [W/m^2 K]
k	Thermal conductivity, (W/m K)
n	Positive integer, Eq. (7), = 1,2,3,...
Nu_a	Local Nusselt number, Eq. (23), $=ha/k$
p	Dimemsionless period of temperature fluctuation
p_1	Dimensionless period of heat flux fluctuation, $=\frac{2\pi}{\omega_1}$
p_2	Dimensionless period of pulsatile velocity, $=\frac{2\pi}{\omega_2}$
Pe	Peclet number, $=Re\cdot Pr$
Pr	Prandtl number, $=\upsilon/\alpha$
q''	Thermal load (Heat flux), [W/m^2]
Re	Reynolds number, $=4u_r a/\upsilon$
t	Time, [s]
T	Temperature, [K]
u	Velocity, [m/s]
x	Axial distance from the entrance of the heated section, [m]
y	Normal coordinate measured from centerline of parallel plate channel, [m]
X	Dimensionless axial coordinate, $=4x/Re\cdot Pr\cdot a$
Y	Dimensionless normal coordinate, $=y/a$

Greek letters

α	Thermal diffusivity, [m^2/s]
ν	Kinematic viscosity, [m^2/s]
ρ	Fluid density, [kg/m^3]
θ	Dimensionless temperature, $=\frac{T-T_0}{q''_r a/k}$
φ	Arbitrary function of X and Fo, Eq. (4)
Ω_1	Angular frequency of the heat flux, [rad/s]
Ω_2	Angular frequency of the fluid velocity, [rad/s]
ω_1	Dimensionless angular frequency of the wall heat flux, $=\Omega_1 a^2/\alpha$
ω_2	Dimensionless angular frequency of the fluid velocity, $=\Omega_2 a^2/\alpha$
τ	Dimensionless arbitrary time
ξ	Dummy Fo variable
ζ	Dummy X variable

Subscripts

0	Inlet
m	Mean or bulk value
w	wall
r	Reference value
s	Step heat flux
$Tr.$	Transition

over a given duty cycle. This study is focused on internal forced convection with arbitrary unsteadiness in flow under arbitrary time-varying heat flux. The results of this work will provide a platform for the design, validation and building new intelligent thermal management systems that can actively and proactively control variable-speed electric pumps to circulate a coolant with instantaneous optimal flow rate in APEEM and similar applications.

1.1. Present literature

Siegel [17] pioneered the study on transient internal forced-convective heat transfer. He conducted several studies to investigate the thermal characteristics of steady tube flow under step wall heat flux/temperature [18–20]. Laminar pulsating flow is also addressed in Siegel's study [21] for planar flow in parallel plates under constant heat flux/wall temperature cases. It is shown that quasi-steady assumption does not give an accurate prediction of the thermal characteristics of the pulsating flow for moderate range of pulsation frequency [21]. Guo and Sung [22] addressed the contradictory results of the Nusselt number for pulsating flow in previous published papers; as some researchers had reported heat transfer enhancement, see Refs. [23,24], while heat transfer reduction had been noted in Ref. [25]. They proposed a new model for the time-averaged Nusselt number of laminar pulsating flow under constant wall heat flux. Such definition was introduced based on the time-averaged differences between the tube-wall and fluid-bulk temperatures over a pulsation period. Hemida et al. [26] argued that the small effects of pulsation, which had been noted in previous studies occurred as a result of the restrictive boundary conditions. Wall temperature/heat flux was assumed constant both in space and time. This may affect the heat exchange process, and reduce the effects of pulsation. This shows the necessity to consider more realistic boundary conditions for the tube wall other than constant heat flux or temperature. Less restrictive boundary conditions might manifest into greater sensitivity to pulsation [26]. This is one of the key issues addressed in the present study. In addition, Brereten and Jiang [27] introduced the idea of fluid flow modulation to increase the time-averaged Nusselt number of pulsating flow under constant heat flux. A summary of literature on laminar pulsating flow is presented in Table 1. Our literature review indicates:

- The existing models for pulsating channel flow are limited to constant wall heat flux/temperature cases.
- Effects of simultaneous oscillation of imposed heat flux and fluid velocity are not investigated in the literature.
- There is no model to determine an optimal velocity frequency for a given harmonic heat flux to maximize the convective heat transfer rate.

To the best of our knowledge, effects of non-constant boundary conditions have not been investigated in the literature neither experimentally nor theoretically. In other words, the answer to the following question is not clear: "can flow pulsation enhance the heat transfer rate in heat exchangers under arbitrary time-dependent loads?"

In our previous studies [31,32], a comprehensive analytical study was performed to predict the thermal characteristics of laminar steady flow under dynamic time-dependent wall heat flux. In the present study, a new analytical model is developed for laminar, single-phase heat transfer between two parallel plates with arbitrary flow unsteadiness under arbitrary time/position dependent wall heat flux. Laminar pulsating flow and harmonic heat flux are considered to obtain exact relationships for: (i) fluid temperature distribution inside the channel; (ii) fluid bulk temperature; and (iii) the Nusselt number. The period of Nusselt number oscillation is obtained under simultaneous oscillation of flow and the imposed wall heat flux. Following Ref. [23], a new definition is introduced to obtain the time-averaged Nusselt number. In addition, optimal pulsating velocity with optimum frequency is found that maximizes

Table 1
Summary of the literature on laminar pulsating channel flow.

Author	Approach	Notes
Siegel and Perlmutter [21]	Analytical (method of characteristics)	√ Reported temperature distribution between two parallel plates √ Covered thermally developing and fully-developed regions × Limited to step wall temperature and heat flux × Nusselt number was defined based on the tube wall and inlet fluid temperature
Hemida et al. [26]	Analytical/numerical (Green's function solution)	√ Reported a closed-form relationship for the temperature distribution in fully-developed region √ Considered different BCs: (i) isoflux; (ii) wall with thermal resistance; (iii) wall with thermal inertia × Treated thermally developing region only numerically
Nield and Kuznetsov [28]	Analytical (perturbation method)	√ Reported transient Nusselt number in circular tubes and parallel plates √ Definition of the Nusselt number similar to [22] × Reported singularity in the solution for $Pr = 1$ × Limited to constant wall heat flux × Limited to oscillations with small amplitudes
Zhao and Cheng [29]	Numerical	√ Proposed a compact relationship for the time averaged Nusselt number for reciprocating flow √ Covered both thermally developing and fully-developed regions × Limited to constant wall temperature
Yan et al. [30]	Analytical/experimental	√ Reported series solutions for temperature distribution and Nusselt number × Limited to constant wall temperature

the heat transfer rate in the channel flow under a given harmonic wall heat flux. An independent numerical study is also performed which compares well with the analytical results; maximum relative difference less than 6%.

To develop the present analytical model, the fluid flow response to a step heat flux is taken into account. A Duhamel's theorem is applied on the thermal response of the fluid flow under the step heat flux, following Ref. [17]. The methodology presented in Ref. [32] is extended to account for arbitrary flow unsteadiness under arbitrary wall heat flux. A harmonic heat flux and pulsating laminar flow are taken into consideration and the thermal characteristics of the fluid flow are determined analytically. Since any time-dependent wall heat flux can be expressed by simple oscillatory functions using a Fourier series transformation [33], the results of this study can be readily applied to determine the pulsating fluid flow response under an arbitrary time-varying heat flux. This approach enables analyzing transient single-phase convective heat transfer under various time-varying conditions, using a superposition technique.

2. Governing equations

Fig. 1 shows fluid flow between two parallel plates with half width of spacing, a, which is thermally insulated in the first sub-region, $x \leqslant 0$, and is heated in the second sub-region, $x > 0$. The entering fluid temperature is maintained at T_0 throughout the heating period. The wall at the second sub-region is given by an arbitrary time-dependent heat flux, $q''(t)$. It should be noted that the second sub-region may be long enough so that the flow can reach thermally fully-developed condition, see Fig. 1. It is intended to determine the evolution of the channel wall temperature, fluid bulk temperature and the Nusselt number as a function of time and space for the entire range of time. Such characteristics are evaluated under dynamic time-dependent heat flux for a fluid flow with arbitrary time-varying velocity.

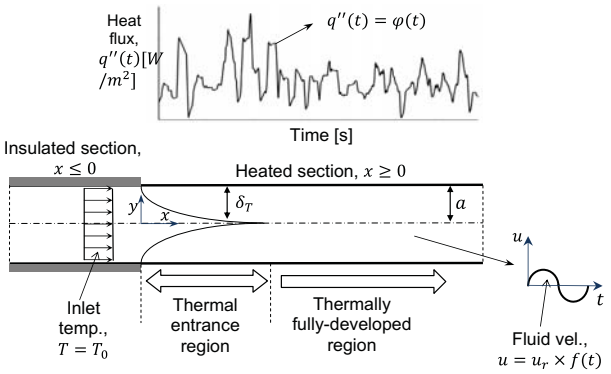

Fig. 1. Schematic of the developing and fully-developed regions, time-dependent wall heat flux and fluid velocity as well as the coordinate system.

The assumptions made in deriving the proposed analytical model are listed below:

- Incompressible flow,
- Constant thermo-physical properties,
- Negligible viscous dissipation,
- Negligible axial heat conduction, i.e., $Pe = Re \times Pr \geqslant 10$ [25],
- No thermal energy sources within the fluid,
- No flow reversal in the duct,
- Fluid flow velocity is only a function of time, i.e., slug flow $u = u(t)$.

The slug flow approximation means consideration of one-dimensional velocity distribution, i.e., the fluid is moving through the channel with a mean velocity that can be a function of time. As demonstrated in Refs. [17,20], the slug flow approximation reveals the essential physical behavior of the system, while it enables obtaining exact mathematical solution for various boundary conditions. Using this simplification one can study the effects of various boundary conditions on transient heat transfer without tedious numerical computations [17,20].

The energy equation for a slug flow inside two parallel plates is then become:

$$\frac{\partial T}{\partial t} + u(t)\frac{\partial T}{\partial x} = \alpha\left(\frac{\partial^2 T}{\partial y^2}\right) \tag{1}$$

where the transient velocity between the parallel plates, $u(t)$, in the energy equation can be written as follows:

$$u(t) = u_r \times f(t) \tag{2}$$

Here u_r is a constant reference velocity, and $f(t)$ is an arbitrary function of time. For a special case where $f(t) = 1$, the channel flow velocity is constant slug flow, $u = u_r$, which was investigated in our

previous works [31,32]. As such, the dimensionless form of the energy equation, Eq. (1), then becomes:

$$\frac{\partial\theta}{\partial Fo}+\frac{u}{u_r}\frac{\partial\theta}{\partial X}=\frac{\partial^2\theta}{\partial Y^2} \tag{3}$$

We define the following dimensionless variables:

$$Fo=\frac{\alpha t}{a^2}\quad X=\frac{4x/a}{Re\cdot Pr}\quad \theta=\frac{T-T_0}{q''_r a/k}\quad Y=\frac{y}{a}\quad Re=\frac{4u_r a}{\upsilon}\quad Pr=\frac{\upsilon}{\alpha}$$

where Fo is the Fourier number and X is the dimensionless axial location that characterizes the flow inside a conduit. As previously mentioned, the goal of this study is to find the transient thermal response of unsteady forced-convective channel flow under arbitrary time-dependent wall heat flux. Therefore, a general wall heat flux is assumed as:

$$q''(X,Fo)=q''_r\cdot\varphi(X,Fo) \tag{4}$$

where q''_r is the heat flux amplitude and φ (X,Fo) is an arbitrary function of space and time, respectively. Consequently, Eq. (4) is subjected to the following initial and boundary conditions:

$$\begin{aligned}&\theta(Y,X,0)=0\quad\text{Initial condition,}\\&\theta(Y,0,Fo)=0\quad\text{Entrance condition,}\\&(\partial\theta/\partial Y)|_{Y=1}=\frac{q''}{q''_r}(X,Fo)=\varphi(X,Fo)\\&\quad\text{Heat flux at the channel wall for } Fo>0,\\&(\partial\theta/\partial Y)|_{Y=0}=0\quad\text{Symmetry at the channel centerline.}\end{aligned} \tag{5}$$

Although the analysis here are performed for fluid flow between parallel plates, the same methodology can be adopted for other geometries, see Ref. [34] for more detail.

3. Model development

In this section, a new all-time model is developed considering; (i) short-time response and (ii) long-time response. When a slab at uniform temperature T_0 is suddenly subjected to a step heat flux $\Delta q''$ at its surface, the temperature response is [17]:

$$\theta_s=\frac{T-T_0}{q''_r a/k}=\frac{\Delta q''}{q''_r}\left[Fo+\frac{3Y^2-1}{6}-2\sum_{n=1}^{\infty}\frac{(-1)^n}{F_n^2}\times\cos(F_nY)\times\exp\left(-F_n^2\times Fo\right)\right] \tag{6}$$

where θ_s is the dimensionless temperature of the fluid under a step wall heat flux, F_n are the eigenvalues which can be found by the following relationship:

$$F_n=n\pi\quad n=1,2,3,\ldots \tag{7}$$

The energy equation, Eq. (1), is linear, therefore; a superposition technique can be used to extend the response of the fluid flow for a step heat flux to the other general cases, as discussed in more detail in [35]. Following Siegel [35], by using Duhamel's integral [36], the thermal response for a step heat flux, Eq. (6), can be generalized for arbitrary time/space variations in wall heat flux.

$$\theta=\int_0^{Fo}\frac{q''(\xi)}{q''_r}d\xi+2\sum_{n=1}^{\infty}(-1)^n\times e^{-F_n^2\times Fo}\times\cos(F_nY)\times\int_0^{Fo}\frac{q''(\xi)}{q''_r}\times\exp\left(F_n^2\times\xi\right)d\xi \tag{8}$$

This expression is only valid when the element is initially isothermal, thus the treatment is limited to the cases where the channel was initially isothermal. However, extension to other cases can be achieved by superposition techniques, as discussed in [35].

As shown in Fig. 2, in an Eulerian coordinate system, where the observer is fixed at a given location x along the channel observing the fluid element passes by. For the considered unsteady flow, Eq. (2), it takes some time, $Fo=Fo_{tr.}$, for the fluid element at the entrance to reach a given axial position say X_1. As such, the relationship between the given axial position X_1 and transition time $Fo_{tr.}$ can be formulated as:

$$X_1=\int_{\xi=0}^{Fo_{tr.}}f(\xi)d\xi \tag{9}$$

Where ξ is the dummy variable, and $Fo_{tr.}$ is the non-dimensional time that takes for the fluid element to reach location X_1. Beyond this distance region, $X\geqslant X_1$, there has not been any penetration of the fluid which was originally outside the channel when the transient began. Hence, the behavior in this region is identical to that of a channel with infinite length in both directions. This means that the convective term in the energy equation, Eq. (1), is zero and a pure transient "heat-conduction" process takes place. This is considered the short-time response of the flow [35]. On the other hand, for $X<X_1$ the observer located at X will see the passing fluid that passed the entrance (insulated) region, when the transient was initiated. This is considered the long-time response of the flow [35]. Therefore, the solution consists of two regions that should be considered separately. The methodology considered in this study is shown schematically in Fig. short-time response, $X\geqslant X_1$

For the sake of generality, we consider a case, where the wall heat flux varies with both time and space, $q''(X,Fo)$. We first consider the region $X\geqslant X_1$. A fluid element that reaches X at time Fo has already passed the heated section at the location $X-\int_{\xi=0}^{Fo}f(\xi)d\xi$ at the beginning of the transient. As this element moves along, it is subjected to the wall heat flux variations in both time and space. At a time τ between 0 and Fo, the element arrives at the location $X-\int_{\xi=\tau}^{Fo}f(\xi)d\xi$. Thus, the heat flux that the element is subjected to at that time is $q''\left(X-\int_{\xi=\tau}^{Fo}f(\xi)d\xi,\tau\right)$. This is substituted into Eq. (8) to find the short-time response for the fluid temperature distribution [35].

$$\theta(X,Fo)=\int_0^{Fo}\frac{q''\left(X-\int_{\xi=\tau}^{Fo}f(\xi)d\xi,\tau\right)}{q''_r}d\tau+2\sum_{n=1}^{\infty}(-1)^n\times\cos(F_nY)\times\exp\left(-F_n^2\times Fo\right)\times\int_0^{Fo}\frac{q''\left(X-\int_{\xi=\tau}^{Fo}f(\xi)d\xi,\tau\right)}{q''_r}\times\exp\left(F_n^2\tau\right)d\tau \tag{10}$$

It should be noted that according to Eq. (10) when the imposed wall heat flux is only a function of time, $q''=q''(Fo)$, the short-time thermal response of the fluid flow is independent of the axial position. However, it is a function of time and the characteristics of the imposed wall heat flux.

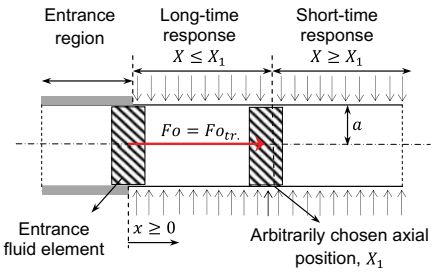

Fig. 2. The methodology adopted to find the thermal response of the unsteady channel flow under arbitrary time-dependent heat flux.

3.1. Transition time, $X = X_1$

As mentioned earlier the transition time, $Fo = Fo_{tr.}$, for a given axial position, $X = X_1$, can be calculated using Eq. (9). Therefore, the time $Fo = Fo_{tr.}$ separates the short-time from the long-time response for a given axial position.

3.2. Long-time response, $X < X_1$

Now we consider $X < X_1$ region. The element that reaches X at time Fo, has entered the channel at the time Fo_0 and already begun to be heated. This time is found from the following implicit relation:

$$X = \int_{Fo_0}^{Fo} f(\xi)d\xi \tag{11}$$

Then for this region, we can use Eq. (10) except that the lower limit of the integrals becomes the initial time, Fo_0. Then by analogy with Eq. (10), for $X < X_1$ we have:

$$\theta(X,Fo) = \int_{Fo_0}^{Fo} \frac{q''\left(X - \int_{\xi=\tau}^{Fo} f(\xi)d\xi, \tau\right)}{q''_r} d\tau + 2\sum_{n=1}^{\infty}(-1)^n \times \cos(F_nY) \times \exp\left(-F_n^2 \times Fo\right) \times \int_{Fo_0}^{Fo} \frac{q''\left(X - \int_{\xi=\tau}^{Fo} f(\xi)d\xi, \tau\right)}{q''_r} \times \exp\left(F_n^2\tau\right)d\tau \tag{12}$$

It should be noted that to find the long-time response, Eqs. (11) and (12) should be solved simultaneously. According to Eq. (12), the long-time thermal response of the fluid flow is a function of time, axial position and the characteristics of the imposed wall heat flux. More detail is presented in Refs. [31,32,37].

4. Heat flux and velocity transients

It is assumed that the transient is initiated by simultaneously changing the fluid flow velocity and channel wall heat flux over time (duty cycle). We develop the present model for a cyclic wall heat flux, as a basic element, noting that the results can be generalized to cover cases with arbitrary time variations in wall heat flux through superposition technique, e.g., Fourier series, Ref. [33]. Throughout this study, the following is considered as a cyclic wall heat flux,

$$\frac{q''}{q''_r}(\Omega_1, t) = [1 + \sin(\Omega_1 t)] \tag{13}$$

where, $q''_r[W/m^2]$ and Ω_1 [rad/s] are the amplitude and the angular frequency of the imposed harmonic heat flux. The dimensionless form of Eq. (13) is given below:

$$q''(\omega_1, Fo) = q''_r[1 + \sin(\omega_1 \times Fo)] \tag{14}$$

where $\omega_1 = \frac{\Omega_1 \times a^2}{\alpha}$ is the dimensionless angular frequency of the imposed wall heat flux. In the following sections, the thermal characteristics of unsteady channel flow are investigated under dynamically varying thermal loads for various forms of transient fluid velocity inside the channel. First, laminar pulsating flow is considered for the fluid velocity. Subsequently, a modified form of pulsation is determined to enhance the convective heat transfer rate inside the parallel plates.

4.1. Laminar pulsating flow

In this section, we assume a pulsatile transient velocity which is caused by superimposing pulsation on a mean flow between parallel plates:

$$\frac{u}{u_r} = f(t) = 1 + \sin(\Omega_2 \times t) \tag{15}$$

where u_r [m/s] and Ω_2 [rad/s] are the amplitude and the angular frequency of the pulsatile flow, respectively. The dimensionless form of Eq. (15) is as follow:

$$\frac{u}{u_r} = 1 + \sin(\omega_2 \times Fo) \tag{16}$$

where ω_2 is the dimensionless angular frequency of the fluid velocity. At the limit where $\omega_2 = 0$, Eq. (16) yields the constant slug flow inside a conduit. In the following sections, we find the temperature distribution and the Nusselt number for the aforementioned wall heat flux, Eq. (14), and transient velocity, Eq. (16).

4.1.1. Temperature distribution inside the fluid

The dimensionless transition time, $Fo_{tr.}$, for a given axial position, $X = X_1$, can be obtained implicitly by substituting Eq. (16) into Eq. (9) as follows:

$$X_1 = Fo_{tr.} + \frac{1}{\omega_2}[1 - \cos(\omega_2 \times Fo_{tr.})] \tag{17}$$

Short-time response, $X \geqslant X_1$:

$$\theta(X,Fo,\omega_1) = Fo + \frac{1}{\omega_1}[1 - \cos(\omega_1 Fo)] + \frac{3Y^2 - 1}{6} + 2\sum_{n=1}^{\infty}(-1)^n \times \cos(F_nY) \times \begin{Bmatrix} \frac{F_n^2 \times \sin(\omega_1 Fo) - \omega_1 \times \cos(\omega_1 Fo) + \omega_1 \times \exp\left(-F_n^2 \times Fo\right)}{\omega_1^2 + F_n^4} \\ -\frac{\exp\left(-F_n^2 \times Fo\right)}{F_n^2} \end{Bmatrix} \tag{18}$$

Long-time response, $X \leqslant X_1$:

$$\theta(X,Fo,\omega_1) = Fo - Fo_0 + \frac{1}{\omega_1}[\cos(\omega_1 Fo_0) - \cos(\omega_1 Fo)] + \frac{3Y^2 - 1}{6} + 2\sum_{n=1}^{\infty}(-1)^n \times \cos(F_nY) \times \begin{Bmatrix} \frac{F_n^2 \times \sin(\omega_1 Fo) - \omega_1 \times \cos(\omega_1 Fo)}{\omega_1^2 + F_n^4} + \\ \frac{\left\{-F_n^2 \times \sin(\omega_1 Fo_0) + \omega_1 \times \cos(\omega_1 Fo_0)\right\} \times \exp\left[F_n^2 \times (Fo_0 - Fo)\right]}{\omega_1^2 + F_n^4} - \\ \frac{\exp\left[F_n^2 \times (Fo_0 - Fo)\right]}{F_n^2} \end{Bmatrix} \tag{19}$$

Where Fo_0 is found from the following relationship:

$$X_1 = Fo - Fo_0 + \frac{1}{\omega_2}[\cos(\omega_2 \times Fo_0) - \cos(\omega_2 \times Fo)] \tag{20}$$

In this study, we considered the first 60 terms of the series solutions, using more terms does not affect the solution up to four decimal digits.

4.1.2. Fluid bulk temperature

The bulk temperature of a constant-property fluid for the slug flow condition can be obtained by the following relationship, Ref. [38]:

$$\theta_m(X,Fo) = \int_0^1 \theta(Y,X,Fo)dY \tag{21}$$

Substituting Eqs. (18) and (19) into Eq. (21), the short-time and long-time fluid bulk temperature can be obtained as follows:

$$\theta_m(X,Fo,\omega_1) = \begin{cases} Fo + \frac{1}{\omega_1}[1 - \cos(\omega_1 Fo)] & X \geqslant X_1 \\ Fo - Fo_0 + \frac{1}{\omega_1}\{\cos(\omega_1 Fo_0) - \cos(\omega_1 Fo)\} & X < X_1 \end{cases} \tag{22}$$

4.1.3. Nusselt number

In most Siegel works [16–21], the transient thermal behavior of a system is evaluated based on the dimensionless wall heat flux considering the difference between the local tube wall and the initial fluid temperature. We are of the opinion that an alternative definition of the local Nusselt number has a more 'physical' meaning, i.e., based on the local difference between the channel wall and the fluid bulk temperature at each axial location; this is consistent with Refs. [22,38]. It should be emphasized that the definition of the Nusselt number is an arbitrary choice and will not alter the final results.

$$Nu_a = \frac{ha}{k} = \frac{1+\sin(\omega_1 Fo)}{\theta_w - \theta_m} \tag{23}$$

where Nu_a is the local Nusselt number and θ_w is the dimensionless wall temperature obtained from Eqs. (18) and (19) with $Y = 1$. Therefore, the short-time and long-time Nusselt numbers are obtained as follows:

Short-time Nusselt number, $X \geqslant X_1$:

$$Nu_a(Fo,\omega_1) = \frac{1+\sin(\omega_1 Fo)}{\frac{1}{3}+2\sum_{n=1}^{\infty}\left\{\begin{array}{l}\frac{F_n^2\times\sin(\omega_1 Fo)-\omega_1\times\cos(\omega_1 Fo)+\omega_1\times\exp\left(-F_n^2\times Fo\right)}{\omega_1^2+F_n^4} \\ -\frac{\exp\left(-F_n^2\times Fo\right)}{F_n^2}\end{array}\right\}} \tag{24}$$

Long-time Nusselt number, $X < X_1$:

$$Nu_a(X,Fo,\omega_1) = \frac{1+\sin(\omega_1 Fo)}{\frac{1}{3}+2\sum_{n=1}^{\infty}\left\{\begin{array}{l}\frac{F_n^2\times\sin(\omega_1 Fo)-\omega_1\times\cos(\omega_1 Fo)}{\omega_1^2+F_n^4}+ \\ \frac{\left\{-F_n^2\times\sin(\omega_1 Fo_0)+\omega_1\times\cos(\omega_1 Fo_0)\right\}\times\exp\left[F_n^2\times(Fo_0-Fo)\right]}{\omega_1^2+F_n^4}- \\ \frac{\exp\left[F_n^2\times(Fo_0-Fo)\right]}{F_n^2}\end{array}\right\}} \tag{25}$$

As previously mentioned in Section 3, the short-time Nusselt number is only a function of time and angular frequency. However, the long-time Nusselt number is a function of time, angular frequency, and the axial location. In addition, Fo_0 is found by Eq. (20). The time-averaged Nusselt number over a period of fluctuation is defined in this study as follows:

$$\overline{Nu}_a(X) = \frac{1}{p}\int_{Fo=0}^{p} Nu_a dFo \tag{26}$$

where $\overline{Nu}_a(X)$ is the local time-averaged Nusselt number and p is the period of temperature oscillation inside the fluid. The latter depends on the period of heat flux, $p_1 = \frac{2\pi}{\omega_1}$, and the fluid flow pulsation, $p_2 = \frac{2\pi}{\omega_2}$. This will be discussed in detail in Section 6.

4.2. Optimum transient velocity

An optimum pulsating velocity can be defined to increase the time-averaged Nusselt number of a pulsating flow compared to its associated constant slug flow condition, see Ref. [27]. This will be discussed in detail in Section 6. This optimal pulsating velocity is considered as follows:

$$\frac{u}{u_r} = 1 + |\sin(\omega_2 \times Fo)| \tag{27}$$

For this transient velocity, the temperature distribution is obtained by Eqs. (18) and (19), while the Nusselt number can be calculated by Eqs. (24) and (25). However, modified forms of Eqs. (9) and (11) should be solved to find $Fo_{tr.}$ and Fo_0 implicitly for a given axial position, $X = X_1$, over time. As a result, Eq. (28) indicates the implicit relationship for dimensionless transition time, $Fo = Fo_{tr.}$, for an arbitrarily chosen axial position, $X = X_1$.

$$X_1 = \int_{\zeta=0}^{Fo_{tr.}} [1+|\sin(\omega_2\zeta)|]d\zeta \tag{28}$$

In addition, to find the long-time response the following implicit relationship can be used to find the parameter Fo_0, for an arbitrary axial position, $X = X_1$.

$$X_1 = \int_{\zeta=Fo_0}^{Fo} [1+|\sin(\omega_2\zeta)|]d\zeta \tag{29}$$

5. Numerical study

In this section, an independent numerical simulation of the axisymmetric flow inside parallel plates is conducted using the commercial software, ANSYS® Fluent [20]. User defined codes (UDFs) are written to apply the dynamic heat flux boundary conditions on the channel wall, Eq. (14), and the transient velocity between the parallel plates, Eq. (16). The assumptions stated in Section 2 are used in the numerical analysis. Grid independency of the results is tested for three different grid sizes, 20×100, 40×200, as well as 80×400, and 40×200 is selected as the final grid size, since the maximum difference in the predicted values for the fluid temperature by the two latter grid sizes is less than 2%. Air is selected as the working fluid for the numerical simulations. The geometrical and thermal properties used in the baseline case for the numerical simulation are listed in Table 2. The maximum relative difference between the analytical results and the numerical data is less than 6%, which are discussed in detail in Section 6.

6. Results and discussion

Variations of the dimensionless channel wall temperature against the Fo number, Eqs. (18) and (19), for three axial positions along the channel are shown in Fig. 3 and compared with the numerical data (markers) obtained in Section 5 of this study. The imposed wall heat flux is assumed to be constant over time, $q'' = q''_r = \text{const.}$, and the fluid velocity fluctuates harmonically over time, $U(Fo) = \frac{u}{u_r} = 1 + \sin(\pi \times Fo)$, respectively.

One can conclude the following from Fig. 3:

- The present model predicts an abrupt transition between the short-time and long-time responses. The numerical results, however, indicate a smoother transition between the responses. This causes the numerical data to deviate slightly from the analytical results as the long-time response begins. The maximum relative difference between the present analytical model and the numerical data occurs at this transition and is less than 6%.
- The abrupt transition between the short- and long-time responses occurs as a result of the limitations of the method of characteristics which is used to solve the energy equation, Eq. (3). More detail is presented in Ref. [31].
- There is an initial transient period of pure conduction during which all of the curves follow along the same line, $Fo \leqslant Fo_{tr.}$.
- When $Fo = Fo_{tr.}$, each curve stems from the common line, i.e., pure conduction response, and moves towards a steady oscillatory behavior at long-time response, Eqs. (18) and (19). The wall temperature increases at larger X values, as expected, because of the increase in the fluid bulk temperature in the axial direction.
- When the heat flux is constant and the fluid velocity is fluctuating over time, the temperature field fluctuates with the same angular frequency. It is also the case when the velocity is constant and the wall heat flux is fluctuating harmonically over

Table 2
Values of the thermal and geometrical properties used for the baseline case in the present numerical simulation.

Properties	Density, ρ[kg/m^3]	Dynamic viscosity, μ[Pa s]	Thermal conductivity, k[W/m/K]	Thermal capacity, c_p[J/kg/K]	Channel half width, a[m]
Values	1.225	1.7894E-5	0.0242	1006.43	0.05

$q''_r = 100$ [W/m^2], $u_r = 0.02$ [m/s], $T_0 = 300$ [K]

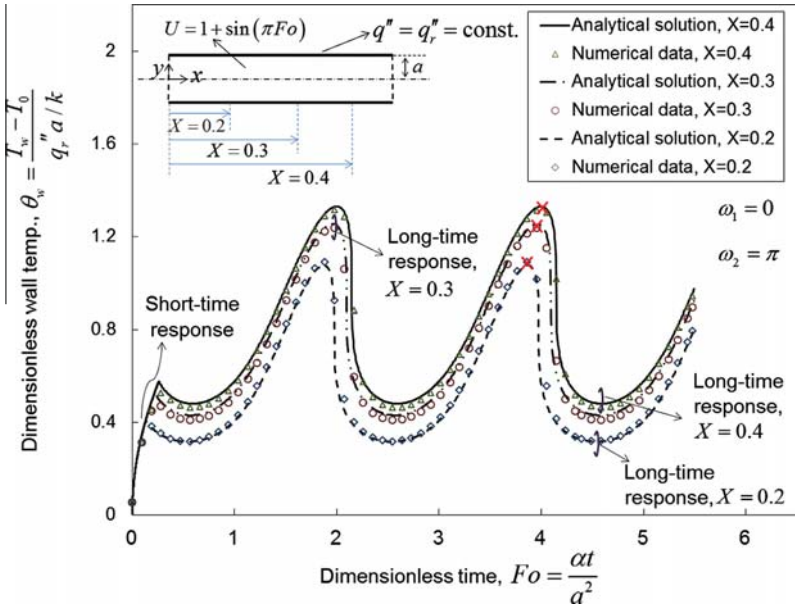

Fig. 3. Channel wall temperature against the dimensionless time, Eqs. (18) and (19), for a few axial positions along the channel, and comparison with the obtained numerical data (markers), when q'' = const. and $U = 1 + \sin(\pi \times Fo)$.

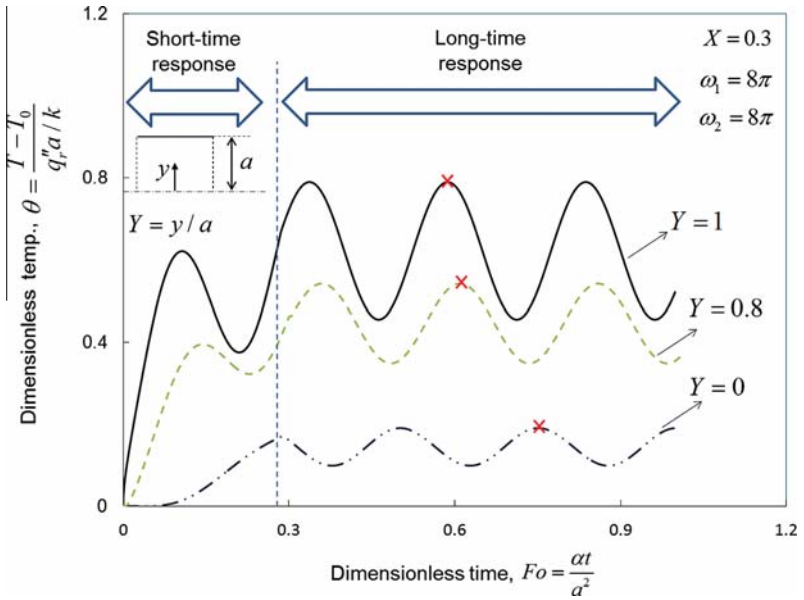

Fig. 4. Variations of the dimensionless fluid temperature at an arbitrarily-chosen axial position of $X = 0.3$ at different vertical positions across the channel against the Fo number where $q''/q''_r = 1 + \sin(8\pi \times Fo)$ and $U(Fo) = u/u_r = 1 + \sin(8\pi \times Fo)$.

time, see Ref. [32] for more detail. The angular frequency of the temperature field inside the fluid when both heat flux and velocity are fluctuating over time will be discussed later in this section.

- The shift between the peaks of the temperature profile is marked at different axial positions. This shows a "thermal lag" (inertia) of the fluid flow, which increases in x-direction towards the downstream of the channel.

Variations of the dimensionless temperature inside the fluid for a few vertical positions across the channel against the dimensionless time are depicted in Fig. 4. The axial position is arbitrarily fixed at $X = 0.3$; the imposed heat flux, and the fluid velocity are varying harmonically over time, i.e., $q''/q''_r = 1 + \sin(8\pi \times Fo)$ and $U(Fo) = 1 + \sin(8\pi \times Fo)$, respectively.

The following can be concluded from Fig. 4:

- At any given axial position, there is an initial transient period, which can be considered as pure conduction, i.e., the short-time response for $Fo \leqslant Fo_{tr.}$. However, as previously mentioned, each axial position shows a steady oscillatory behavior for $Fo > Fo_{tr.}$ at the long-time response.
- Regarding Eq. (17), for a given axial position of $X = 0.3$, the long-time response begins at $Fo_{tr.} = 0.28$, and shows the same behavior at all-time thereafter.
- The shift between the peaks of the temperature profile is marked at different vertical positions. This shows a "thermal lag" (inertia) of the fluid flow, which increases towards the centerline of the channel in the$y$-direction. In fact, this happens due to the thermal inertia of the fluid, and the harmonic heat flux imposed on the channel wall, $q''/q''_r = 1 + \sin(8\pi \times Fo)$.
- At a given axial position, the fluid temperature increases in radial locations closer to the channel wall. This occurs since; (i) the heat flux is imposed at the channel wall; and (ii) the fluid thermal inertia is less in regions near the wall.

Fig. 5 shows the variations of the local Nusselt number versus the Fourier number for three axial positions along the channel. The imposed wall heat flux and the fluid velocity are considered to vary harmonically over time, i.e., $\frac{q''}{q''_r} = 1 + \sin(8\pi \times Fo)$ and $U = 1 + \sin(8\pi \times Fo)$, respectively.

The following can be concluded from the trends in Fig. 5:

- At early times, before the initiation of the long-time response, "pure-conduction-like" heat transfer occurs, and the Nusselt number of all axial positions is only a function of time.
- The troughs of the Nusselt number at different axial positions are the same corresponding to the times, when the wall heat flux is zero.
- The values of the Nusselt number decrease at higher axial locations, i.e., further downstream. This is attributed to the boundary layer growth which insulates the channel wall, and reduces the rate of the heat transfer.
- For axial positions$X \geqslant 0.3$, the Nusselt number varies less than 4% with an increase in axial position. This indicates the existence of a fully-developed region similar to that of the constant slug flow under dynamic thermal load, see Ref. [32]. At $X = 0.3$, the boundary layers on the channel wall merge and the Nusselt number reaches its cyclic fully-developed value.
- In thermal fully-developed region: defined as the region where $X \geqslant 0.3$, the Nusselt number for pulsating channel flow under harmonic heat flux does not vary with the axial location any further. However, it can be an arbitrary function of time and the characteristics of the imposed heat flux.
- The main characteristic of the defined fully-developed region, $X \geqslant 0.3$, is the fact that the pulsation effect is fully damped. As such, the fully-developed Nusselt number for pulsating flow with a given angular frequency yields that of the constant slug flow condition.
- Using a curve fitting technique, the following compact relationship is developed in this study. This relationship can be used to find the fully-developed Nusselt number for laminar pulsating flow under dynamic heat flux for $\pi \leqslant \omega_1 \leqslant 10\pi$, $\pi \leqslant \omega_2 \leqslant 15\pi$, and $X \geqslant 0.3$. The maximum relative difference between the exact series solution, Eq. (25), and Eq. (30) is less than 10%.

$$Nu_a = \frac{1 + \sin(\omega_1 \times Fo)}{\frac{1}{3} + 0.16 \times \sin(\omega_1 \times Fo - 0.7)} \tag{30}$$

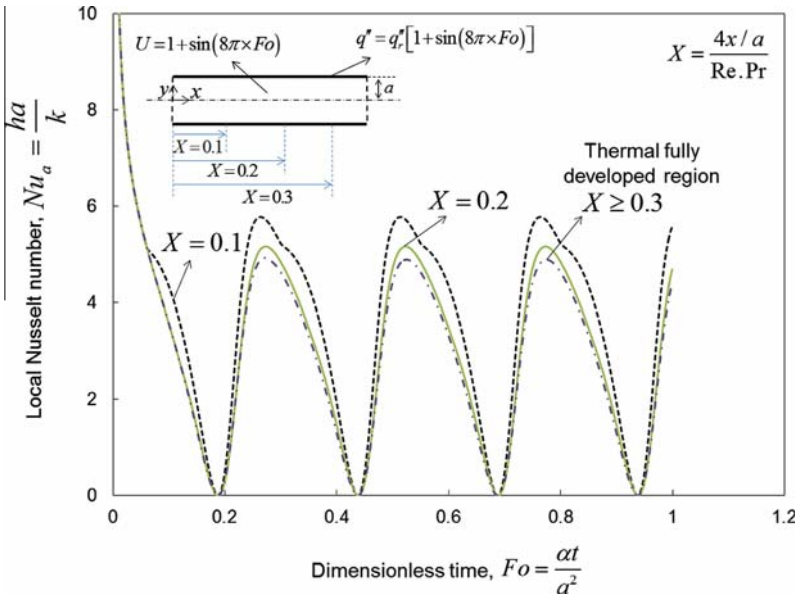

Fig. 5. Variations of the local Nusselt number against the Fourier number at different axial positions along the channel, when $\frac{q''}{q''_r} = 1 + \sin(8\pi \times Fo)$ and $U = 1 + \sin(8\pi \times Fo)$.

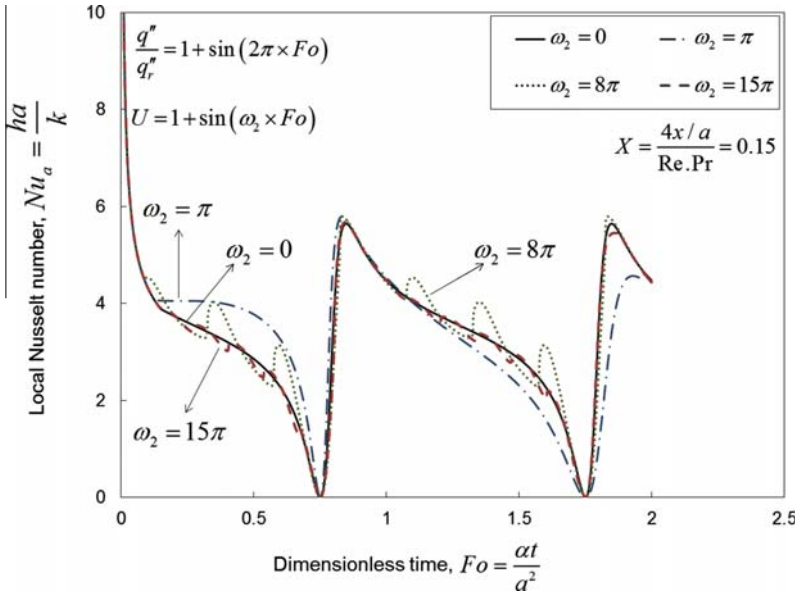

Fig. 6. Variations of the local Nusselt number versus dimensionless time (*Fo* number), for different values of the pulsation frequency ω_2, where $\frac{q''}{q''_r} = 1 + \sin(2\pi \times Fo)$.

Depicted in Fig. 6 are the variations of the local Nusselt number against the dimensionless time, *Fo*, for different values of the pulsation angular frequency, ω_2. The imposed wall heat flux is assumed to vary harmonically over time, i.e., $\frac{q''}{q''_r} = 1 + \sin(2\pi \times Fo)$. The results are shown for an arbitrary axial position, $X = 0.15$. The trends for other axial positions are similar.

The following conclusions can be drawn from Fig. 6:

- The local Nusselt number is zero at times when the imposed wall heat flux is zero.
- When the periods of the heat flux and pulsating velocity are $p_1 = \frac{2\pi}{\omega_1}$ and $p_2 = \frac{2\pi}{\omega_2}$, respectively, the period of fluid temperature is the least common multiple (LCM) of the periods. As such, as shown in Fig. 6, when $\omega_1 = 2\pi$ and $\omega_2 = 8\pi$, the period of the long-time temperature inside the fluid is:

$$\begin{cases} p_1 = \frac{2\pi}{\omega_1} = 1 \\ p_2 = \frac{2\pi}{\omega_2} = \frac{1}{4} \end{cases} \Rightarrow p = LCM(p_1, p_2) = 1 \tag{31}$$

- For a pulsating velocity with high angular frequency, the fluid does not follow the cycles of the velocity due to its thermal inertia, i.e., the fluctuations are filtered out. Therefore, for high angular frequencies, the flow acts as if the fluid velocity is constant at the average value associated with zero frequency for the sinusoidal term of the pulsating velocity, for this case. This is called the "cut-off" pulsation frequency.
- Dimensionless cut-off pulsation frequency: defined in this study as the angular frequency beyond which the pulsating Nusselt number lies within ± 5% of that of steady slug flow condition. As such, for a pulsating flow between parallel plates subjected to harmonic wall heat flux, $\omega_2 = \frac{\Omega_2 \times a^2}{\alpha} = 15\pi$ is the cut-off angular frequency.
- Regarding Eq. (15), the dimensionless cut-off frequency is a function of pulsation angular frequency, Ω_2 [rad/s], channel half width, $a[m]$, and fluid thermal diffusivity, $\alpha\left[\frac{m^2}{s}\right]$.

Fig. 7 shows the variations of the local Nusselt number at an arbitrarily chosen axial position, $X = 0.1$, against the Fourier number. Pulsating flow, $U = 1 + \sin(\pi/8 \times Fo)$, and constant slug flow, $U = \frac{u}{u_r} = 1$, are considered for the fluid velocity. In addition, the imposed wall heat flux is chosen arbitrarily as $\frac{q''}{q''_r} = 1 + \sin(\pi \times Fo)$. The following conclusions can be drawn from Fig. 7:

- For a constant velocity inside the conduit, the long-time Nusselt number fluctuates with the angular frequency of the imposed heat flux. In mathematical notation, $\omega_2 = 0 \Rightarrow p = p_1 = \frac{2\pi}{\omega_1} = 2$.
- For the considered pulsating velocity, $p_2 = \frac{2\pi}{\omega_2} = 16$, and the period of the imposed wall heat flux is, $p_1 = 2$. Therefore the period of fluctuations of the local Nusselt number for this instance is: $p = LCM(2,16) = 16$. The results will be repeated periodically from that time thereafter, $Fo \geqslant 16$.
- Over the first half cycle of the pulsation, $Fo \leqslant \frac{p_2}{2}$, the Nusselt number of pulsating velocity is higher than that of constant slug flow. In fact, this happens since during the first half cycle the sinusoidal term of pulsating velocity is positive. As a result, the flow rate inside the conduit is higher than that of constant slug-flow case.
- On the other hand, over the second half cycle, $\frac{p_2}{2} \leqslant Fo \leqslant p_2$, the sinusoidal term of the pulsating velocity becomes negative which in turn decreases the local Nusselt number of the pulsating flow compared to its constant slug-flow case.
- The time averaged *Nu* number is the area under the local Nu curves presented in Fig. 7, see Eq. (26). As such, over the defined period of fluctuation, $0 \leqslant Fo \leqslant p$, the time-averaged *Nu* number for pulsating flow is equal to that of constant slug-flow case.
- Modulating the pulsating velocity to maintain the oscillatory term positive can remarkably enhance the local Nusselt number at a given axial position, see Ref. [27]. This is called the "optimal pulsating velocity" which can be defined as, $U = \frac{u}{u_r} = 1 + |\sin(\omega_2 Fo)|$.

Fig. 8 depicts the variations of the local *Nu* number against the *Fo* number for different values of angular frequencies of the "optimal pulsating velocity", i.e., $U = \frac{u}{u_r} = 1 + |\sin(\omega_2 Fo)|$. The axial position is arbitrarily chosen at $X = 0.1$, and the imposed heat flux is assumed as, $\frac{q''}{q''_r} = 1 + \sin(\pi \times Fo)$.

The following can be concluded from Fig. 8:

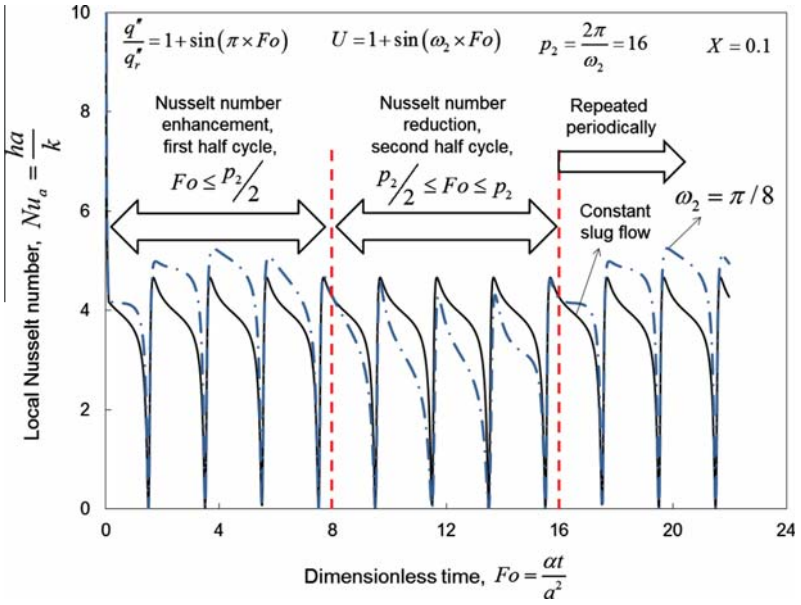

Fig. 7. Variations of the local Nusselt number at a given axial position, $X = 0.1$, against dimensionless time when $U = 1 + \sin(\frac{\pi}{8} \times Fo)$, and comparison with constant slug flow condition, $U = \frac{u}{u_r} = 1$.

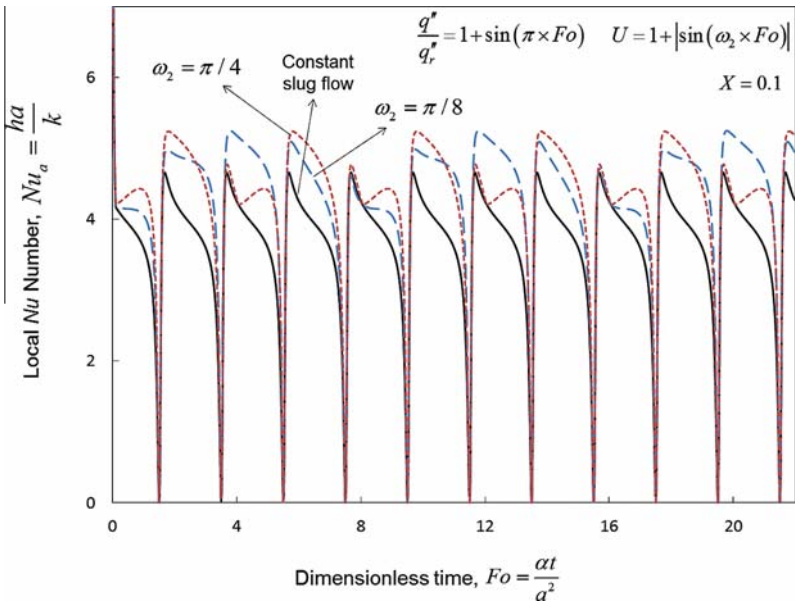

Fig. 8. Variations of the local *Nu* number against the *Fo* number for different angular frequencies where $U = 1 + |\sin(\omega_2 Fo)|$ and $\frac{q''}{q''_r} = 1 + \sin(\pi \times Fo)$.

- Irrespective of the angular frequency over a given period of time, the Nusselt number of the optimal pulsating flow is higher than that of the constant slug flow case.
- Comparing Figs. 7 and 8, it is evident that the local *Nu* number reduction which happened for the second half cycle of pulsating flow, $U = 1 + \sin(\omega_2 \times Fo)$, does not exist when using optimal pulsating flow, i.e., $U = 1 + |\sin(\omega_2 Fo)|$.
- As previously mentioned, the time averaged Nusselt number is the area below the local Nu curves presented in Fig. 8. Since this area is not the same for different angular frequencies, the time averaged Nusselt number depends on the angular frequency of the optimal pulsating flow.
- For a given harmonic wall heat flux, there is an "optimum angular frequency" which maximizes the time-averaged *Nu* number of optimal pulsating flow, $U = 1 + |\sin(\omega_2 Fo)|$, compared to its constant slug flow case, $U = \frac{u}{u_r} = 1$.

Fig. 9 shows the enhancement of time averaged Nusselt number as a result of using the optimal pulsating flow compared to the corresponding steady slug flow inside a duct. Three axial positions along the duct are chosen arbitrarily to show the time averaged *Nu* number enhancement. Note that the heat transfer enhancement is defined by the following relationship:

$$\Delta\overline{Nu} = \overline{Nu}_{\omega_{2\neq 0}} - \overline{Nu}_{\omega_{2=0}} \tag{32}$$

where $\Delta\overline{Nu}$ is the enhancement of the time-averaged *Nu*. In addition, $\overline{Nu}_{\omega_{2\neq 0}}$, and $\overline{Nu}_{\omega_{2=0}}$ are the time-averaged *Nu* for pulsating flow,

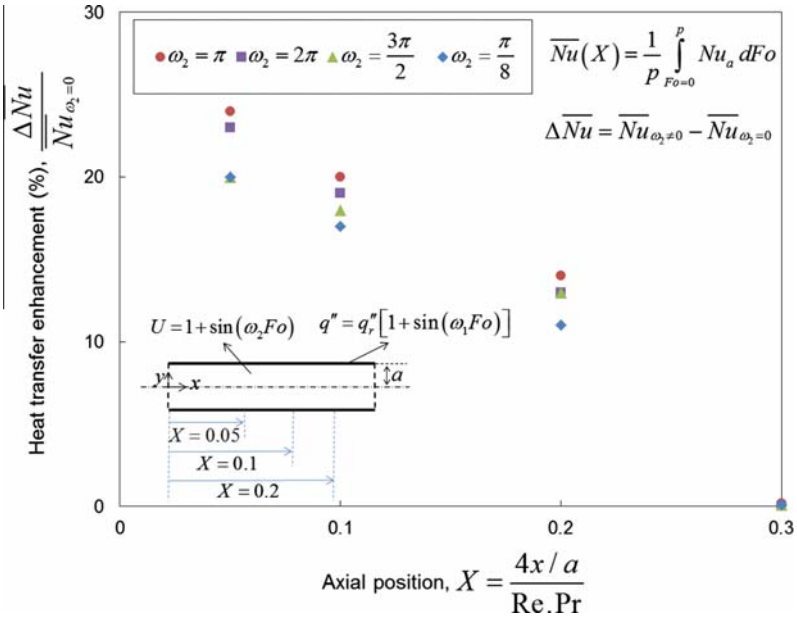

Fig. 9. Time averaged Nusselt number enhancement at different axial positions along the duct for various pulsation frequencies where $q'' = q_r''[1+\sin(\pi Fo)]$.

and its corresponding steady slug flow, respectively. As previously mentioned, the time averaged *Nu* in this study is defined over a period of fluctuation $0 \leqslant Fo \leqslant p$, see Eq. (26).

The following can be concluded from Fig. 9:

- Irrespective of angular frequency, the optimal pulsating flow, $U = 1 + |\sin(\omega_2 Fo)|$, increases the time averaged *Nu* number compared to constant slug flow condition.
- The time averaged Nusselt number increases up to 27% at the axial position, $X = 0.05$, compared to the corresponding constant slug-flow inside the duct.
- There is an "optimum frequency" which maximizes the *Nu* number enhancement. This value depends on the frequency of the imposed harmonic wall heat flux. For instance, when $\omega_1 = \pi$ this optimum value is, $\omega_{2,opt.} = \pi$.
- Downstream of the channel, the pulsation effects decrease; as a result, the heat transfer enhancement drops. For $X \geqslant 0.3$ the effects of pulsation are completely damped, and there is no heat transfer enhancement in the channel. Therefore, it is beneficial to design heat exchangers considering this length.
- The cost of using a controlled unsteady flow to enhance the Nusselt number is an increase in the input pumping power. This power requirement is a function of pressure gradient and flow rate in unsteady flow. The present model provides a platform for optimization analyses needed to design cost-effective 'green' cooling systems.

7. Conclusion

A new all-time range analytical model is developed to predict the thermal characteristics of pulsating channel flow under dynamic time-dependent heat flux and can be used to evaluate: (i) temperature distribution inside the fluid; (ii) fluid bulk temperature; and (iii) the Nusselt number. Compact relationships are developed to obtain the thermal entrance length and fully-developed Nusselt number. For the first the concept of optimal pulsating flow with an optimum frequency is introduced to maximize the time averaged Nusselt number. The highlights of this study can be listed as follows:

- The period of the temperature and Nusselt fluctuation inside the fluid is the least common multiple of the periods of the heat flux and the pulsating flow.
- There is a cut-off angular frequency for pulsating flow, i.e. $\omega_2 = 15\pi$, beyond which the Nusselt number yields that of the constant slug-flow condition.
- Effects of pulsation along the duct decrease as the thermal boundary layer grows. As such, for $X \geqslant 0.3$ the pulsation effects are fully-damped and the fluid flow reaches thermally fully-developed condition.
- There is an optimal pulsating flow with an optimum frequency which increases the heat transfer rate remarkably compared to the constant flow condition. Heat transfer enhancements of up to 27% can be achieved at the thermal entrance region.
- The optimum frequency depends on the angular frequency of the imposed heat flux. In other words, for an imposed harmonic wall heat flux, there is an optimum value for the pulsation frequency which maximizes the heat transfer enhancement.

The question whether the flow pulsation increases or reduces the heat transfer rate of convective cooling systems under time dependent thermal load is answered here as follows: the time averaged *Nu* number of pulsating flow is equal to that of steady flow over a period of fluctuation. However, within the context of "optimal velocity" up to 27% heat transfer enhancement is noted compared to steady slug flow case.

Conflict of interest

None declared.

Acknowledgments

This work was supported by Automotive Partnership Canada (APC), Grant No. APCPJ 401826-10. The authors would like to thank the support of the industry partner, Future Vehicle Technologies Inc. (British Columbia, Canada).

References

[1] M. Marz, A. Schletz, Power electronics system integration for electric and hybrid vehicles, in: 6th Int. Conf. Integr. Power Electron. Syst., 2010: Paper 6.1.
[2] K. Chau, C. Chan, C. Liu, Overview of permanent-magnet brushless drives for electric and hybrid electric vehicles, IEEE Trans. Ind. Electron. 55 (2008) 2246–2257.
[3] J. Garrison, M. Webber, Optimization of an integrated energy storage scheme for a dispatchable wind powered energy system, in: ASME 2012 6th Int. Conf. Energy Sustain. Parts A B San Diego, California, USA, 2012, pp. 1009–1019.
[4] J. Garrison, M. Webber, An integrated energy storage scheme for a dispatchable solar and wind powered energy system and analysis of dynamic parameters, Renew. Sustain. Energy. 3 (2011) 1–11.
[5] I. Mudawar, Assessment of high-heat-flux thermal management schemes, IEEE Trans. Components Packag. Technol. 24 (2001) 122–141.
[6] M.R.O. Panão, A.M. Correia, A.L.N. Moreira, High-power electronics thermal management with intermittent multijet sprays, Appl. Therm. Eng. 37 (2012) 293–301.
[7] M. O'Keefe, K. Bennion, A comparison of hybrid electric vehicle power electronics cooling options, in: Veh. Power Electron. Cool. Options, 2007, pp. 116–123.
[8] T.J. Lu, Thermal management of high power electronics with phase change cooling, Int. J. Heat Mass Transfer 43 (2000) 2245–2256.
[9] D.H. Lim, S.C. Kim, M.S. Kim, Thermal analysis of an electric water pump for internal combustion engine vehicles, Int. J. Autom. Technol. 14 (2013) 579–585.
[10] J.-S. Park, B.-G. Gu, J.-H. Choi, I.-S. Jung, Development of BLDC motor drive for automotive water pump systems, J. Int. Counc. Electr. Eng. 1 (2011) 395–399.
[11] R. Scott Downing, G. Kojasoy, Single and two-phase pressure drop characteristics in miniature helical channels, Exp. Therm. Fluid Sci. 26 (2002) 535–546.
[12] H. Bhowmik, C.P. Tso, K.W. Tou, Thermal behavior of simulated chips during power-off transient period, Packag. Technol. 65 (2003) 497–500.
[13] J.A. Clarck, V.S. Arpaci, Dynamic response of heat exchangers having internal heat sources, Trans. ASME 80 (1958) 612–624.
[14] J.A. Clarck, V.S. Arpaci, Dynamic response of heat exchangers having internal heat sources- Part II, Trans. ASME 80 (1958) 625–634.
[15] E.M. Sparrow, F.N. De Farias, Unsteady heat transfer in ducts with time-varying inlet temperature and participating walls, Int. J. Heat Mass Transfer 11 (1968) 837–853.
[16] K. Bennion, M. Thornton, Integrated vehicle thermal management for advanced vehicle propulsion technologies, SAE(2010-01-0836), 2010.
[17] R. Siegel, Transient heat transfer for laminar slug flow in ducts, Appl. Mech. 81 (1959) 140–144.
[18] E.M. Sparrow, R. Siegel, Thermal entrance region of a circular tube under transient heating conditions, in: Third U.S. Natl. Congr. Appl. Mech., 1958, pp. 817–826.
[19] R. Siegel, E.M. Sparrow, Transient heat transfer for laminar forced convection in the thermal entrance region of flat ducts, Heat Transfer 81 (1959) 29–36.
[20] R. Siegel, Heat transfer for laminar flow in ducts with arbitrary time variations in wall temperature, Trans. ASME. 27 (1960) 241–249.
[21] R. Siegel, M. Perlmutter, Heat transfer for pulsating laminar duct flow, Heat Transfer 84 (1962) 111–122.
[22] Z. Guo, H. Sung, Analysis of the Nusselt number in pulsating pipe flow, Int. J. Heat Mass Transfer 40 (1997) 2486–2489.
[23] M. Faghri, K. Javdani, A. Faghri, Heat transfer with laminar pulsating flow in a pipe, Lett. Heat Mass Transfer 6 (1979) 259–270.
[24] S. Uchida, The pulsating viscous flow superposed on the steady laminar motion of incompressible fluid in a circular pipe, Z. Angew. Math. Phys. 7 (1956) 403–422.
[25] R. Siegel, Influence of oscillation diffusion on heat transfer in a uniformly heated channel, Trans. ASME 109 (1987) 244–249.
[26] H.N. Hemida, M.N. Sabry, a. Abdel-Rahim, H. Mansour, Theoretical analysis of heat transfer in laminar pulsating flow, Int. J. Heat Mass Transfer 45 (2002) 1767–1780.
[27] G.J. Brereton, Y. Jiang, Convective heat transfer in unsteady laminar parallel flows, Phys. Fluids. 18 (2006) 103602.
[28] D.a. Nield, a.V. Kuznetsov, Forced convection with laminar pulsating flow in a channel or tube, Int. J. Therm. Sci. 46 (2007) 551–560.
[29] T. Zhao, P. Cheng, A numerical solution of laminar forced convection in a heated pipe subjected to a reciprocating flow, Int. J. Heat Mass Transfer 38 (1995) 3011–3022.
[30] B.H. Yan, L. Yu, Y.H. Yang, Forced convection with laminar pulsating flow in a tube, Heat Mass Transfer 47 (2010) 197–202.
[31] M. Fakoor-Pakdaman, M. Andisheh-Tadbir, M. Bahrami, Transient internal forced convection under arbitrary time-dependent heat flux, in: Proc. ASME Summer Heat Transfer Conf., Minneapolis, MN, USA, 2013.
[32] M. Fakoor-Pakdaman, M. Andisheh-Tadbir, M. Bahrami, Unsteady laminar forced-convective tube flow under dynamic time-dependent heat flux, J. Heat Transfer 136 (2013) 041706-1–041706-10.
[33] E. Kreyszig, H. Kreyszig, E.J. Norminton, Advanced Engineering Mathematics, tenth ed., John Wiley & Sons, n.d.
[34] M. Fakoor-Pakdaman, M. Ahmadi, M. Bahrami, Unsteady internal forced-convective flow under dynamic time-dependent boundary temperature, J. Thermophys. Heat Transfer 28 (2014) 463–473.
[35] R. Siegel, M. Perlmutter, Laminar heat transfer in a channel with unsteady flow and wall heating varying with position and time, Trans. ASME 85 (1963) 358–365.
[36] T. Von Karman, M.A. Biot, Mathematical Methods in Engineering, McGraw-Hill, New York, 1940.
[37] R. Siegel, Forced convection in a channel with wall heat capacity and with wall heating variable with axial position and time, Int. J. Heat Mass Transfer 6 (1963) 607–620.
[38] A. Bejan, Convection Heat Transfer, third ed., USA, 2004.

Appendix C
Temperature-aware time-varying convection over a duty cycle for a given system thermal-topology

International Journal of Heat and Mass Transfer 87 (2015) 418–428

Contents lists available at ScienceDirect

International Journal of Heat and Mass Transfer

journal homepage: www.elsevier.com/locate/ijhmt

Temperature-aware time-varying convection over a duty cycle for a given system thermal-topology

M. Fakoor-Pakdaman, Mehran Ahmadi, Majid Bahrami *

Laboratory for Alternative Energy Conversion (LAEC), School of Mechatronic Systems Engineering, Simon Fraser University, Surrey, BC, V3T 0A3, Canada

ARTICLE INFO

Article history:
Received 28 September 2014
Received in revised form 2 April 2015
Accepted 2 April 2015
Available online 24 April 2015

Keywords:
Convection
Dynamic systems
Transient
Experiment
Duty cycle

ABSTRACT

Smart dynamic thermal management (SDTM) is a key enabling technology for optimal design of the emerging transient heat exchangers/heat sinks associated with advanced power electronics and electric machines (APEEM). The cooling systems of APEEM undergo substantial transition as a result of time-varying thermal load over a duty cycle. Optimal design criteria for such dynamic cooling systems should be achieved through addressing internal forced convection under time-dependent heat fluxes. Accordingly, an experimental study is carried out to investigate the thermal characteristics of a laminar fully-developed tube flow under time-varying heat fluxes. Three different transient scenarios are implemented under: (i) step; (ii) sinusoidal; and (iii) square-wave time-varying thermal loads. Based on the transient energy balance, exact closed-form relationships are proposed to predict the coolant bulk temperature over time for the aforementioned scenarios. In addition, based on the obtained experimental data and the methodology presented in Fakoor-Pakdaman et al. (2014), semi-analytical relationships are developed to calculate: (i) tube wall temperature; and (ii) the Nusselt number over the implemented duty cycles. It is shown that there is a 'cut-off' angular frequency for the imposed power beyond which the heat transfer does not feel the fluctuations. The results of this study provide the platform for temperature-aware dynamic cooling solutions based on the instantaneous thermal load over a duty cycle.

1. Introduction

Smart dynamic thermal management (SDTM) is a transformative technology for efficient cooling of advanced power electronics and electric machines (APEEM). APEEM has applications in: (i) emerging cleantech systems, e.g., powertrain and propulsion systems of hybrid/electric/fuel cell vehicles (HE, E, FCV) [1,2]; (ii) sustainable/renewable power generation systems (wind, solar, tidal) [3,4]; (iii) information technology (IT) services (data centers) and telecommunication facilities [5–7]. The thermal load of APEEM substantially varies over a duty cycle; Downing and Kojasoy [8] predicted heat fluxes of $150-200$ [W/cm^2] and pulsed transient heat loads up to 400 [W/cm^2], for the next-generation insulated gate bipolar transistors (IGBTs). The non-uniform and time-varying nature of the heat load is certainly a key challenge in maintaining the temperature of the electronics within its safe and efficient operating limits [9]. As such, the heat exchangers/heat sinks associated with APEEM operate periodically over time and never attain a steady-state condition. Conventionally, cooling systems are conservatively designed for a nominal steady-state or worst-case scenarios, which may not properly represent the thermal behavior of various applications or duty cycles [10]. The state-of-the-art approach is utilizing SDTM to devise a variable-capacity cooling infrastructure for the next-generation APEEM and the associated engineering applications [7]. SDTM responds to thermal conditions by adaptively adjusting the power-consumption profile of APEEMs on the basis of feedback from temperature sensors [5]. Therefore, supervisory thermal control strategies can then be established to minimize energy consumption and safeguard thermal operating conditions [9]. As such, the performance of transient heat exchangers is optimized based on the system "thermal topology", i.e., instantaneous thermal load (heat dissipation) over a duty cycle. For instance, utilizing SDTM in designing the cooling systems of a data center led to significant energy saving, up to 20%, compared to conventionally cooled facility [7]. In addition, in case of the HE/E/FCV, SDTM improves the vehicle overall efficiency, reliability and fuel consumption as well as reducing the weight and carbon foot print of the vehicle [11].

Therefore, there is a pending need for an in-depth understanding of instantaneous thermal characteristics of transient cooling systems over a given duty cycle. However, there are only a few analytical/experimental studies in the open literature on this topic.

* Corresponding author. Tel.: +1 (778) 782 8538; fax: +1 (778) 782 7514.
E-mail addresses: mfakoorp@sfu.ca (M. Fakoor-Pakdaman), mahmadi@sfu.ca (M. Ahmadi), mbahrami@sfu.ca (M. Bahrami).

http://dx.doi.org/10.1016/j.ijheatmasstransfer.2015.04.011
0017-9310/

Nomenclature

a	heat flux amplitude, [W/m^2]
c_p	heat capacity, [J/kg/K]
c_n	coefficients in Eq. (10)
D	tube diameter, [m]
Fo	Fourier number, $= \alpha t/R^2$
h	heat transfer coefficient, [W/m^2/K]
J	Bessel function
k	thermal conductivity, [W/m/K]
L	length, [m]
m	integer number, Eq. (21)
$\dot{m}$	mass flow rate, [kg/s]
Nu_D	local Nusselt number, $= [h(x,t) \times D]/k$
$\overline{Nu}_D$	average Nusselt number, $\frac{1}{L_2}\int_0^{L_2} Nu_D dx$
P	power, [W]
p	period of the imposed power, [s]
Pr	Prandtl number, $= \nu/\alpha$
q''	thermal load (heat flux), [W/m^2]
R	tube radius, [m]
r	radial coordinate measured from tube centerline, [m]
Re	Reynolds number, $= UD/\upsilon$
T	temperature, [K]
t	time, [s]
U	velocity, [m/s]
X	dimensionless axial distance, $= 4x/\mathrm{Re}\cdot\mathrm{Pr}\cdot D$
x	axial distance from the entrance of the heated section, [m]

Greek letters

α	thermal diffusivity, [m^2/s]
ν	kinematic viscosity, [m^2/s]
ρ	fluid density, [kg/m^3]
λ_n	Eigenvalues in Eq. (10)
Λ_n	values defined in Eq. (10)
θ	dimensionless temperature, $= \frac{T-T_{in}}{q''_r D/k}$
Ψ	a function defined in Eq. (23)
Υ	a function defined in Eq. (18)
β_n	positive roots of the Bessel function, $J_1(\beta_n) = 0$
ω_1	angular frequency of the sinusoidal heat flux, $= (2\pi R^2)/(p_1\alpha)$
ω_m	dimensionless number characterizing the square-wave heat flux, $= [(2m+1)\pi R^2]/(p_2\alpha)$

Subscripts

1	sinusoidal scenario
2	square-wave scenario
in	inlet
m	mean or bulk value
out	outlet
r	reference value
w	wall

This study is focused on transient internal forced convection as the main representative of the thermal characteristics of dynamic heat exchangers under arbitrary time-varying heat fluxes. In fact, such analyses lead to devising "temperature-aware" cooling solutions based on the system thermal topology (power management) over a given duty cycle. The results of this work will provide a platform for the design, validation and building new smart thermal management systems that can actively and proactively control the cooling systems of APEEMs and similar applications.

1.1. Present literature

Siegel [12–17] pioneered study on transient internal forced-convective heat transfer. Siegel [12] studied laminar forced convection heat transfer for a slug tube-flow where the walls were given a step-change in the heat flux or alternatively a step-change in the temperature. Moreover, the tube wall temperature of channel slug flows for particular types of position/ time-dependent heat fluxes was studied in the literature [17,18]. Most of the pertinent literature was done for laminar slug flow inside a duct. The slug flow approximation reveals the essential physical behavior of the system, while it enables obtaining exact mathematical solution for various boundary conditions. Using this simplification, one can study the effects of various boundary conditions on transient heat transfer without tedious numerical computations [12,15]. Siegel [15] investigated transient laminar forced convection with fully developed velocity profile following a step change in the wall temperature. The obtained solution was much more complex than the response for slug flow which was presented in [12]. It was reported that the results for both slug and fully-developed flows showed the same trends; however, the slug flow under-predicted the tube wall temperature compared to the Poiseuille flow case. Fakoor-Pakdaman et al. [19–22] conducted a series of analytical studies on the thermal characteristics of internal forced convection over a duty cycle to reveal the thermal characteristics of the emerging dynamic convective cooling systems. Such thermal characteristics were obtained for steady slug flow under: (i) dynamic thermal load [19,20]; (ii) dynamic boundary temperature [21]; and (iii) unsteady slug flow under time-varying heat flux [22]. Most literature on this topic is analytical-based; a summary is presented in Table 1.

Table 1
Summary of existing literature on convection under dynamically varying thermal load.

Author	Notes
Siegel [12]	✓ Reported temperature distribution inside a circular tube and between two parallel plates × Limited to step wall heat flux × Limited to slug flow condition × Limited to an analytical-based approach without validation/verification
Siegel [15]	✓ Reported temperature distribution inside a circular tube or between two parallel plates ✓ Covered thermally developing and fully-developed regions ✓ Considered fully-developed velocity profile × Limited to step wall temperature × Nusselt number was defined based on the tube wall and inlet fluid temperature × Limited to an analytical-based approach without validation/verification
Fakoor-Pakdaman et al. [20]	✓ Reported temperature distribution inside a circular tube ✓ Defined the Nusselt number based on the tube wall and fluid bulk temperature × Limited to slug flow condition × The analytical results were only verified numerically
Fakoor-Pakdaman et al. [22]	✓ Reported temperature distribution inside a circular tube ✓ Considered transient velocity profile for the fluid flow × Limited to sinusoidal wall heat flux. × The analytical results were only verified numerically

Our literature review indicates:

- There is no experimental work on transient internal forced-convection over a duty cycle under a time-varying thermal load.
- The presented models in literature for internal flow under dynamic thermal load are limited to slug flow conditions.
- No analytical model exists to predict the thermal characteristics of fully developed flow over a harmonic duty cycles.

Although encountered quite often in practice, the unsteady convection of fully-developed tube flow under time-varying thermal load over a duty cycle has never been addressed in literature; neither experimentally nor theoretically. In other words, the answer to the following question is not clear: "how the thermal characteristics of emerging dynamic cooling systems vary over a duty cycle under time-varying thermal loads (heat fluxes) of the electronics and APEEM?".

An experimental testbed is fabricated to investigate the thermal characteristics of a fully-developed tube flow under different transient scenarios: (i) step; (ii) sinusoidal; and (iii) square-wave heat fluxes. Based on the transient energy balance, exact closed-form relationships are proposed to predict the fluid bulk temperature under the studied transient scenarios (duty cycles). The accuracy of the experimental data is also verified by the obtained results for the fluid bulk temperature. Based on the obtained experimental data and the methodology presented in [13,18], semi-analytical relationships are developed to calculate the: (i) tube wall temperature; and (ii) the Nusselt number over the studied duty cycles. Moreover, easy-to-use relationships are presented as the short-time asymptotes for tube wall temperature and the Nusselt number for the case of step wall heat flux. At early times, $Fo < 0.2$, such asymptotes deviate only slightly from the obtained series solutions as the short-time responses; maximum deviation less than 2%.

2. Real-time data measurement

2.1. Experimental setup

The experimental setup fabricated for this work is shown schematically in Fig. 1. The fluid, distilled water, flows down from an upper level tank and enters the calming section. Adjusting the installed valves, the water level inside the upper-level tank is maintained constant during each experiment to attain the desired values of the constant flow during each experiment.

Following [23], the calming section is long enough so that the fluid becomes hydrodynamically fully-developed at the beginning of the heated section. A straight copper tube with 12.7 ± 0.02 [mm] outer diameter, and 11.07 ± 0.02 [mm] inner diameter is used for the calming and heated sections. The length of the former is $L_1 = 500$ [mm], while the heated section is $L_2 = 1900$ [mm] long. Two flexible heating tapes, STH series Omega, are wrapped around the entire heated section. Four T-type thermocouples are mounted on the heated section at axial positions in [mm] of T1(300), T2(600), T3(1000), and T4(1700) from the beginning of the heated section to measure the wall temperature. In addition, two T-type thermocouples are inserted into the flow at the inlet and outlet of the test section to measure the bulk temperatures of the distilled water. The heating tapes are connected in series, while each is 240 [V] and 890 [W]. To apply the time-dependent power on the heated section, two programmable DC power supplies (Chroma, USA) are linked in a master and slave fashion, and connected to the tape heaters. The maximum possible power is 300 [W]. To reduce heat losses towards the surrounding environment, a thick layer (5 [cm]) of fiber-glass insulating blanket is wrapped around the entire test section including calming and heated sections. After the flow passes through the test section, the flow rate is measured by a precise micro paddlewheel flow meter, FTB300 series Omega. Finally, the fluid returns to the surge tank which is full of ice-water mixture. As a result, the fluid is cooled down, and then is pumped to the main tank at the upper level. All the thermocouples are connected to a data acquisition system composed of an SCXI-1102 module, an SCXI-1303 terminal and an acquisition board; all these components are from National Instrument. The programmable DC power supplies are controlled via standard LabVIEW software (National Instrument), to apply the time-dependent powers. As such, different unsteady thermal duty cycles are attained by applying three different scenarios for the imposed power: (i) step; (ii) sinusoidal; and (iii) square-wave. As such, real-time data are obtained for transient thermal characteristics of the system over such duty cycles; see Section 2.2 for more detail. The accuracy of the measurements and the uncertainties of the derived values are given in Table 2.

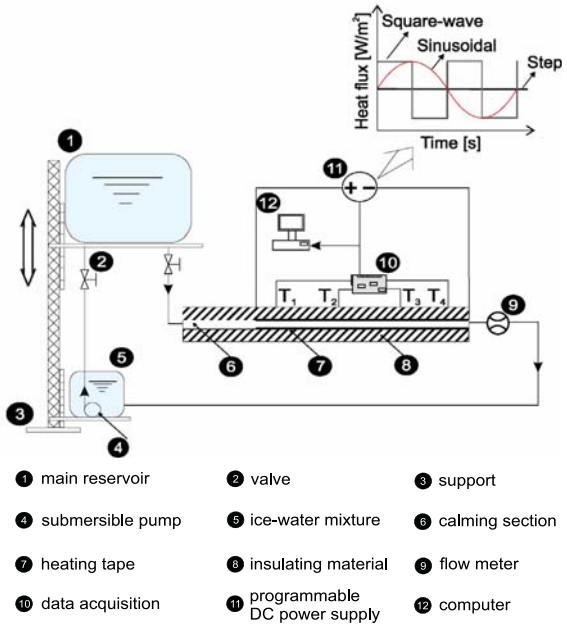

Fig. 1. Schematic view of the fabricated experimental setup.

Table 2
Summary of calculated experimental uncertainties.

Primary measurements		Derived quantities	
Parameter	Uncertainties	Parameter	Uncertainties (%)
$\dot{m}$	6%	Re	7.6
P [W]	3%	h [W/m^2/K]	8.1
$T(T_{in}, T_{out}, T_m)$	0.5[°C]	Nu	8.3

2.2. Data processing

In most Siegel works [13,18], the transient thermal behavior of a system is evaluated based on the dimensionless wall heat flux considering the difference between the local tube wall and the initial fluid temperature. We are of the opinion that an alternative definition of the local Nusselt number has a more 'physical' meaning, i.e., based on the local difference between the channel wall and the fluid bulk temperature at each axial location; this is consistent with [24,25]. It should be emphasized that the definition of the Nusselt number is an arbitrary choice and will not alter the final results. As such, the overall transient convective heat transfer coefficient is defined as follows:

$$\overline{h}(L_2,t)=\frac{q''(t)}{\overline{T_w}(t)-\overline{T_m}(t)} \tag{1}$$

where $q''(t)$ is the applied time-dependent heat flux, $\overline{T_w}(t)$ is the average tube wall temperature, and $\overline{T_m}(t)$ is the arithmetic average of inlet and outlet fluid bulk temperatures. Therefore, the definitions of different parameters in Eq. (1) are given below:

$$\overline{T_w}(t)=\frac{1}{4}\sum_{i=1}^{4}T_i(t) \tag{2}$$

$$\overline{T_m}(t)=\frac{T_{in}(t)+T_{out}(t)}{2} \tag{3}$$

$$q''(t)=\frac{P(t)}{\pi DL_2} \tag{4}$$

where T_{in} and T_{out} are the inlet and outlet fluid temperatures, respectively. Moreover, $P(t)$ is the applied transient power and L_2 is the length of the heated section. The overall Nusselt number is also obtained by the following relationship.

$$\overline{Nu}_D(L_2,t)=\frac{\overline{h}(L_2,t)\times D}{k} \tag{5}$$

where, D and k are the tube diameter and fluid thermal conductivity, respectively. The thermo-physical properties of the distilled water used in this study are determined at the arithmetic average temperature, $\overline{T_m}(t)$, from [23].

3. Model development

In this section, it is intended to present closed-form solutions for the thermal characteristics of laminar tube flow under the transient scenarios, i.e., (i) step; (ii) sinusoidal; and (iii) square-wave heat fluxes. Following Siegel [13] and Fakoor-Pakdaman et al. [20,22], closed-form relationships are obtained to calculate: (i) tube wall temperature; (ii) fluid bulk temperature; and (iii) the Nusselt number, for the above-mentioned time-dependent heat fluxes.

The methodology presented in [13] proceeds as follows: consider a position x in the channel through which the fluid is flowing with average velocity U. A fluid element starting from the entrance of the channel will require time duration $t=x/U$ to reach the x location. In the region where $x/U \geqslant t$, i.e., short-time response, there is no penetration of the fluid which was at the entrance when the transient began. Therefore, the short-time response corresponds to pure transient heat conduction, and the effect of heat convection is zero. However, for the region $x/U \leqslant t$, the heat transfer process occurs via the fluid that entered the channel after the transient was initiated. This forms the long-time response which is equal to short time response at the transition time, i.e., $t=x/U$. Therefore, the solution composed of two parts that should be considered separately: (i) short-time and (ii) long-time responses. More detail regarding the short- and long-time responses were presented elsewhere [19–22].

3.1. Step power (heat flux)

For this scenario, the imposed heat flux is considered in the following form:

$$q''(t)=\begin{cases}0 & t<0\\ q_r''=\text{const.} & t\geqslant 0\end{cases} \tag{6}$$

where q_r'' (offset), is a constant value over the entire heating period. When a tube flow is suddenly subjected to a step heat flux, the short-time response for the tube wall temperature is obtained as follows [12]:

$$\theta_w=Fo+\frac{1}{8}-\sum_{n=1}^{\infty}\frac{e^{-\beta_n^2 Fo}}{\beta_n^2} \tag{7}$$

where β_n are the positive roots of $J_1(\beta)=0$, and $J_1(\beta)$ are the first-order Bessel functions of the first kind, respectively. In addition, θ_w and Fo are the dimensionless wall temperature and dimensionless time, respectively. Such dimensionless numbers are defined as follows:

$$\theta_w=\frac{T_w-T_{in}}{q_r''D/k};\quad Fo=\frac{\alpha t}{R^2} \tag{8}$$

where T_w, T_{in}, k, and α are tube wall temperature, inlet temperature, fluid thermal conductivity, and diffusivity, respectively. It should be noted that when $Fo\to 0$, Fakoor-Pakdaman and Bahrami [26], presented a compact easy-to-use relationship for Eq. (7) as the short-time asymptote for the tube wall temperature. For $Fo<0.2$, the maximum deviation between the series solution, Eq. (7), and the compact model, Eq. (9), is less than 2%.

$$\theta_{w,Fo\to 0}=\left(\sqrt{\frac{\pi}{Fo}}-\frac{\pi}{4}\right)^{-1} \tag{9}$$

In addition, the long-time asymptote can be obtained by a well-known Graetz solution [25] as given below:

$$\theta_w=X+\frac{11}{48}+\frac{1}{2}\sum_{n=1}^{\infty}C_n\Lambda_n\exp\left(-\frac{\lambda_n^2 X}{2}\right) \tag{10}$$

where $X=\frac{4x/D}{\mathrm{Re}\cdot\mathrm{Pr}}$ is the dimensionless axial location. Besides, the values of λ_n and $C_n\Lambda_n$ are tabulated in [25]. In addition, the fluid bulk temperature can be obtained by performing a heat balance on an infinitesimal differential control volume of the flow;

$$\dot{m}c_pT_m+q''(\pi D)dx-\left(\dot{m}c_pT_m+\dot{m}c_p\frac{\partial T_m}{\partial x}dx\right)=\rho c_p\left(\frac{\pi D^2}{4}\right)\frac{\partial T_m}{\partial t}dx \tag{11}$$

where $\dot{m}$ is the fluid mass flow rate, c_p and T_m are specific heat and fluid bulk temperature, respectively. The dimensionless form of Eq. (11) is:

$$\frac{q''(X,Fo)}{q_r''}=\frac{\partial\theta_m}{\partial Fo}+\frac{\partial\theta_m}{\partial X} \tag{12}$$

where q_r'' is the offset around which the imposed heat flux fluctuates. Eq. (12) is a first-order partial differential equation which can be solved by the method of characteristics [27]. The short- and long-time asymptotes for the fluid bulk temperature for the case of step heat flux are [26];

$$\theta_m=\begin{cases}Fo & \text{short}-\text{time asymptote}\\ X & \text{Long}-\text{time asymptote}\end{cases} \tag{13}$$

Following Fakoor-Pakdaman and Bahrami [26], the short-time asymptote for the average Nusselt number under a step heat flux can be calculated by a compact relationship, Eq. (14).

$$Nu_D(t)_{Fo\to 0}=\frac{h(t)\times D}{k}=\sqrt{\frac{\pi}{Fo}} \tag{14}$$

In addition, the following well-known Shah equation [28] is used as the long-time asymptote for the average Nusselt number of laminar flow under constant wall heat flux.

$$Nu_{0-x,D}=\begin{cases}1.953X^{-1/3} & \text{for}\quad X\leqslant 0.03\\ 4.364+\frac{0.0722}{X} & \text{for}\quad X>0.03\end{cases} \tag{15}$$

3.2. Sinusoidal power (heat flux)

For this case, the applied heat flux is considered in the following form.

$$q'' = q''_r + a \times \sin\left(\frac{2\pi}{p_1}t\right) \tag{16}$$

where, q''_r [W/m^2], a [W/m^2], and p_1 [s] are the offset, amplitude, and period of the imposed heat flux. The dimensionless form of Eq. (16) is:

$$\frac{q''}{q''_r} = 1 + \left(\frac{a}{q''_r}\right) \times \sin(\omega_1 Fo) \tag{17}$$

where, $\omega_1 = \frac{2\pi R^2}{p_1 \alpha}$ is the dimensionless angular frequency of the imposed heat flux, and R [m] is the tube radius. Substituting Eq. (17) into Eq. (12), closed-form relationships are obtained for the short- and long-time responses for fluid bulk temperature, see Eqs. (18.a) and (18.b). In addition, following the methodology presented in [20], semi-analytical relationships are proposed to predict the tube wall temperature, Eqs. (19.a) and (19.b). Table 3 presents a summary of the results obtained for short- and long-time responses of tube wall and fluid bulk temperatures under a sinusoidal heat flux. It should be noted that C_1 in Eqs. (19.a) and (19.b), is a coefficient which depends on the velocity profile of the fluid inside the tube. It takes the value of unity for slug flow inside the duct, i.e., uniform velocity across the tube, see [20]. For a parabolic velocity profile (poiseuille flow), the value of such coefficient is obtained in this study empirically, and will be discussed in Section 4, where the functions $\Upsilon_{1,n}$ and $\Upsilon_{2,n}$ are defined as:

$$\begin{cases} \Upsilon_{1,n} = \frac{e^{-\beta_n^2 Fo}}{\beta_n^2} + \frac{\omega_1 (a/q''_r)}{\omega_1^2 + \beta_n^4} \times \left[\cos(\omega_1 Fo) - \frac{\beta_n^2}{\omega_1} \times \sin(\omega_1 Fo) - e^{-\beta_n^2 Fo}\right] \\ \Upsilon_{2,n} = \frac{e^{-\beta_n^2 X}}{\beta_n^2} + \frac{\omega_1 (a/q''_r)}{\omega_1^2 + \beta_n^4} \times \left\{\cos(\omega_1 Fo) - \frac{\beta_n^2}{\omega_1} \times \sin(\omega_1 Fo) + e^{-\beta_n^2 X} \times \begin{Bmatrix} \frac{\beta_n^2}{\omega_1} \times \sin[\omega_1 (Fo - X)] - \\ \cos[\omega_1 (Fo - X)] \end{Bmatrix}\right\} \end{cases} \tag{18}$$

In addition, the short- and long-time local Nusselt numbers can be calculated by the following relationship:

$$Nu_D(x,t) = \frac{q'' D/k}{T_w - T_m} = C_2 \left[\frac{1 + \sin(\omega_1 Fo)}{\theta_w - \theta_m}\right] \tag{19}$$

Again C_2 is a coefficient which takes a value of unity for slug flow inside the duct [20]. The value of such coefficient for a parabolic velocity in this study is obtained empirically, and discussed in Section 4 of this study. Accordingly, the average Nusselt number over the entire length of the heated section, L_2, is calculated as follows:

$$\overline{Nu_D}(L_2,t) = \frac{1}{L_2}\int_0^{L_2} Nu_D dx \tag{20}$$

3.3. Square-wave power (heat flux)

The Fourier series for a square-wave heat flux with offset q''_r, amplitude a, and period p_2 is, [29]:

$$q'' = q''_r + a \times \sum_{m=0,1,2}^{\infty} \frac{1}{2m+1} \sin\left[\frac{(2m+1)\pi}{p_2}t\right] \tag{21}$$

The dimensionless form of Eq. (21) is:

$$\frac{q''}{q''_r} = 1 + \left(\frac{a}{q''_r}\right) \times \sum_{m=0,1,2}^{\infty} \frac{1}{2m+1} \sin(\omega_m Fo) \tag{22}$$

where $\omega_m = \frac{(2m+1)\pi R^2}{p_2 \alpha}$ is a dimensionless number which characterizes the behavior of the square-wave heat flux. Substituting Eq. (22) into Eq. (12), closed-form relationships are obtained for the short- and long-time responses for fluid bulk temperature, see Eqs. (25.a) and (25.b). In addition, following the methodology presented in [20], semi-analytical relationships are proposed to predict the tube wall temperature, Eqs. (26.a) and (26.b). Table 4 presents a summary of the results obtained for short- and long-time responses of tube wall and fluid bulk temperatures under a square-wave heat flux.

Table 3
Tube wall and fluid bulk temperatures for transient scenario II: sinusoidal heat flux, [20].

Short-time response, $X \leqslant Fo$	Long-time response, $X \geqslant Fo$
Fluid bulk temperature, $\theta_m = \frac{T_m - T_{in}}{q''_r D/k}$	
$= Fo + \frac{(a/q''_r)}{\omega_1}[1 - \cos(\omega_1 Fo)]$ (18.a)	$= X + \frac{(a/q''_r)}{\omega_1}\{\cos[\omega_1(Fo - X)] - \cos(\omega_1 Fo)\}$ (18.b)
Tube wall temperature, $\theta_w = \frac{T_w - T_{in}}{q''_r D/k}$	
$= C_1 \left\{ \begin{matrix} Fo + \frac{(a/q''_r)}{\omega_1} \times [1 - \cos(\omega_1 Fo)] \\ + \frac{1}{8} - \sum_{n=1}^{\infty} \Upsilon_{1,n} \end{matrix} \right\}$ (19.a)	$= C_1 \left\{ \begin{matrix} X + \frac{(a/q''_r)}{\omega_1} \times \begin{Bmatrix} \cos[\omega_1(Fo - X)] \\ -\cos(\omega_1 Fo) \end{Bmatrix} \\ + \frac{1}{8} - \sum_{n=1}^{\infty} \Upsilon_{2,n} \end{matrix} \right\}$ (19.b)

Table 4
Tube wall and fluid bulk temperatures for transient scenario III: square-wave heat flux, Ref. [20].

Short-time response, $X \leqslant Fo$	Long-time response, $X \geqslant Fo$
Fluid bulk temperature, $\theta_m = \frac{T_m - T_{in}}{q''_r D/k}$	
$= X + \left(\frac{a}{q''_r}\right) \times \sum_{m=0,1,2}^{\infty} \frac{1}{\omega_m (2m+1)} \begin{Bmatrix} \cos[\omega_m (Fo - X)] \\ -\cos(\omega_m Fo) \end{Bmatrix}$ (25.a)	$= X + \left(\frac{a}{q''_r}\right) \times \sum_{m=0,1,2}^{\infty} \frac{1}{\omega_m (2m+1)} \begin{Bmatrix} \cos[\omega_m (Fo - X)] \\ -\cos(\omega_m Fo) \end{Bmatrix}$ (25.b)
Tube wall temperature, $\theta_w = \frac{T_w - T_{in}}{q''_r D/k}$	
$= C_2 \left\{ \begin{matrix} Fo + \\ (a/q''_r) \times \sum_{m=0,1,2}^{\infty} \frac{1}{\omega_m (2m+1)} \times \begin{bmatrix} 1 \\ -\cos(\omega_m Fo) \end{bmatrix} \\ + \frac{1}{8} - \sum_{n=1}^{\infty} \Psi_{1,n} \end{matrix} \right\}$ (26.a)	$= C_2 \left\{ \begin{matrix} X + \\ \frac{(a/q''_r)}{\omega_m} \times \sum_{m=0,1,2}^{\infty} \frac{1}{\omega_m (2m+1)} \times \begin{Bmatrix} \cos[\omega_m (Fo - X)] \\ -\cos(\omega_m Fo) \end{Bmatrix} \\ + \frac{1}{8} - \sum_{n=1}^{\infty} \Psi_{2,n} \end{matrix} \right\}$ (26.b)

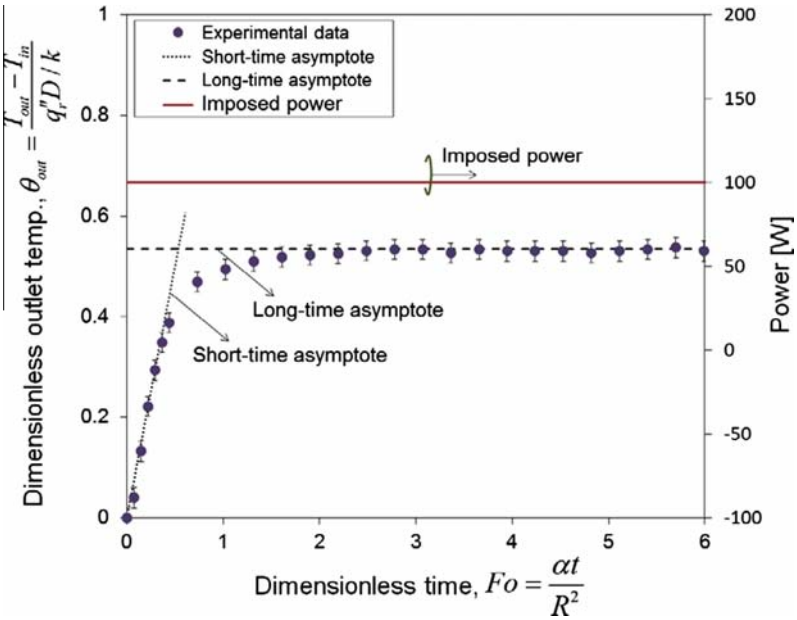

Fig. 2. Short- and long-time asymptotes for outlet fluid bulk-temperature and comparison with experimental data for the step power. ($\dot{m} = 3.3 \pm 0.198$ [gr/s]).

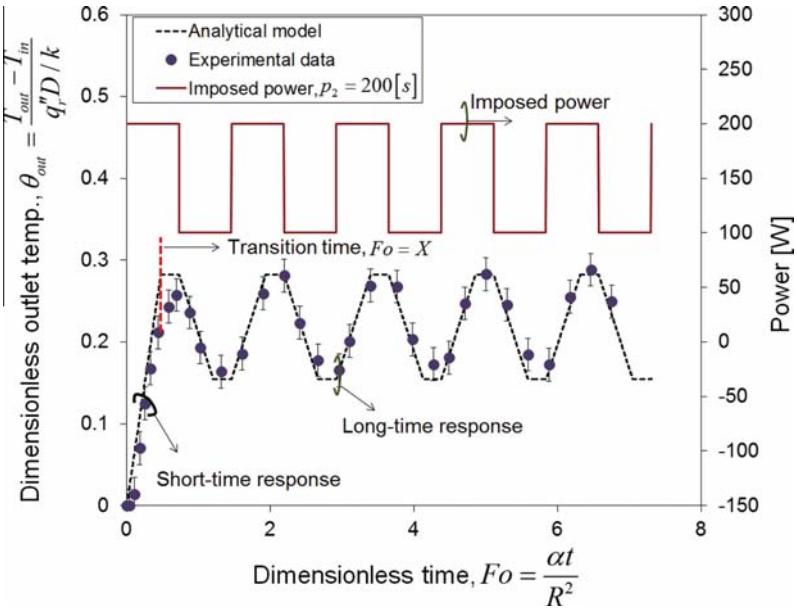

Fig. 3. Short- and long-time responses for outlet fluid bulk temperature and comparison with experimental data for the square-wave power. ($\dot{m} = 3.6 \pm 0.216$ [gr/s]).

The functions $\Psi_{1,n}$ and $\Psi_{2,n}$ are defined as:

$$\begin{cases} \Psi_{1,n} = \frac{e^{-\beta_n^2 Fo}}{\beta_n^2} + (a/q''_r) \times \sum_{m=0,1,2}^{\infty} \frac{\omega_m}{(2m+1)(\omega_m^2+\beta_n^4)} \times \left[\cos(\omega_m Fo) - \frac{\beta_n^2}{\omega_m} \times \sin(\omega_m Fo) - e^{-\beta_n^2 Fo}\right] \\ \Psi_{2,n} = \frac{e^{-\beta_n^2 X}}{\beta_n^2} + (a/q''_r) \times \sum_{m=0,1,2}^{\infty} \frac{\omega_m}{(2m+1)(\omega_m^2+\beta_n^4)} \times \left\{ \begin{cases} \cos(\omega_m Fo) - \frac{\beta_n^2}{\omega_m} \times \sin(\omega_m Fo) + \\ e^{-\beta_n^2 X} \times \left\{ \frac{\beta_n^2}{\omega_m} \times \sin[\omega_m (Fo - X)] - \\ \cos[\omega_m (Fo - X)] \end{cases} \right\} \end{cases} \tag{23}$$

In addition, the short- and long-time local Nusselt numbers can be obtained by the following relationship:

$$Nu_D(x,t) = \frac{q'' D/k}{T_w - T_m} = C_2 \left[\frac{1 + \left(\frac{a}{q''_r}\right) \times \sum_{m=0,1,2}^{\infty} \frac{1}{2m+1} \sin(\omega_m Fo)}{\theta_w - \theta_m} \right] \tag{24}$$

Similar to Section 3.2, the average Nusselt number over the entire length of the heated section is:

$$\overline{Nu_D}(L_2,t) = \frac{1}{L_2} \int_0^{L_2} Nu_D dx \tag{25}$$

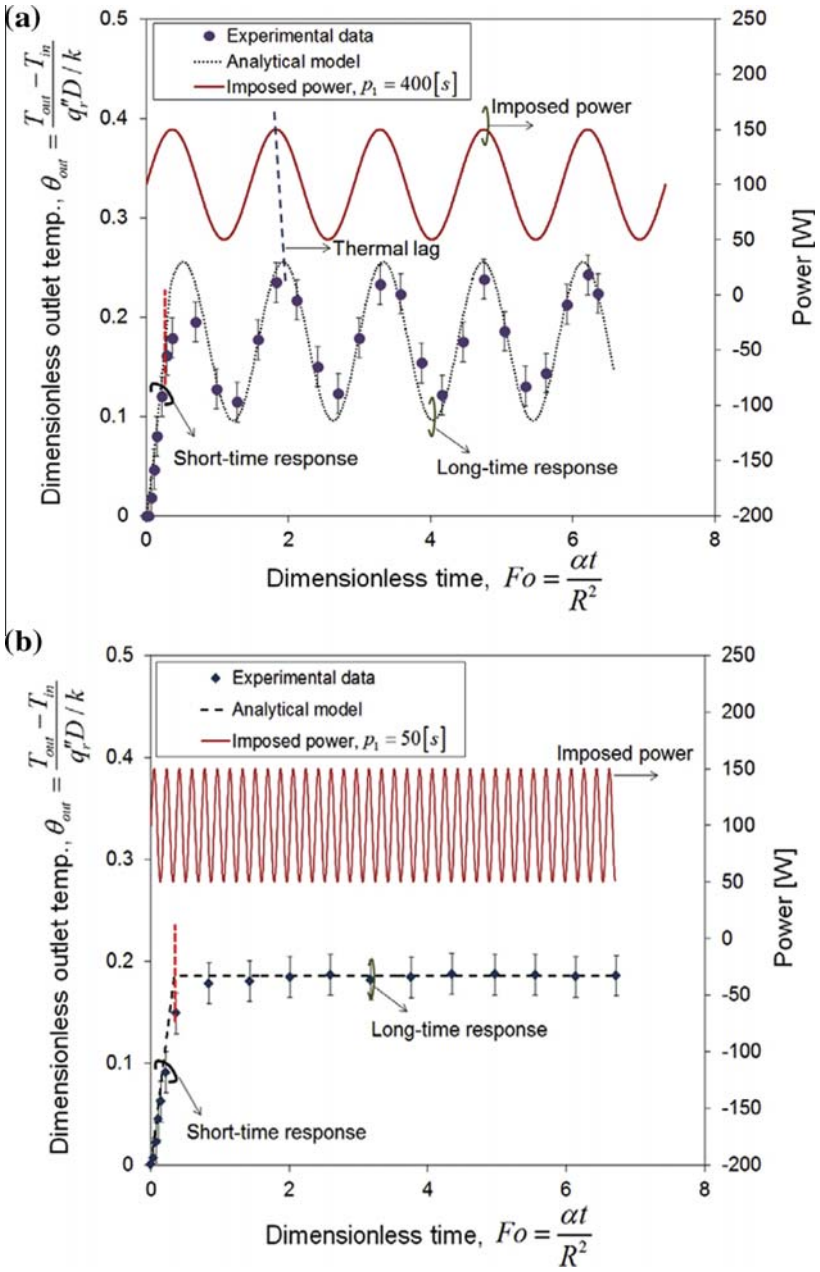

Fig. 4. Short- and long-time responses for outlet temperature and comparison with experimental data for sinusoidal power with different periods: (a) $p_1 = 400$ [s] and (b) $p_1 = 50$ [s]. ($\dot{m} = 3.6 \pm 0.216$ [gr/s]).

4. Results and discussion

4.1. Validation tests/outlet fluid bulk-temperature

Fig. 2 shows the dimensionless short- and long-time asymptotes, Eq. (13), for the outlet fluid bulk-temperature against the dimensionless time (Fourier number) for a step power. The exact analytical results are also compared with the obtained experimental data in Fig. 2.

The following highlights the trends in Fig. 2:

- There is an excellent agreement between the exact analytical solutions and the obtained experimental data. The maximum relative difference between the derived asymptotes and the experimental data is less than 8%.
- The good agreement between the analytical results and the experimental data verifies the accuracy of the experimental setup and the measuring instruments.
- As the heating is applied, the outlet fluid bulk-temperature increases to reach the steady-state value at the long-time asymptote.
- The experimental data show a smooth transition between the short- and long-time responses.

Fig. 3 depicts the variations of dimensionless outlet fluid bulk-temperature against the Fourier number for a square-wave power. The exact analytical results are also compared with the obtained experimental data in Fig. 3. The following conclusions can be drawn from Fig. 3:

- There is a good agreement between the analytical results and the obtained experimental data; the maximum relative difference less than 12%.
- The good agreement between the analytical results and the experimental data verifies the accuracy of the experimental setup and the measuring instruments.
- As the heating is applied, the temperature of the fluid rises to show steady oscillatory behavior after the transition time, $X = Fo$. This time is demarcated on Fig. 3 by a vertical dash line.
- There is an initial transient period, which can be considered as pure conduction, i.e., the short-time response for $X \geqslant Fo$. However, as pointed out earlier, each axial position shows steady oscillatory behavior for $X < Fo$ at the long-time response.
- There is a slight discrepancy between the analytical results and experimental data around the transition time. Referring to [12,20], this happens as a result of the limitations of the mathematical method "method of characteristics" that is used in [20] to solve the energy equation. Such mathematical method predicts an abrupt transition from short- to long-time responses while experimental data show a smooth transition.
- As expected the fluid temperature fluctuates with time in case of a square-wave heat flux. For a step heat flux, the solution does not fluctuate over time. The temperature fluctuates with the period of the imposed heat flux.

4.2. Cut-off angular frequency

Fig. 4 shows the dimensionless outlet fluid bulk-temperature versus the Fourier number under a sinusoidal power. To investigate the effects of the angular frequency of the applied heat flux on the coolant behavior, "slow" and "fast" functions are taken into account for the imposed power. Fig. 4a shows a "slow" transient scenario where the angular frequency of the applied power is $p_1 = 400$ [s], while the corresponding value in the "fast" case in Fig. 4b is $p_1 = 50$ [s]. The following highlights the trends in Fig. 4:

- There is a shift between the peaks of the applied power and the outlet fluid bulk-temperature. This shows a "thermal lag" (inertia) of the fluid flow. This thermal lag is attributed to the fluid thermal inertia.
- When a sinusoidal cyclic heat flux with high angular frequency is imposed on the flow, the fluid does not follow the details of the heat flux behavior. Therefore, for very high angular frequencies, the fluid flow acts as if the imposed heat flux is constant at "the average value" associated with zero frequency for the sinusoidal heat flux.
- For high angular frequencies, i.e., $p \to 0$ or $\omega \to \infty$, the fluid flow response yields that of a step heat flux. This is called the "cut-off" pulsation frequency.
- Dimensionless cut-off angular frequency: defined in this study as the angular frequency beyond which the fluid response lies within $\pm 5\%$ of that of step heat flux. As such, following [22], for a fully developed tube flow subjected to a sinusoidal wall heat flux, $\omega_1 = \frac{2\pi R^2}{p_1 \alpha} = 15\pi$ is the cut-off angular frequency.
- The dimensionless cut-off frequency is a function of heat flux period, p_1 [s], tube radius, R [m], and fluid thermal diffusivity, α $[\frac{m^2}{s}]$.
- Irrespective of Fo number, the amplitude of the dimensionless fluid bulk-temperature decreases remarkably as the angular frequency increases. As mentioned earlier, this happens due to the fact that for high angular frequencies the fluid flow response approaches to that of the step heat flux.

4.3. Tube wall temperature

Fig. 5 shows variations of short- and long-time asymptotes for tube wall temperature, Eqs. (7) and (10), against the dimensionless time (Fourier number). A comparison is also made in Fig. 6 between the presented asymptotes, Eqs. (7) and (10), and the obtained experimental data. Step heat flux, Eq. (6), is imposed on the tube wall and the experimental data are reported for the thermocouples T_1 and T_4 which are corresponding to axial locations $X = 0.15$ and 0.4, respectively. The trends for other axial locations are similar.

The following conclusions can be drawn from Fig. 5:

- As heating is applied, the wall temperature rises and then levels out at a steady state value, i.e., long-time asymptote.

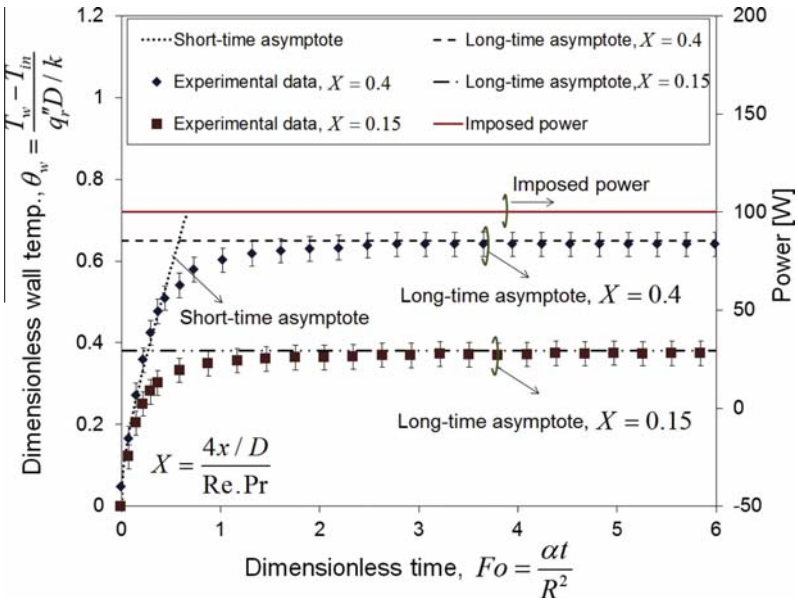

Fig. 5. Short- and long-time asymptotes for tube wall temperature and comparison with experimental data for the step power. ($\dot{m} = 3.3 \pm 0.198$ [gr/s]).

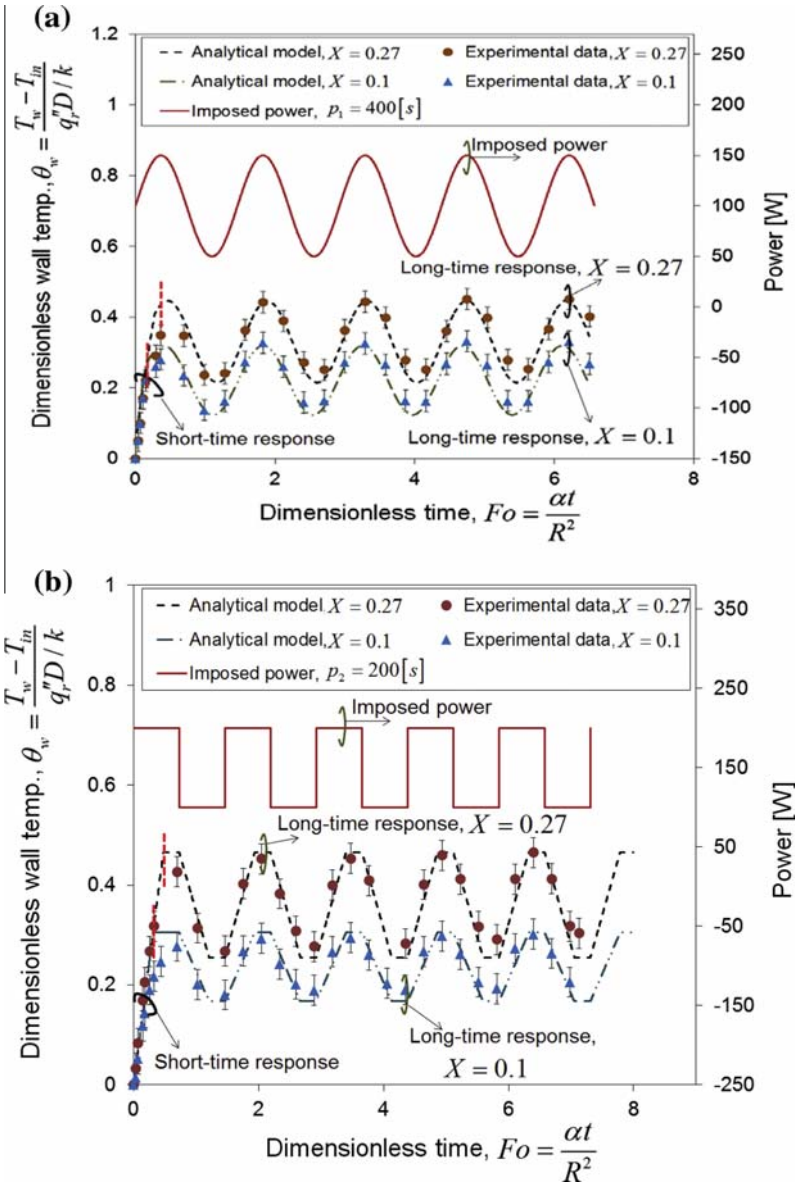

Fig. 6. Short- and long-time responses for tube wall temperature and comparison with experimental data for: (a) sinusoidal and (b) square-wave power. ($\dot{m} = 3.6 \pm 0.216$ [gr/s]).

- There is a good agreement between the experimental data and the short- and long-time asymptotes, Eqs. (9) and (10); maximum relative difference less than 9.2%.
- The obtained experimental data show a smooth transition between the short- and long-time asymptote.
- Around the transition time, the experimental data branch off from the short-time asymptote and plateau out at the long-time asymptote, Eq. (10).

Fig. 6 depicts the variations of closed-form solutions and experimental results for tube wall temperature over the dimensionless time (Fourier number) for: (a) sinusoidal power, Eqs. (19.a) and (19.b); and (b) square-wave power, Eq. (26.a) and (26.b). The experimental data are reported for the thermocouples T_1 and T_3 which are corresponding to $X = 0.1$ and 0.27, respectively. The trends for other axial locations are similar. The following highlights the trends in Fig. 6:

- There is an initial transient period of pure conduction, i.e., short-time response, during which all of the curves follow along the same line, $X \geqslant Fo$.
- When $Fo = X$, each curve moves away from the common line, i. e., pure conduction response and adjusts towards a steady oscillatory behavior at long-time response. The transition time for the axial locations considered in Fig. 6, are indicated by vertical dash lines.
- The wall temperatures become higher for larger X values, as expected, because of the increase in the fluid bulk temperature in the axial direction.
- As mentioned before, the value of C_1 is unity for slug flow, while it should be obtained empirically for other velocity profiles. Based on the obtained experimental data, the value of C_1 is considered equal to 1.7; in mathematical notation, $C_1 = 1.7$. As such, there is an excellent agreement between the closed-form relationships Eqs. (16) and (22), and the experimental data over the short-and long-time responses.

- There is a small discrepancy between the experimental data and analytical results around the transition time, $X = Fo$. As mentioned before, this is attributed to the limitations of the mathematical approach "method of characteristics" that cannot predict the results around the transition time accurately. The maximum relative difference between the present analytical model and the experimental data is less than 10.1%.

4.4. Nusselt number

Variations of the average Nusselt number against the Fourier number for a step power are depicted in Fig. 7. Short- and long-time responses are shown in Fig. 7, and compared with the obtained experimental data. Moreover, a relationship is proposed as an all-time Nusselt number based on the blending technique [30]. The following can be concluded from Fig. 7:

- There is a good agreement between the short-time asymptote, Eq. (14), and the obtained experimental data at early times, $Fo \to 0$.
- Around the transition time, the experimental data branch off from the short-time asymptote and adjust towards the long-time asymptote.
- Based on the blending technique [31], the following relationship is proposed as an all-time model for the average Nusselt number under a step heat flux.

$$\overline{Nu}_D(t,x) = \left\{ [(Nu_D(t)_{Fo\to 0})]^3 + [Nu_{0-x,D}]^3 \right\}^{(1/3)} \tag{26}$$

where $Nu_D(t)$ and $Nu_{0-x,D}$ are the short- and long-time asymptotes, Eqs. (14) and (15). In addition, $\overline{Nu}_D(t,x)$ is the all-time model presented for the average Nusselt number for a step power.

- The maximum relative difference between the proposed all-time model and the experimental data is less than 7%.

Fig. 8 shows the variations of the average Nusselt number against the Fourier number for the sinusoidal imposed heat flux. Different periods are considered for the imposed power and the semi-analytical results are compared with obtained experimental data. Regarding Fig. 8, the conventional "quasi-steady" model is a simplified model which assumes that the convective heat transfer coefficient is constant, equal to the fully developed condition in the channel [13]. It should be noted that based on the obtained experimental data, the value of the coefficient C_2 is considered equal to

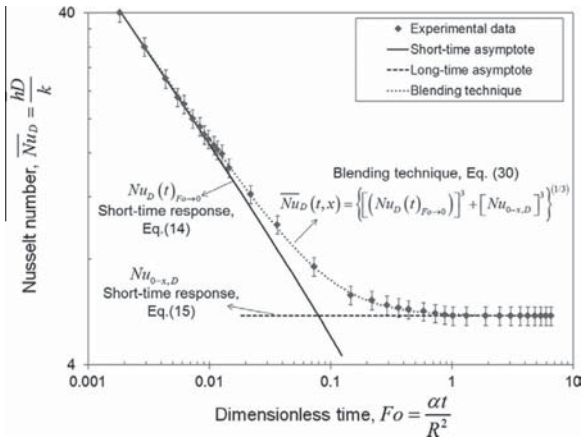

Fig. 7. Short- and long-time responses as well as the proposed all-time model for the average Nusselt number, and comparison with the obtained experimental data for the step power. ($\dot{m} = 3.3 \pm 0.198$ [gr/s]).

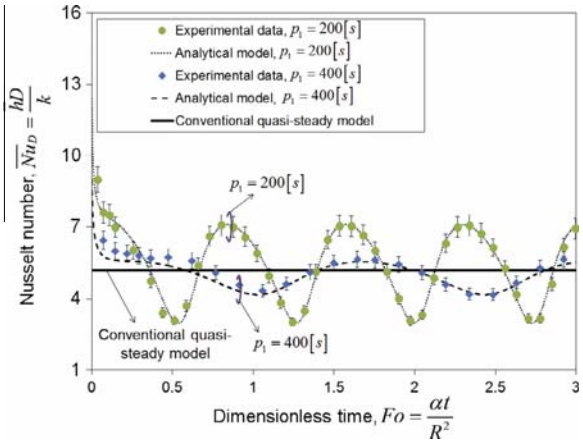

Fig. 8. All-time Nusselt number for sinusoidal transient scenario with different periods of $p_1 = 200$ [s] and $p_1 = 400$ [s], and comparison with quasi-steady model and the obtained experimental data. ($\dot{m} = 3.6 \pm 0.216$ [gr/s]).

0.54. Such value minimizes the difference between the experimental and semi-analytical results; maximum relative difference less than 10%. The following highlights the trends in Fig. 8.

- The values of the average Nusselt number vary significantly with the angular frequency of the imposed heat flux, while the conventional models, e.g., quasi-steady model fail to predict such variations of the Nusselt number with time.
- The Nusselt number oscillates with the angular frequency of the imposed heat flux.
- Regardless of the angular frequency, at very initial transient period, the Nusselt number is much higher than that of the long-time response.
- The fluctuations of the transient Nusselt number occur somewhat around the fully-developed steady-state value. Considering the slug flow inside a circular tube, the value of the fully-developed Nusselt number for the steady-state condition is: $Nu_D = 4.36$ as predicted by the quasi-steady model [25].

6. Conclusion

An experimental study is carried out to investigate the thermal characteristics of a fully-developed tube flow under time-varying heat fluxes. Three different scenarios are considered for the applied time-dependent heat fluxes: (i) step; (ii) sinusoidal; and (iii) square-wave. Exact closed-form relationships are proposed to find the fluid bulk temperature for the implemented scenarios. As such, the accuracy of the experimental data and the measuring instruments are verified. Semi-analytical relationships are proposed to predict; (i) tube wall temperature and (ii) the Nusselt number for all the implemented scenarios. The question "how the thermal characteristics of the dynamic cooling systems vary over a duty cycle" is answered here as follows: The imposed heat flux (thermal load) is the dominant parameter that characterizes the thermal behavior of a cooling system. As such;

- The temperature and the Nusselt number fluctuate with the period of the applied thermal load.
- For fast transients, there is a cut-off angular frequency for the imposed heat flux beyond which the fluid does not follow the details of the imposed thermal load. The fluid response then becomes that of step heat flux.
- The fluid response consists of two main parts: (i) short-time response and (ii) long-time response. The former is corresponding to early times during which pure conduction occurs inside

the fluid domain. On the other hand, long-time response refers to a period of time starting after the transition time; the fluid yields steady-oscillatory behavior.

- The conventional steady-state models fail to predict the thermal behavior of dynamic cooling systems under time-varying thermal load.

Conflict of interest

None declared.

Acknowledgments

This work was supported by Automotive Partnership Canada (APC), Grant No. APCPJ 401826-10. The authors would like to thank the support of the industry partner, Future Vehicle Technologies Inc. (British Columbia, Canada).

References

[1] M. Marz, A. Schletz, Power electronics system integration for electric and hybrid vehicles, in: 6th Int. Conf. Integr. Power Electron. Syst., 2010, pp. Paper 6.1.
[2] K. Chau, C. Chan, C. Liu, Overview of permanent-magnet brushless drives for electric and hybrid electric vehicles, IEEE Trans. Ind. Electron. 55 (2008) 2246–2257.
[3] J. Garrison, M. Webber, Optimization of an integrated energy storage scheme for a dispatchable wind powered energy system, in: ASME 2012 6th Int. Conf. Energy Sustain. Parts A B San Diego, CA, USA, 2012, pp. 1009–1019.
[4] J. Garrison, M. Webber, An integrated energy storage scheme for a dispatchable solar and wind powered energy system and analysis of dynamic parameters, Renew. Sustain. Energy 3 (2011) 1–11.
[5] C. Crawford, Balance of power: dynamic thermal management for Internet data centers, IEEE Internet Comput. 9 (2005) 42–49.
[6] R.R. Schmidt, E.E. Cruz, M. Iyengar, Challenges of data center thermal management, IBM J. Res. Dev. 49 (2005) 709–723.
[7] Y. Joshi, P. Kumar, B. Sammakia, M. Patterson, Energy Efficient Thermal Management of Data Centers, Springer, US, Boston, MA, 2012.
[8] R. Scott Downing, G. Kojasoy, Single and two-phase pressure drop characteristics in miniature helical channels, Exp. Therm. Fluid Sci. 26 (2002) 535–546.
[9] S.V. Garimella, L. Yeh, T. Persoons, Thermal Management Challenges in Telecommunication Systems and Data Centers Thermal Management Challenges in Telecommunication Systems and Data Centers, CTRC Res. Publ, 2012. pp. 1–26.
[10] M. O'Keefe, K. Bennion, A comparison of hybrid electric vehicle power electronics cooling options, in: Veh. Power Electron. Cool. Options, 2007, pp. 116–123.
[11] C. Mi, F.Z. Peng, K.J. Kelly, M.O'. Keefe, V. Hassani, Topology, design, analysis and thermal management of power electronics for hybrid electric vehicle applications, Int. J. Electr. Hybrid Veh. 1 (2008) 276–294.
[12] R. Siegel, Transient heat transfer for laminar slug flow in ducts, Appl. Mech. 81 (1959) 140–144.
[13] R. Siegel, M. Perlmutter, Laminar heat transfer in a channel with unsteady flow and wall heating varying with position and time, Trans. ASME 85 (1963) 358–365.
[14] R. Siegel, M. Perlmutter, Heat transfer for pulsating laminar duct flow, Heat Transfer 84 (1962) 111–122.
[15] R. Siegel, Heat transfer for laminar flow in ducts with arbitrary time variations in wall temperature, Trans. ASME 27 (1960) 241–249.
[16] M. Perlmutter, R. Siegel, Two-dimensional unsteady incompressible laminar duct flow with a step change in wall temperature, Trans. ASME 83 (1961) 432–440.
[17] M. Perlmutter, R. Siegel, Unsteady laminar flow in a duct with unsteady heat addition, Heat Transfer 83 (1961) 432–439.
[18] R. Siegel, Forced convection in a channel with wall heat capacity and with wall heating variable with axial position and time, Int. J. Heat Mass Transfer 6 (1963) 607–620.
[19] M. Fakoor-Pakdaman, M. Andisheh-Tadbir, M. Bahrami, Transient internal forced convection under arbitrary time-dependent heat flux, in: Proc. ASME Summer Heat Transf. Conf., Minneapolis, MN, USA, 2013.
[20] M. Fakoor-Pakdaman, M. Andisheh-Tadbir, M. Bahrami, Unsteady laminar forced-convective tube flow under dynamic time-dependent heat flux, J. Heat Transfer 136 (2014) 041706.
[21] M. Fakoor-Pakdaman, M. Ahmadi, M. Bahrami, Unsteady internal forced-convective flow under dynamic time-dependent boundary temperature, J. Thermophys. Heat Transfer 28 (2014) 463–473.
[22] M. Fakoor-Pakdaman, M. Ahmadi, M. Andisheh-Tadbir, M. Bahrami, Optimal unsteady convection over a duty cycle for arbitrary unsteady flow under dynamic thermal load, Int. J. Heat Mass Transfer 78 (2014) 1187–1198.
[23] F.P. Incropera, D.P. Dewitt, T.L. Bergman, A.S. Lavine, Introduction to Heat Transfer, fifth ed., John Wiley & Sons, USA, 2007.
[24] Z. Guo, H. Sung, Analysis of the Nusselt number in pulsating pipe flow, Int. J. Heat Mass Transfer 40 (1997) 2486–2489.
[25] A. Bejan, Convection Heat Transfer, third ed., USA, 2004.
[26] M. Fakoor-Pakdaman, M. Bahrami, Transient internal forced convection under step wall heat flux, in: Proc. ASME 2013 Summer Heat Transf. Conf. HT2013, 2013.
[27] T. Von Karman, M.A. Biot, Mathematical Methods in Engineering, McGraw-Hill, New York, 1940.
[28] R.K. Shah, Thermal entry length solutions for the circular tube and parallel plates, in: Proceeding 3rd Natl. Heat Mass Transf. Conf., Indian Institute of Technology, Bombay, 1975, pp. HMT–11–75.
[29] E. Kreyszig, H. Kreyzig, E.J. Norminton, Advanced Engineering Mathematics, 10th ed., John Wiley & Sons, n.d.
[30] S.W. Churchill, R. Usagi, A general expression for the correlation of rates of transfer and other phenomena, Am. Inst. Chem. Eng. 18 (1972) 1121–1128.
[31] R. Siegel, E.M. Sparrow, Transient heat transfer for laminar forced convection in the thermal entrance region of flat ducts, Heat Transfer 81 (1959) 29–36.